ANALYSIS OF SPREAD MULTI-JET VTOL AIRCRAFT IN HOVER

Final Technical Report

by

Leroy F. Albang

Prepared for the

NATIONAL AERONAUTICS AND SPACE ADMINISTRATION
LANGLEY RESEARCH CENTER
HAMPTON, VIRGINIA 23665

Under
Master Contract Agreement NAS1-11707
Task Authorization No. 68
A. Sidney Roberts , Jr., Principal Investigator

SCHOOL OF ENGINEERING
OLD DOMINION UNIVERSITY
NORFOLK, VIRGINIA 23508

December 1974

Technical Report

74-54

ANALYSIS OF SPREAD MULTI-JET VTOL AIRCRAFT IN HOVER

FINAL TECHNICAL REPORT

By

Leroy F. Albang

Prepared for the
NATIONAL AERONAUTICS AND SPACE ADMINISTRATION
Langley Research Center
Hampton, Virginia

Under
Master Contract Agreement NAS1-11707
Task Authorization No. 68
A. Sidney Roberts, Jr., Principal Investigator

School of Engineering
Old Dominion University
Technical Report 74-T8

Submitted by the
Old Dominion University Research Foundation
P.O. Box 6173
Norfolk, Virginia

December 1974

ANALYSIS OF SPREAD MULTI-JET VTOL AIRCRAFT IN HOVER

By

Leroy F. Albang[1]

SUMMARY

An investigation of vertical takeoff and landing (VTOL) aircraft lift losses in hover has been conducted to evaluate a method for a simplified test technique.

Three flat plate models were tested to determine their usefulness in predicting hover characteristics by comparing results between plate and three-dimensional models. Attempts to correlate the out of ground effect results for the plate models with the empirical expression for calculating jet induced loads were successful for the models which used engine simulators producing efflux characteristics similar to the three-dimensional model engines. Data for the model using engine simulators with characteristics unlike those of the three-dimensional model simulators could not be correlated in this manner.

In ground effect, comparisons of induced lift loads indicated correlations between the plate and three-dimensional models were within 2 percent of thrust in the height range dominated by the fountain effect. However, small outward deflection of the lift engine exhaust was found to cause a decrease in beneficial fountain on the order of 5 to 10 percent of thrust. Dashpots proved useful in eliminating data scatter caused by flow-induced model vibration. The engine arrangement of a midspan-pod VTOL lift-fan transport model showed a strong adverse effect on lift

---

[1] Graduate Research Assistant, School of Engineering, Old Dominion University, Norfolk, VA 23508

loss due to engine deflection. Data obtained for the plate models could be correlated to three-dimensional results by the application of a geometrical equivalent height correction factor $\Delta h\ D_e$. The correlation of plate and tunnel models indicated that lift losses in ground effect were essentially independent of the efflux characteristics for the engine simulators.

INTRODUCTION

In recent years, the evolution of vertical takeoff and landing (VTOL) aircraft has brought about a need to determine thrust-induced lift losses during hover. These thrust effects occur when the vehicle takes off or lands vertically. Out of ground effect, the entrainment of flow caused by the vertically directed propulsion system is the predominant cause. The velocity of the induced flow causes a static pressure drop on the lower surface of the vehicle which results in a lift loss. As a vehicle approaches the ground, additional effects such as recirculation and reingestion, wall jet and fountain effects, all of which are highly dependent on the vehicle configuration, influence the flow. Therefore, procedures must be developed to predict the flow-induced loads, since the design of VTOL aircraft requires a detailed knowledge of the associated aerodynamic lift-loss characteristics.

A number of experimental tests, references [1 to 4], have been conducted to examine the lift losses associated with various aircraft configurations.

Reference [1] indicated that lift losses for clustered lift thrust systems could be predicted out of ground effect by an empirical equation based on jet and model geometry and the maximum dynamic-pressure decay of the lift jets. In reference [2] static ground effect lift-loss tests for a single round centrally located lifting jet indicated that an empirical equation based on jet and planform surface geometry could predict the lift

loss as a function of ground height. The correlations of reference [2] were obtained using planform plates rather than three-dimensional models as in reference [1].

At the present time, most investigations are primarily directed towards contemporary configurations with spread lift-thrust systems to determine the level of the lift losses. The understanding of the physical processes is inadequate to develop an analytical model to predict the resultant model forces. Therefore, more experimental work is needed with proposed vehicle designs to increase the understanding of the associated phenomena and consequently to improve the design. In an effort to simplify the investigation of spread multi-jet VTOL aircraft, two-dimensional models based on an aircraft projected planform and cut from sheet metal were used in hover tests. Three different flatplate model configurations were tested in the MPA of the Langley V/STOL tunnel to study the effect of contoured aircraft surface as opposed to flat plates on induced lift losses. The prime objective of this study was to determine the applicability of flat plate models as a simple and inexpensive method for assessing induced forces and moments in hover.

SYMBOLS

A_j	jet exit area, cm^2 ($in.^2$)
D	diameter of jet exit, cm (in.)
D_e	effective diameter, diameter of a circle equivalent in area to total jet exit area of a given configuration, cm (in.)
h	height from jet exit to downstream pressure rake or from bottom of the model at the center of gravity to the ground, cm (in.)
Δh	difference between tunnel model height and equivalent plate model height, cm (in.)

ΔL	load induced on model (force referenced with respect to body axis system), N (lb)
ΔPM	pitching moment induced on model, cm-N (in.-lb)
ΔRM	rolling moment induced on model, cm-N (in.-lb)
p	ambient static pressure, N/cm^2 ($lb/in.^2$)
p_t	total pressure in the jet wake, N/cm^2 ($lb/in.^2$)
q	dynamic pressure, N/cm^2 ($lb/in.^2$)
q_e	jet impact pressure at exit, N/cm^2 ($lb/in.^2$)
q_h	impact pressure measured at a distance h downstream from jet exit, N/cm^2 ($lb/in.^2$)
$\overline{q_h}$	average dynamic pressure at a downstream distance h from jet exit, N/cm^2 ($lb/in.^2$)
rpm	revolutions per minute
S	plate or wing-plus-fuselage planform area, cm^2 ($in.^2$)
T	jet thrust
β	spread angle of the jet
δ_L	lift engine louver deflection from vertical axis
δ_{Lc}	lift-cruise engine hood deflection from horizontal axis
θ	pitch angle
ϕ	roll angle

Subscripts:

i	point of maximum rate of change of decay parameter
max	maximum
plate	referenced to plate model
tunnel	referenced to tunnel model

MODELS AND APPARATUS

Description of Test Apparatus

The model support frame used with the present static ground effect investigation is shown in Figure 1. Several stings were designed to accomodate the different balances and mounting positions required for each model. Since the expected induced loads were only a small percentage of the total jet thrust, it was considered necessary to mount the plates models independently of the plenum chamber and model engine assemblies. The plenum chamber on the bottom of the frame was connected to a high pressure air supply, with the airflow into the chamber remotely regulated. Manual valves on the plenum chamber allowed differential adjustments of the airflow to the model engines for individual thrust settings. Figure 1 also shows the inverted model arrangement as it was located beneath the 3.63 m x 3.63 m (12 ft x 12 ft) plywood groundboard. Threaded screwjacks enabled the board to be set at various heights and removed to simulate hover out-of-ground effect. The board was canted with respect to the model to simulate various model pitch and roll orientations.

A 24-port straight rake was used to obtain total pressure profiles downstream of all model engines to determine engine efflux dynamic pressure decay characteristics.

The model fans used magnetic sensors to measure fan rpm. For the midspan pod plate model the close spacing of the wing nozzles (due to the small scale) prevented side-by-side mounting of the ejectors. The plate model V/STOL fighter ejectors were spaced far enough apart so that they could be mounted in their original configuration. Small dashpots (with a 1.27 cm [0.5 in.] spherical piston having about 2.54 cm [1.0 in.] of travel in highly viscous oil) were located on both wingtips of the midspan pod plate model; wingtips, nose and tail of the V/STOL fighter plate model, and the wingtips for a few selected runs on the wingtip pod plate model. They were used to reduce the model fluctuations created by flow turbulence.

Description of Flat Plate Models

The present investigation used three different flat plate model configurations to simulate lift-fan transport and advanced VTOL fighter aircraft. These aircraft use lift engines and cruise engine thrust deflection for lift in hover. A scale factor based on the ratio of the model fan diameter to the full-scale fan diameter was used to size the models. Table I lists the important features of the engine configuration used in these models. For those configurations where the exit area was measured in the plane of the fan hub, the annular area was used. The inside (hub) diameter was included for these engines. Table II illustrates which engine configurations were used for each model. These models were built from aluminum sheet metal cut to the shape of the aircraft's projected planform.

Wingtip pod VTOL lift-fan transport model. Model 1, a wingtip pod VTOL lift-fan transport design, is illustrated in Figures 2 and 3. An aluminum plate box formed the center of the model to which the front and rear fuselage sections were attached. The wings could be mounted to the sides of the box at various heights to represent low-, mid-, and high-wing configurations. Small aluminum angles, bolted to the underside of the plate, provided additional stiffness for the model. The model fans were mounted so they exhausted through the plate and were perpendicular to it, with no contact between the fan cowl and the plate (Figure 4). These fans were used to simulate the lift fans located in the forward fuselage and in pods on each wingtip, and the lift/cruise fans located on the aft portion of the fuselage.

For direct comparison with the plate model, a balsa wood contour, which represented the three-dimensional lower fuselage shape, was designed to be mounted directly on the plate (Figure 5). These cylindrical sleeves were installed to prevent any direct thrust forces from acting on the model, so that only induced surface effects were felt by the model. These sleeves are not

shown in Figure 5. The moment reference center of plate and contour model is located on the thrust centerline of the wing pod fans.

Midspan pod VTOL lift-fan transport model. Model 2, a midspan pod VTOL lift-fan transport model, is illustrated in Figures 6 and 7. This flat plate model was cut from a single piece of aluminum sheet. High pressure air ejectors (Figure 8) were used to simulate the lift fans and lift/cruise fans for this model. The forward ejectors exhausting through the wing pods made use of a bullet-shaped centerbody in the nozzle to approximate the distortion of the exit pressure profile caused by a fan hub. Since the rear ejectors represented deflected-fan exhausts, the simple nozzle was expected to provide a reasonable representation of exit pressure characteristics. The ejectors were mounted to exhaust in a perpendicular direction. As shown in Figure 8, the lip of the plate was beveled to reduce the gap between the lip and the nozzle exit. The ejectors with centerbodies used to simulate the lift fans were located in the wing pods and the lift/cruise fans located on the aft portion of the fuselage. The moment reference center of Model 2 is located 35.26 cm (13.88 in.) aft of the nose of the aircraft.

Advanced V/STOL fighter model. Model 3, an advanced V/STOL fighter model, is illustrated in Figures 9 and 10. A single sheet of aluminum plate was also used for this model. High pressure air ejectors (Figure 8) were used to simulate the lift and lift/cruise engines for this model. Centerbodies were not used on any of these ejectors. The forward ejector represented the lift engine and the two rear ejectors represented the lift/cruise engines. The moment reference center of Model 3 is located 89.54 cm (35.25 in.) aft of the nose of the aircraft.

Description of Tunnel Models

Tunnel Model 1 (Figure 11) results were the basis of comparison for the data from plate Model 1. A forward fuselage

lift fan drawing (Figure 12) shows the variable louver system used for the four Model 1 lift fans. The lift/cruise fan, 90° deflection hood, and nozzle are shown in Figure 13.

Tunnel Model 2 (Figure 14) results were the basis of comparison for the data from plate Model 2. A lift fan drawing (Figure 15) is shown with the fixed louvers used for the four Model 2 lift fans. The lift/cruise fan, 90° deflection hood, and nozzle for Model 2 are shown in Figure 16.

Tunnel Model 3 (Figure 17) results were the basis of comparison for the data from plate Model 3. The lift engine (Figure 8) for tunnel Model 3 is the same as that for the plate model lift engine. The same ejectors (Figure 8) are used for the cruise engines but are deflected by the 90° extensions.

TEST PROCEDURES

Engine Test Procedures

Thrust calibrations. It was necessary to obtain thrust calibrations for all of the engine simulators. The tip reaction fans of Model 1 were calibrated for thrust as a function of fan rpm. The ejectors used for Models 2 and 3 were calibrated for thrust as a function of the ejector plenum pressure. One ejector was also tested with a ground plate set at various distances perpendicular to the ejector nozzle exit to determine the influence of ground effect on the thrust calibrations.

Efflux characteristics of flat plate model engines. Previous investigations [1] of thrust-induced lift losses for a model hovering out of ground effect indicated a relationship between jet efflux decay characteristics and jet-induced forces on the model. Therefore, total pressure profiles were taken across the flow at various distances downstream of the exit for all configurations of model engines used during lift loss tests. By assuming axial symmetry about the thrust centerline, a radial profile was used to represent the pressure contour at each

downstream station. For Model 1, an 8-blade fuselage fan (A) and a 4-blade wing pod fan (B) were examined. The same two fans were also tested with the extension sleeves (A', B', respectively) used with the balsa wood contoured model. For these fan h/D was measured from the edge of the cowl for the plate configuration, and the edge of the cowl closest to the fan for the cutout sleeve extensions used for the contour model. For Model 2, the ejector configurations studied were the basic ejector and nozzle without centerbody (F), the forward wing pod ejector and nozzle with centerbody and short exit extension (G'), and the rear wing pod ejector and nozzle with centerbody and long exit extension (G). For all of these ejectors, h/D was measured from the nozzle exit. Model 3 used only the basic ejector and nozzle without center body configuration (F).

Efflux characteristics of tunnel model engines. In order to provide a base comparison for engine characteristics, exit profiles were taken for the lift and lift/cruise engines of Models 1 and 2. Since the four Model 2 lift engines were identical, a profile series was taken for one engine with h/D measured from the fan exit. A profile series was obtained for the lift/cruise engine of Model 2 with h/D measured from the most upstream point on the uneven nozzle. Since the Model 1 fuselage and wing pod lift fans were identical, efflux characteristics were taken for a forward fuselage fan with h/D measured from the lower edge of the middle louver. Identical fan units were used for the lift/cruise engines of Models 1 and 2 with different nozzle exits areas. It was assumed that the efflux characteristics would be the same and the Model 2 lift/cruise engine was used to represent the Model 1 lift/cruise engine.

In the previous analysis by Gentry and Margason [1] the decay parameter q_h/q_e was used where q_h was the maximum

dynamic pressure at each downstream station h. No corrections for compressibility were applied. This parameter, q_h/q_e (the maximum q-decay), was determined for the engine simulators of the present study. However, the irregular exit profiles of the fans implied that it might be worthwhile to look also at an average q-decay found to correlate characteristics for certain irregular nozzles [14]. All of the profiles were corrected for compressibility, then averaged over the area to yield an average efflux dynamic pressure q_h for each downstream station. In order to provide consistent comparisons, q_e was calculated from

$$q_e = T/2A_j$$

where A_j is the exit area at the point where h/D was 0 and T is the thrust available from force measurements or from calibration data.

Model Test Procedures

Force measurements on each plate model were conducted with thrust, ground board height, pitch, and roll as the variables. For each model and ground board orientation the height (h) of the model was defined as the distance from the model (and balance) center of gravity to the ground board, measured perpendicular to the plate model. Additional tests with no pitch or roll variation were run for Model 1 to examine several aspects of the testing method. Check runs were conducted to define the sensitivity to wing position variations. For one comparison series of runs for both plate and balsa contour model, the gaps between fan cowl and the model were covered with dental dam to ascertain any influence due to the gaps on lift loss. In an attempt to reduce flow induced model fluctuation and determine its influence on force measurements, dashpots were mounted between the wingtips and the test frame. Again a series of runs was made for both the plate and balsa contour models.

PRESENTATION OF RESULTS

The results are presented in the following figures:

ENGINE SIMULATOR CHARACTERISTICS

		Figure No.
Pressure Ratio Profiles		
Configuration	**A**	**18**
	A'	**19**
	B	**20**
	B'	**21**
	C	**22**
	D	**23**
	E	**24**
	F	**25**
	G	**26**
	G'	**27**
Dynamic Pressure Decay		
Effect of assumed spread angle		**28**
Thrust effects	**- plate Model 1 fan**	**29**
	- tunnel Model 1 fan	**30**
	- plate Models 2 and 3 ejector	**31**
	- tunnel Model 2 fan	**32**
Comparison of plate and tunnel model engines		
	Model 1 cruise	**33**
	Model 1 lift	**34**
	Model 2 cruise	**35**
	Model 2 lift	**36**

MODEL HOVER CHARACTERISTICS - LEVEL CONFIGURATIONS

Plate Model 1		
Thrust effects		**37**
Thrust effects with balsa contour		**38**
Effects of dashpots and dental dam		**39-41**
Effects of wing height variation		**42**

DISCUSSION OF RESULTS

Engine Simulator Characteristics

The engines will be examined first in terms of the efflux pressure profiles. The maximum dynamic pressure from each profile, and an average dynamic pressure from an integration of the profile, will be studied for each engine configuration.

Analysis of efflux pressure ratio profile Efflux pressure ratio profiles (Figures 18 to 27) were obtained from the various configurations of fans and ejectors for all of the models tested.

The ratio of total pressure to ambient pressure is plotted as a function of the radial distance from engine centerline non-dimensionalized by engine exit radius. The profile was taken from engine centerline outward and axial symmetry was assumed. The profiles are sketched to the right of the data to indicate the downstream location of the profile. The efflux profiles (Figures 18 to 21) for the Model 1 were taken only across the exit area of the fans at each downstream location. The maximum dynamic pressure decay parameter is measured within this area. To determine the effect of this discrepancy on the average q-decay parameter an exhaust spread angle was assumed with a pressure ratio of 1 at the edge. The new profile, linear from the last data point to the edge, was integrated and the calculated thrust from the average q was compared to the measured exit thrust. Since the thrust downstream must be less than or equal to the exit thrust a maximum spread angle was defined. The profile sketches (Figures 22 to 27) are all taken directly from the actual data. The pressure profiles reveal how the efflux spreads and mixes with the ambient air. The gradient of the profile at the edge is an indicator of the amount of mixing.

Comparison of the plate and tunnel Model 1 lift/cruise fans (Figures 18 and 23) for comparable h/D values shows a higher shear (indicated by the steeper pressure profile gradient at the edge of the profile) for the plate model fans. This is due to the shape of the blades which produce a higher velocity away from the hub. This implies that the tunnel fan exhaust is mixing and dissipating more quickly. It should be noted that at the exits the lift fans have an annular exit area which tends to coalesce downstream while the lift/cruise fan exhaust has started mixing in the deflection hood.

The four lift fans for the plate Model 1 (Figures 18 to 21) when compared to the tunnel Model 1 lift fan (Figure 22) show a similar higher boundary shear due to the high exit velocity near the edge. Similarly this would indicate that for Model 1 the plate fans would not tend to mix as quickly with ambient air as would the tunnel fans.

The plate Model 2 ejector representing the 90° deflected cruise fan shows a flat exit velocity (pressure) profile (Figure 25). This results in a high velocity at the edge of the jet creating a large velocity shear which persisted a large distance from the exit before mixing with the ambient air. The tunnel Model 2 lift/cruise fan shows a lower pressure profile gradient (Figure 23) indicating earlier mixing.

The lift ejectors (with centerbodies) show profiles (Figures 26 and 27) which are very similar to the tunnel Model 2 lift fan (Figure 24). The velocity peaks and profile gradient comparisons indicate the ejectors should produce mixing very much like the tunnel Model 2 lift fan.

Since the cruise engines of tunnel Model 3 used the same ejector units but with a 90° extension to the nozzle it was assumed that the plate and tunnel Model 3 engine exit profiles would be similar. When the tunnel Model 3 tests were made previously, exit profiles were not taken.

The lift engine for tunnel Model 3 used the same type of ejector unit used in the plate model. Therefore, the lift engine should produce the same mixing characteristics (Figure 25).

Analysis of dynamic pressure decay. The dynamic pressure decay curves (Figures 28 to 36) show the ratio of the average and the maximum dynamic pressure q_h at each rake position downstream to the exit dynamic pressure q_e as a function of the downstream position. Average q decays for one of the plate Model 1 fans (8-blade with sleeve) presented in Figure 28 indicates a difference between the decay curve based on the data as taken, and the data corrected to an assumed spread angle. This is expected, since for the lower curve the assumption of the spread angle includes additional area at a lower q which decreases the average value. Far downstream, where the difference between the curves is greater, the magnitude of the average q (hence pressure) approaches the accuracy of the pressure transducer. However, the trends of the curves are consistent and the

differences are felt to be significant for comparison with other results. Therefore, the data for all plate Model 1 fans have been corrected to a half angle spread of 3.5°. The results are plotted for the two definitions of dynamic pressure decay based on maximum dynamic pressure and average dynamic pressure.

The q decay curves (Figures 29 to 32) for engines from plate Models 1 and 2 and from tunnel Models 1 and 2 indicate there is some change due to varying the thrust level, but it is small. The differences between the maximum and average q decay definitions can also be seen for the different types of engines. The average q decay for all engines tends to be very steep initially, then continues with a decreasing magnitude slope. The ejector q decays (Figure 31) maintain a high peak value much farther downstream, then drop off at a slope less steep than the initial slope for the fans. The maximum decay for the ejectors follows the pattern of the high pressure air nozzles of reference [1].

While thrust effects are small and in most cases are negligible, wherever possible comparisons of plate and tunnel engines have been made for equivalent thrusts based on the scaled thrust of each model. This was obtained by matching the thrusts with a planform loading parameter S/T. The plate and tunnel Model 1 cruise fans are seen to correlate slightly better for the average q decay parameter than for the max q decay (Figure 33). This trend (Figure 34) is also true for the different lift fans of plate and tunnel Model 1. The Model 2 cruise engines indicate a large difference in q decay (Figure 35) between the fans and the original ejector configuration, but the correlation is better for the average q decay definition than for the maximum q decay. It should be noted that the tunnel Model 2 lift fan and the ejectors with centerbody, which show the most similar average decay correlation and maximum q decay correlation (Figure 36), also show the closest correlation of efflux profiles.

Model Hover Characteristics

The model characteristics (forces and moments) will first be examined in terms of the thrust effects. Several aspects of the testing procedure and the effects of certain parameters will be examined along with the verification of several assumptions made previously. Comparisons will then be made between the tunnel models and the plate models to determine the accuracy of the plate model representations.

Thrust effects and procedural verification. The effects of thrust level for each flat plate model and tunnel Models 1 and 2 are presented in Figures 37 to 49 for non-dimensional induced lift, induced pitching moment, and induced rolling moment versus ground height. There is a large amount of scatter attributable to the model vibrations caused by the turbulent flow for both plate and contour Model 1 data (Figures 37 and 38). As a result, in order to simplify comparisons the curves were faired through the numerical average of the three thrusts taken for each height and model orientation for all models. Where thrust averaging was used, the results have been referred to as thrust averaged data. In all other cases, the results are actual data points.

Tests were conducted to determine the effectiveness of using dashpots to filter out the high frequency turbulent flow vibrations observed for Model 1. Comparison of induced lift with and without dashpots (Figure 39) for plate Model 1 indicates a small decrease in the data scatter for dashpots mounted on the wingtips. Of equal importance is whether the dashpots affected the forces or moments. The peak values of about 6.5 percent of thrust compare favorably, as well as the minimum of -1 percent at h/De of 0.85, with and without dashpots. Comparing the induced pitching moment with and without dashpots (Figure 40) shows the dashpot curve minimum and maximum points occurring at the same location below h/De of 3. The rolling moment results (Figure 41) support the conclusion that the dashpots have no appreciable effect on the forces. However, the small reductions in scatter

indicate a need to match the dashpot damping characteristics more closely to each model.

A second factor to be considered was the sealing of the gap (Figures 4 and 8) between the engine simulators and plates by taping dental dam loosely between both surfaces. The effects of dental dam on induced lift, pitching moment, and rolling moment are included in Figures 39 to 41. The induced lift curve (Figure 39) peak of 6.5 percent and minimum of 0.5 percent indicate a negligible change in lift due to the gaps around the fan cowls. The induced pitching moment (Figure 40) and induced rolling moment (Figure 41) show little effect due to the dental dam. At h/De of 0.85, the dental dam was stretched and may have influenced the induced pitching moment (Figure 40).

Another variable examined (Figure 42) was the wing height on plate Model 1. The wing for plate Model 1 was about 36 percent of the total planform area. The three symbols represent thrust averaged data for the respective configurations. Although the magnitudes of maximum induced lift for the three wing heights are about the same, 6 to 7 percent of thrust, the peaks do not coincide at a given height. For the high wing, the peak is at h/De of 2.75; for the mid wing (where test program data were taken) the peak is at an h/De of 2; and for the low wing, the peak is at an h/De of 3.5. These results show that both the fountain and wall jet effects influence the low wing configuration at a higher height than for the high wing. For Model 1 where the wing area is 36 percent of the total planform, the mid wing receives more positive induced lift than the high wing, but less negative induced lift closer to the ground than for the low wing.

Plate Model 2 was tested keeping in mind the indicated trends and lessons learned from the difficulties encountered with Model 1. The resultant forces and moments (Figure 43) show much less scatter and information was obtained over a larger height range. Variation of thrust for this model is shown to have no appreciable effect.

Induced loads (Figures 44 and 45) of plate Model 3, where dashpots were again used, indicate that the results show no effect due to thrust variation. It is interesting to note the variation of the induced lift curve for Model 3 (fighter configuration) as compared to the transport Models 1 and 2. The lower lift forces obtained in the h/De range between 2 and 6 (Figure 44) indicate a weaker fountain formed by the three jets when compared to the fountain formed by the 6-fan configuration (Figures 37 and 43).

The induced loads for tunnel Models 1 and 2 are presented in Figures 46 to 49. The measured lift force included the thrust, which had to be calculated from rpm calibration curves. The induced lift was found by subtracting the thrust from the measured lift. The effect of thrust variation for tunnel Model 1 (Figure 46) is negligible. Some scatter due to flow-induced vibration was produced but the model was heavy enough to decrease the frequency. Similar effects are evident for the tunnel Model 2 results (Figure 47). The induced lift curve for tunnel Model 2 indicates a good deal less lift than might be anticipated from plate Model 2 (Figure 43). One prominent difference of tunnel Model 2 was the outboard cant of the wing pod lift fans due to the 3° dihedral of the wing. In an effort to study this factor more closely, tunnel Model 1, which had thrust deflection louvers for the lift engines, was tested for inward (+10°) and outward (-10°) thrust deflection for comparison with the initial 0° deflection results. A comparison of the thrust averaged data (Figure 48) indicates considerable additional lift loss when the flow is deflected outwards, since this tends to remove the positive influence of the fountain.

An assumption made for Models 1 and 2 with a T-tail was that the tail would not influence hover characteristics. To verify this, tunnel Model 2 was tested with and without the tail. The thrust averaged results presented in Figure 49 indicate that there is no effect on induced lift, pitching moment, or rolling moment due to the T-tail.

Data for tunnel Model 3 can be obtained in reference [3].

Comparison of plate and tunnel model results. A comparison of results for plate and tunnel models is presented in Figures 50 to 57 as thrust averaged data. For the flat-plate models, the height parameter h/De was referenced to the center of gravity location on the bottom plate surface. Tunnel Models 1 and 2 were originally referenced to the center of gravity of the models while the balsa wood contour of Model 1 and tunnel Model 3 were referenced to the bottom of the fuselage. For consistency, all of the three-dimensional models were referenced to the fuselage surface below the center of gravity. For the pitch and roll orientations, the height was measured from the bottom of the model below the center of gravity to the ground, perpendicular to the axes of the model. An apparent shift in the induced lift curves along the h/De axis was noted between the plate and tunnel models (Figures 50, 53, and 56). In an effort to correlate these results for an equivalent h/De it was necessary to find $\Delta h/De$ for which the plate results would coincide with the three-dimensional model data (Sketch A).

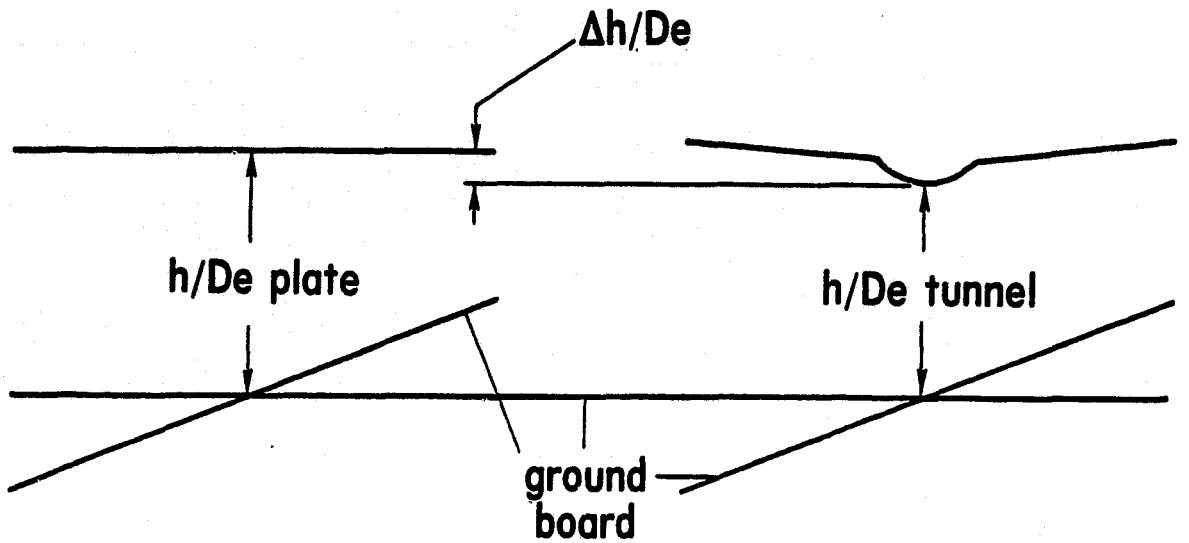

Sketch A

For

$$h/De)_{tunnel} = h/De)_{plate} - \Delta h/De \qquad (1)$$

the following definition was used:

$$\Delta h/De = \frac{\sum h_j S_j}{\sum S_j}\left(\frac{1}{De}\right) \qquad (2)$$

The planform of each three-dimensional model was divided into areas denoted by the subscript j. The height h_j was defined as the median distance of each area S_j above the bottom of the fuselage. The data presented in Figures 50 to 57 has incorporated the correction for $\Delta h/De$ for each model. Table III lists the final geometric correction factors h/De for each of the three configurations tested.

The thrust averaged data for Model 1 is presented in Figures 50 to 52 for the level attitude, +10° pitch, and +10° roll, respectively. For the level attitude, the tunnel model shows small (3 to 4 percent) lift increments (Figure 50) over the plate and contour data for h/De below 0.5 and above 2.5. At h/De of 2.5, the plate data does not correspond as well to the tunnel data as does the low wing data of Figure 42. This would indicate that the mid wing was not an appropriate representation. For the model at a +10° pitch angle and below h/De of 1.5, the induced lift curve (Figure 51) indicates a weaker flow influence for the inclined models, with the plate model gaining a slightly larger positive induced lift. The induced pitch for the tunnel model shows a nondimensional increment of 6 percent, possibly due to an axisymmetry of the initial thrust setting about the pitch axis. For +10° roll the maximum h/De of the tunnel model is 2 (Figure 52). However, for the short overlap, the induced pitch and lift curves agree. There is a noticeable difference in the induced rolling moment curve for the tunnel model and there is

not enough information available to explain its occurrence. However, the 4° dihedral of the tunnel model should be considered when comparisons are made with the flat plate model.

The thrust averaged data for Model 2 is presented in Figures 53 to 55. The induced lift for all model attitudes exhibits similarly shaped curves and maximum and minimum lift at similar heights for plate and tunnel models. However, the tunnel model data is below that of the plate model by a factor of 10 percent of thrust. This is due primarily to the increased lift loss caused the outward lift-thrust deflection, a trend indicated by results of Figure 48. The effect cannot be directly correlated since tunnel Model 2 did not have variable louver deflection capability.

The plate results (Figure 53) show a peak rolling moment at an h/De of 3. Since the plate was parallel to the ground this was unexpected. Use of tufts for flow-visualization showed that the engine arrangement for this model produced a flow pattern indicating a very intense centerline fountain. It should be noted that four of the six engines were outboard and aligned on axes parallel to the centerline of the model, which apparently caused the centerline ridge of the fountain to impinge along the centerline axis of the model. As a result small changes in symmetry between the engines, or a slight geometrical asymmetry of the model, caused the plate to roll violently, since the unstable condition would be reinforced by the additional flow to the deflected side. For the tunnel model, the fountain influence appeared to be less intense, but the rolling moment asymmetry is observed.

For the models at a +10° pitch angle the lift curves (Figure 54) show different trends at low h/De (less than 2).

The thrust averaged data for Model 3 is presented in Figures 56 and 57. Comparisons have only been made for the level model orientation because tunnel models tests with the circular ejector nozzles were only obtained for this configuration. In the region

of maximum fountain influence h/De of 1 to 4 the corrected plate data and tunnel model data show excellent correlation (Figure 56).

The major variation in pitching moment (Figure 57) below h/De of 4 may be due to suckdown on the plate model tail since for this test the tunnel model had a T tail. This would indicate that the presence of the tail on the plate model was an inappropriate representation. The plate Model 3 results indicate a variation in rolling moment for this model similar to that for Model 2.

Effect of Engine Characteristics on Model Characteristics

Out of ground effect. An attempt was made to determine the applicability of the out of ground effect hovering lift loss parameter of Gentry and Margason [1] to the data obtained during the present test. For the out of ground effect case the plate models were tested with the ground board removed so that the nearest interference was caused by the ceiling of the model preparation area, about 20 feet above the model. The maximum elevation for the tunnel models was about 4 feet as the sting systems were arranged so that the models could go down to the floor of the test section. For Models 1, 2, and 3, the maximum plate h/De were about 15, 20, and 60, respectively. Therefore, it appears that the models may not have been completely out of ground effect for any of the three tunnel models tested, thus the correlation results shown in Figure 58 were only applied to the plate model data. For plate Model 1 the induced lift loss was positive and could not be included in Figure 58. The q decay results (Figure 29) were obtained for the 8-blade fan and applied to the contour Model 1 hover results, which were negative out of ground effect. The Model 2 plate data used the q decay information from Figure 36, since 4 of the 6 ejectors were of the configuration with centerbodies. For plate Model 3 all of the ejectors were without centerbodies so that Figure 31 was a good representation of the q decay characteristics. The data

points (Figure 58) for Models 2 and 3 when plotted against the line representing the fairing for the correlations of Gentry and Margason show very good agreement. Model 1 data (Figure 58), however, does not correlate well with this parameter. It should be noted that plate models which use simulators with efflux characteristics similar to those of the tunnel models engines produced good correlation with reference [1], while those engines which did not have similar efflux characteristics between plate and tunnel model engines did not produce a good correlation of force data with reference [1].

In ground effect. All of the induced lift data for level model orientation for Models 1, 2, and 3 in ground effect are shown in Figure 59. The data for the plate and tunnel models were examined in view of the correlations of their respective engine efflux characteristics. Plate and contour Models 1 used the same fans while tunnel Model 1 used a different type of fan. As noted previously, these two types of fan produced dissimilar efflux characteristics but the three induced lift curves for Model 1 correlate well. Plate and tunnel Model 3 used the same ejectors with nozzle variations as discussed previously. The induced lift curves for Model 3 showed excellent correlation. The best correlation of efflux characteristics was for the lift engines of Model 2. The induced lift curves for Model 2 do not coincide; however, the difference in lift engine deflection for the plate and tunnel models was shown to be a critical parameter. Based on Models 1 and 3, it appears that for a number of different types of engine simulators with varying efflux characteristics, the overall results for plate and three-dimensional models were similar and within 2 percent of thrust in the region where the fountain between engines is the predominant effect on lift loss. These results imply that the lift losses obtained in ground effect are essentially independent of the correlations of efflux characteristics for the engine simulators.

CONCLUSIONS

An investigation of VTOL aircraft lift losses in hover has been conducted with the following conclusions. Attempts were made to correlate the out of ground effect results for the plate Models with the empirical expression for calculating jet induced loads. This was successful for the models which used engine simulators producing efflux characteristics similar to the three-dimensional model engines. Data for the model using engine simulators with characteristics unlike those of the three-dimensional model engines could not be correlated in this manner.

In ground effect comparisons of induced lift loads indicated correlations between the plate and three-dimensional models were within 2 percent of thrust in the height range dominated by the fountain effect. However, small outward deflection of the lift engine exhaust was found to cause a decrease in beneficial fountain on the order of 5 to 10 percent of thrust. The engine arrangement of Model 2 showed a strong adverse effect on lift loss due to engine deflection. Dashpots proved useful in eliminating data scatter caused by flow-induced model vibration. Data obtained for the plate models could be correlated to three-dimensional results by the application of a geometrical equivalent height correction factor $\Delta h/D_e$. The correlation of plate and tunnel models indicated that lift losses obtained in ground effect were essentially independent of the efflux characteristics for the engine simulator.

Use of flat plate models can be expected to yield reasonable results for most spread-jet VTOL models in hover. However, the best results will be obtained through the ground height range where the impinging fountain between the engines produces the maximum lift increment.

The simplicity of this testing technique makes it a valuable tool to use in parametric investigations. The data obtained in this manner will provide understanding of the physical

processes of thrust induced effects, as well as the characteristics of the particular aircraft configuration being tested.

REFERENCES

1. Gentry, Carl L. and Margason, Richard J.: Jet-Induced Lift Losses on VTOL Configuration Hovering In and Out of Ground Effect. NASA TN D-3166, 1966.

2. Wyatt, L.A.: Static Test of Ground Effect on Planforms Fitted with a Centrally-Located Round Lifting-Jet. Aeronautical Res. Council Current Papers, CP No. 749, 1964.

3. Shumpert, P.K. and Tibbetts, J.G.: Model Test of Jet Induced Lift Effects on a VTOL Aircraft in Hover. NASA CR-1297, 1969.

4. Wooten, W.H. and Hoff, G.E.: Deflected Exhaust Jet Effects on V/STOL Fighter Performance. G.E. Rep. R73AEG279, July 1973.

5. Hoad, Danny R.: Longitudinal Aerodynamic Characteristics of an Externally Blown Flap Powered-Lift Model with Several Propulsive System Simulators. NASA TN D-6760, 1974.

TABLE I

ENGINE SIMULATOR CONFIGURATIONS

Designation	Type	Outside diameter	Inside diameter	Configuration
A	tip reaction fan	15.88 (6.25)	N/A	8 blade without sleeve
A′	↓	15.88 (6.25)	N/A	8 blade with sleeve
B	↓	17.15 (6.75)	N/A	4 blade without sleeve
B′	↓	17.15 (6.75)	N/A	4 blade with sleeve
C	tip turbine fan	13.97 (5.50)	N/A	lift fan with variable exit louvers
D	↓	12.20 (4.80)	N/A	cruise fan with 90° deflector hood
E	↓	13.97 (5.50)	7.49 (2.95)	lift fan with fixed exit louvers
F	ejector	5.08 (2.00)	N/A	original cruise simulator nozzle
G	↓	5.08 (2.00)	2.41 (0.95)	long exit extension and centerbody
G′	↓	5.08 (2.00)	2.41 (0.95)	short exit extension and centerbody

TABLE II

APPLICATION OF ENGINE SIMULATORS

Model / Engine	1	2	3
Plate lift/cruise	A	F	F
Plate lift	A fuselage B wing pod	G rear pod G′ forward pod	F
Contour lift/cruise	A	N/A	N/A
Contour lift	A′ fuselage B′ wing pod	N/A	N/A
Tunnel lift/cruise	D	D	information not available
Tunnel lift	C } fuselage wing pod	E	F

TABLE III

AIRCRAFT THICKNESS CORRECTIONS

Model / Factor	1	2	3
Δh/De	0.421	0.169	1.148

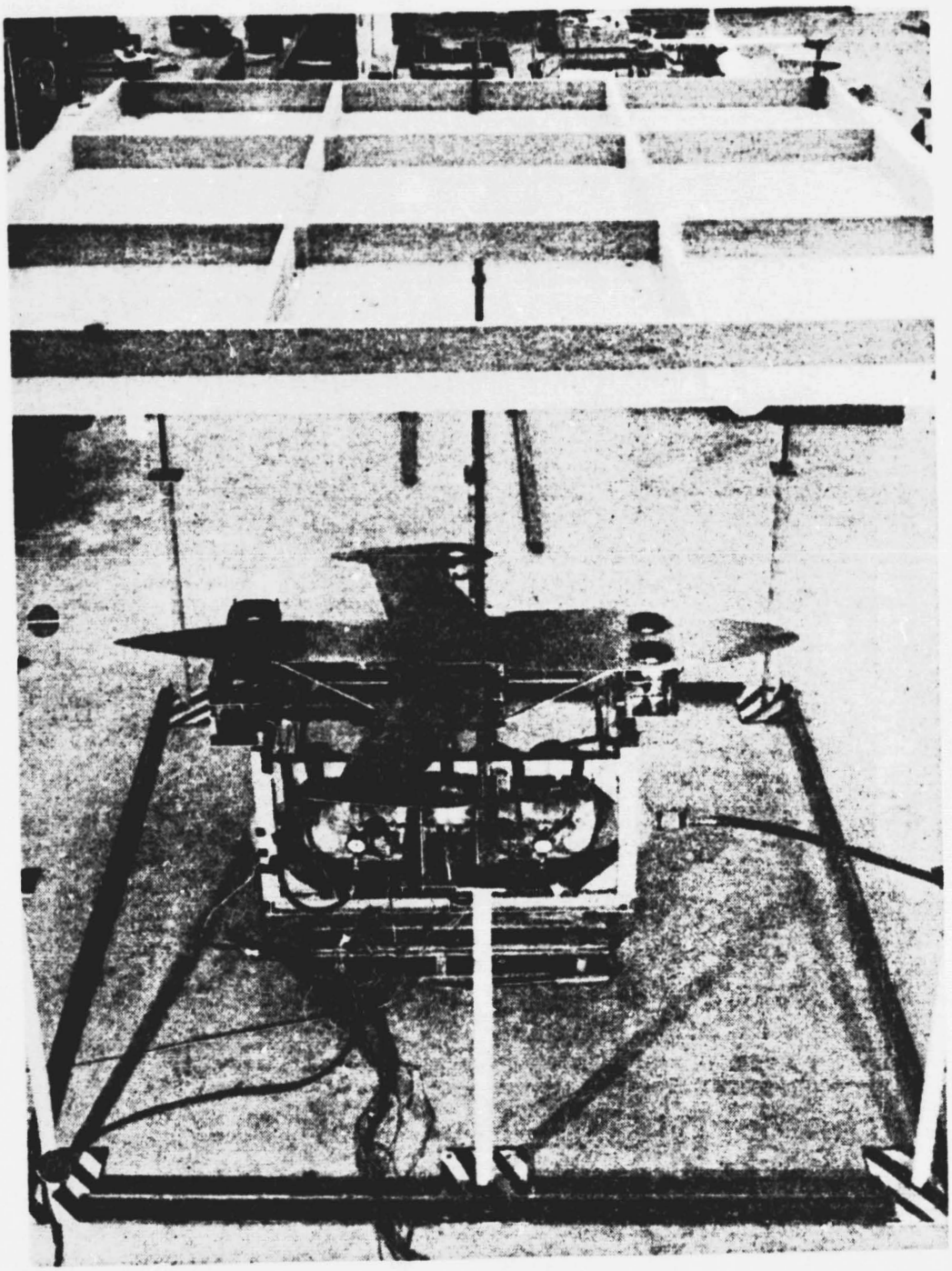

Figure 1. Test rig with plenum chamber and plate model 1 shown beneath the ground board.

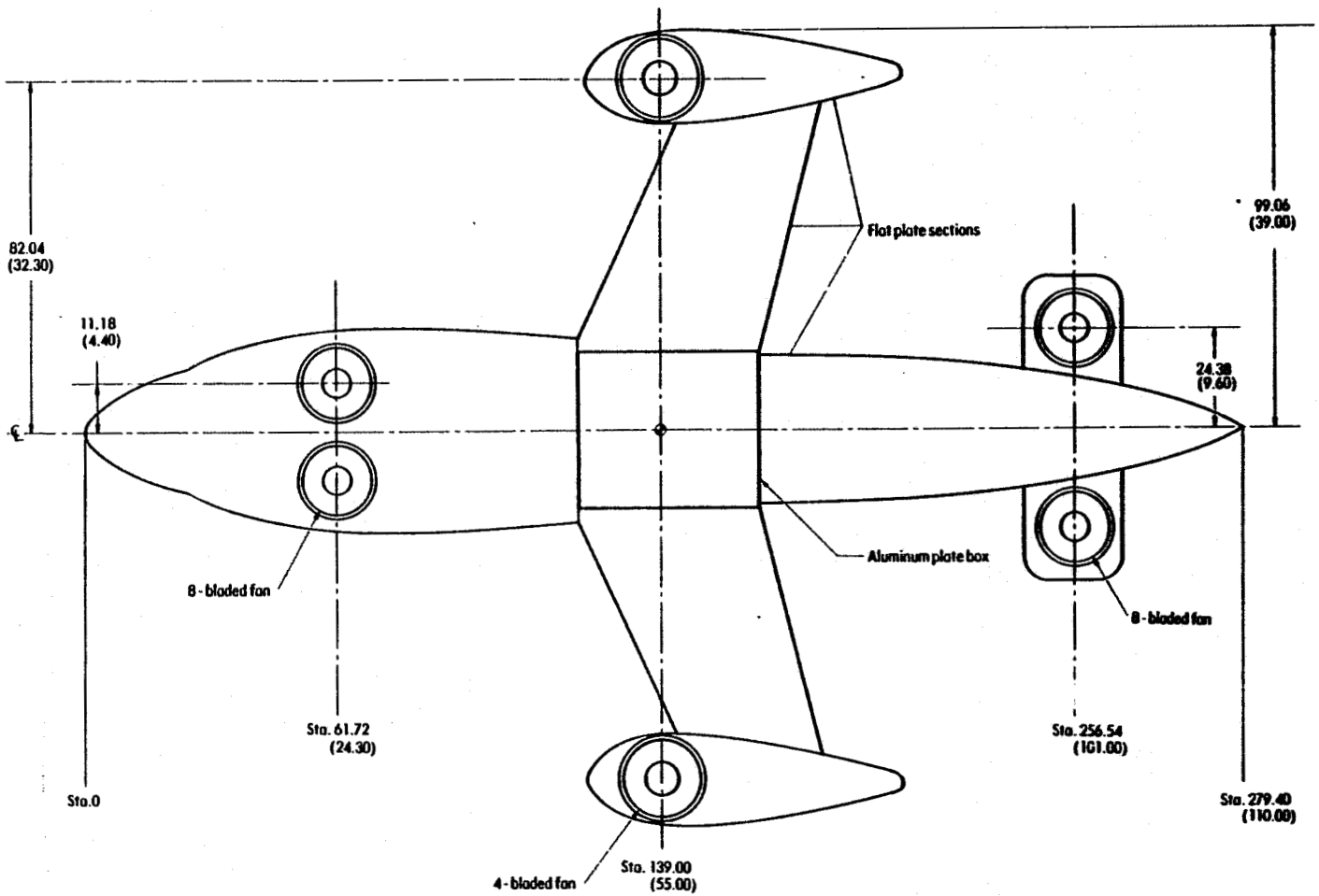

Figure 2. Dimensions of plate model 1 showing fan arrangement. Flat sections are 0.318 (.125) and plate box 0.635 (.250) thick. All dimensions are in cm (in.).

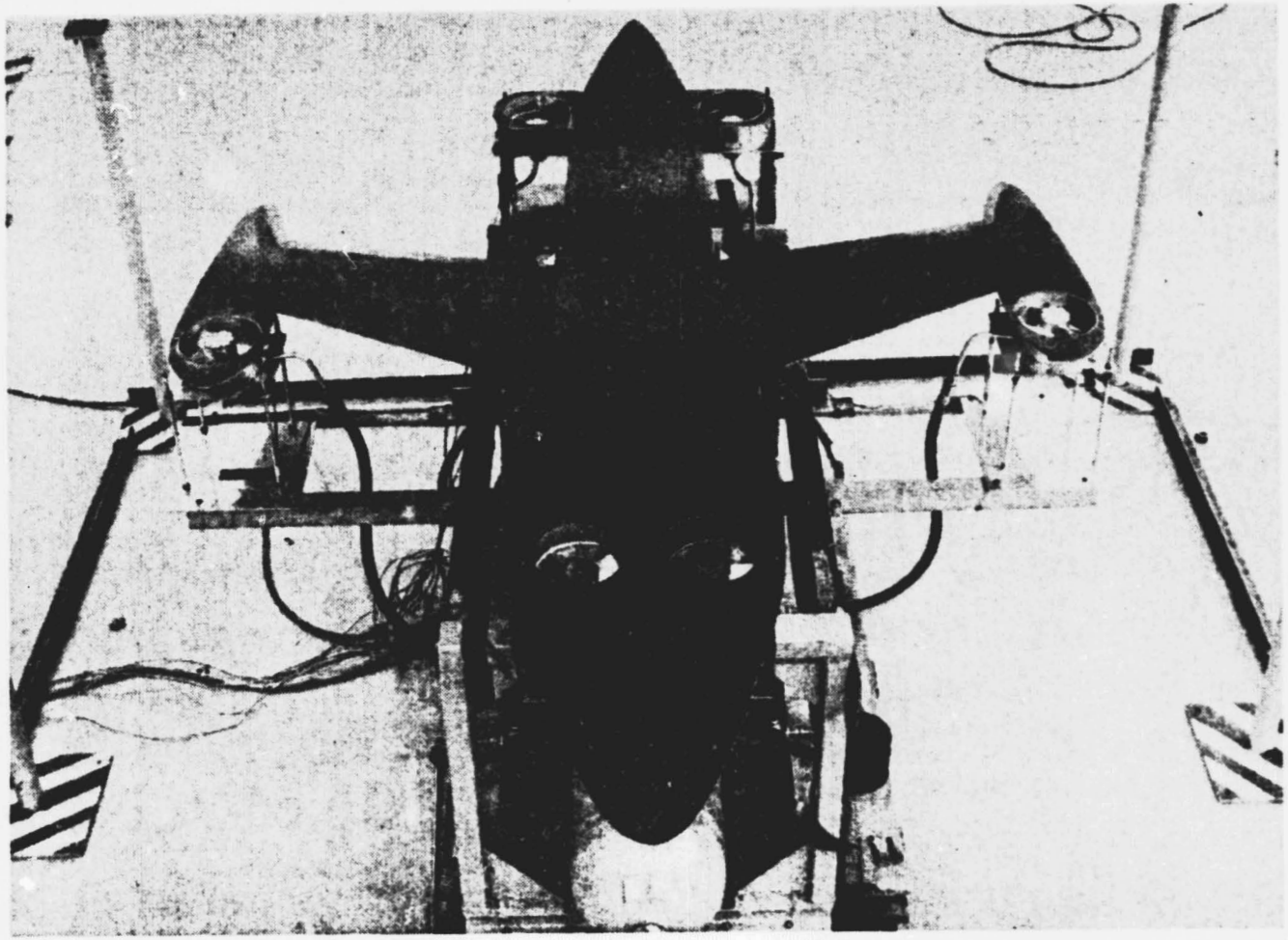

Figure 3. Plate model 1 mounted on the test rig.

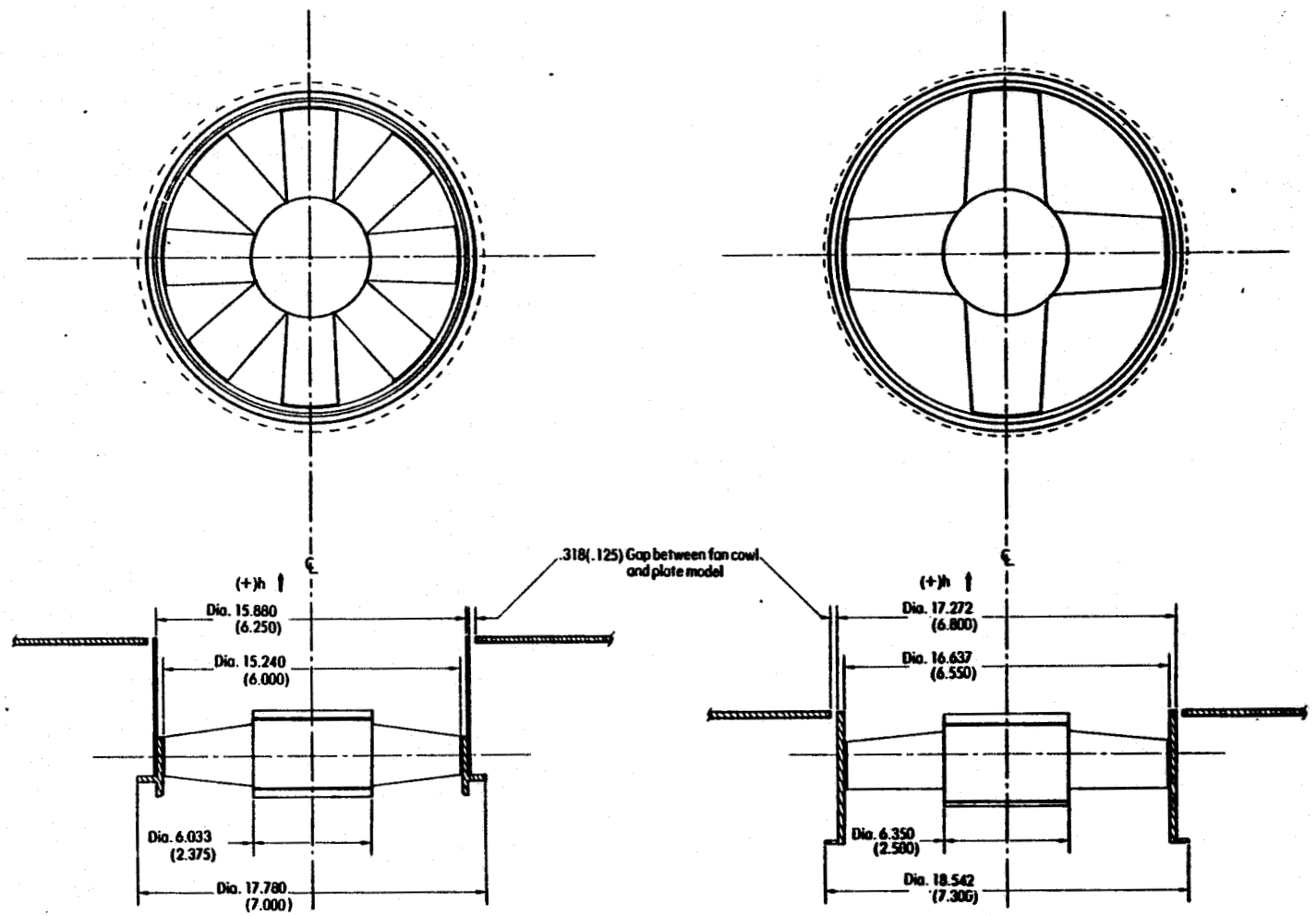

Figure 4. Tip driven fans, 4 and 8 blade shown in the plate model 1 configuration (without sleeve extensions). All dimensions are in cm (in.).

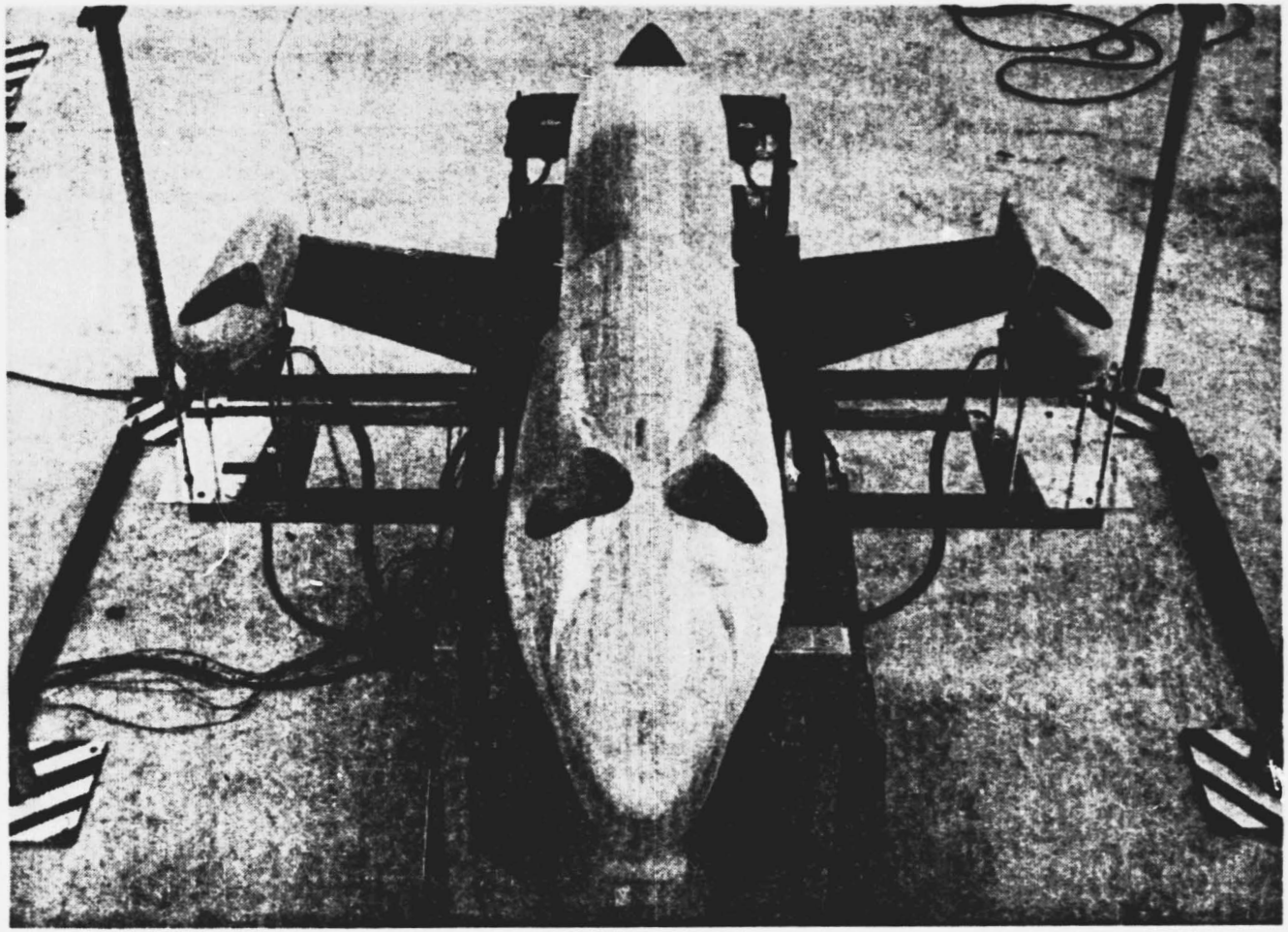

Figure 5. Photograph of balsa wood contour mounted on plate model 1. Shown without extension sleeve.

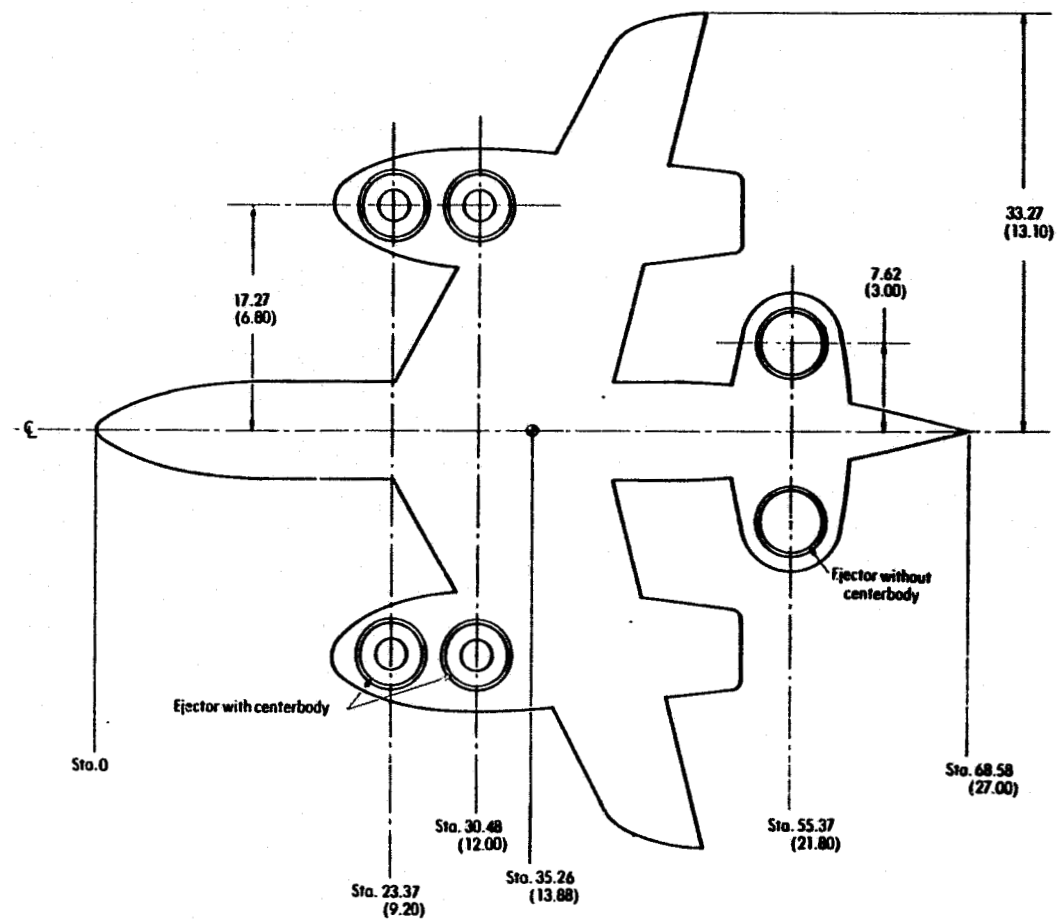

Figure 6. Dimensions of plate model 2 showing ejector arrangement. Plate is 0.318 (.125) thick. All dimensions are in cm (in.).

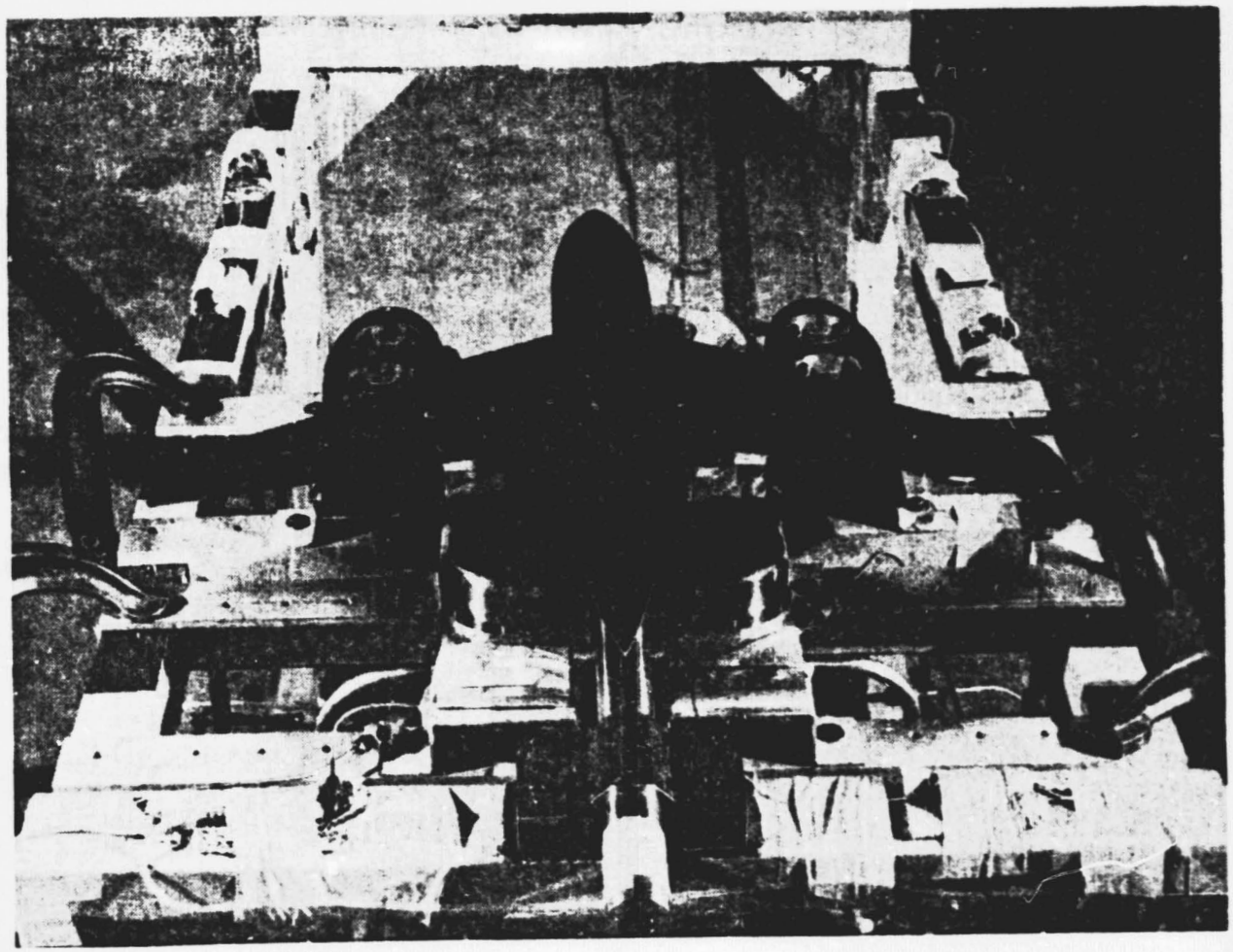

Figure 7. Plate model 2 mounted on the test rig.

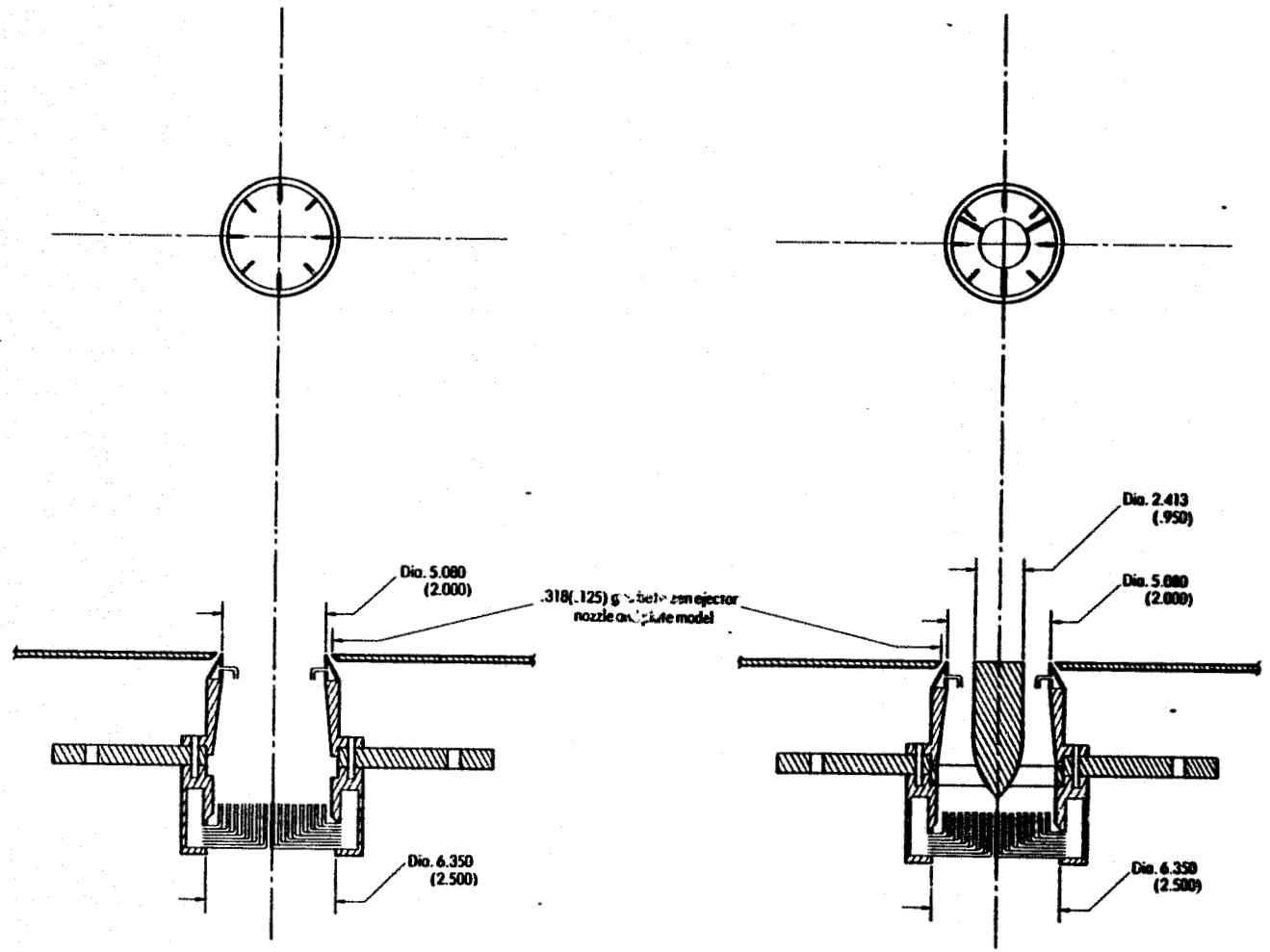

Figure 8. Basic lift engine ejectors of plate models 2 and 3 and fan simulator ejector with centerbody for model 2. All dimensions are in cm (in.).

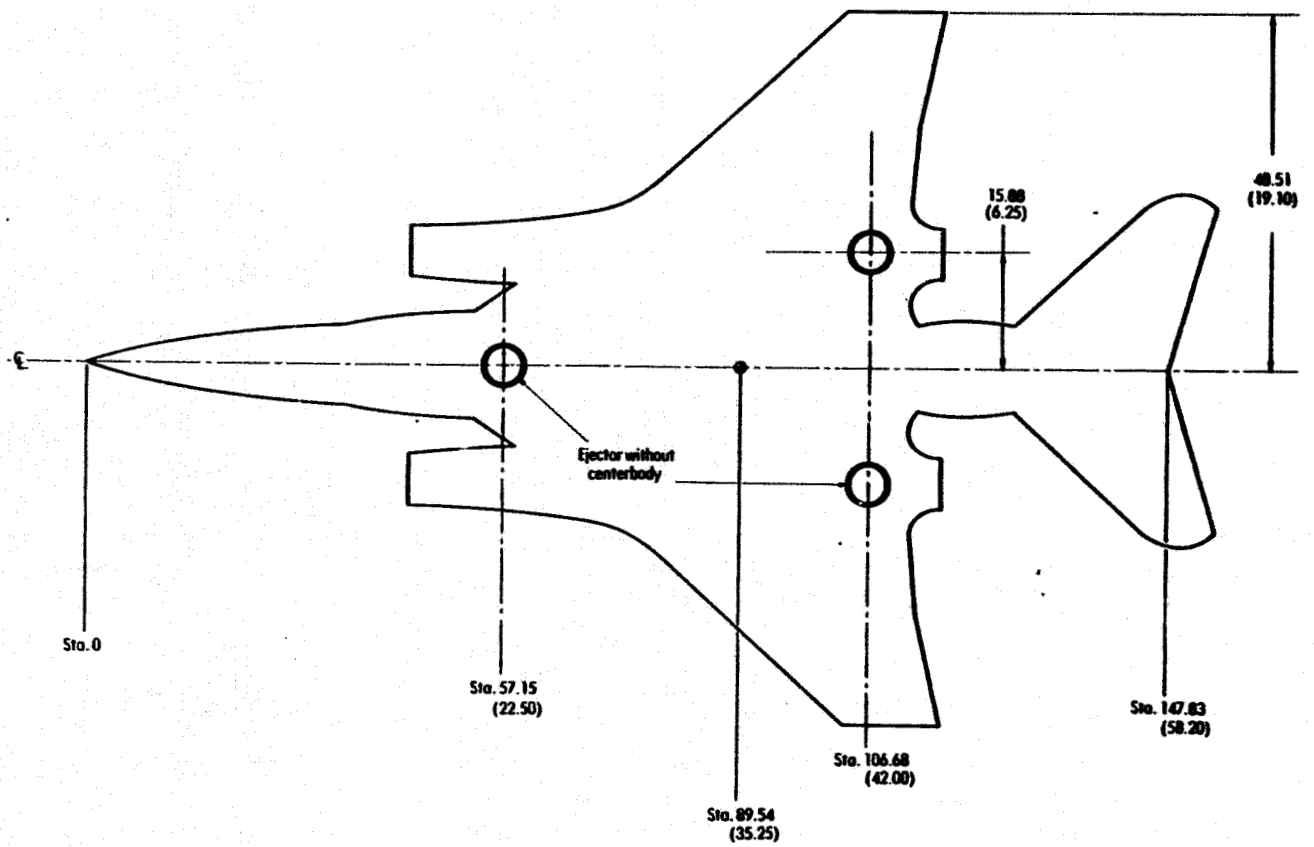

Figure 9. Dimensions of plate model 3 showing ejector arrangement. Plate is 0.952 (.375) thick. All dimensions are in cm (in.).

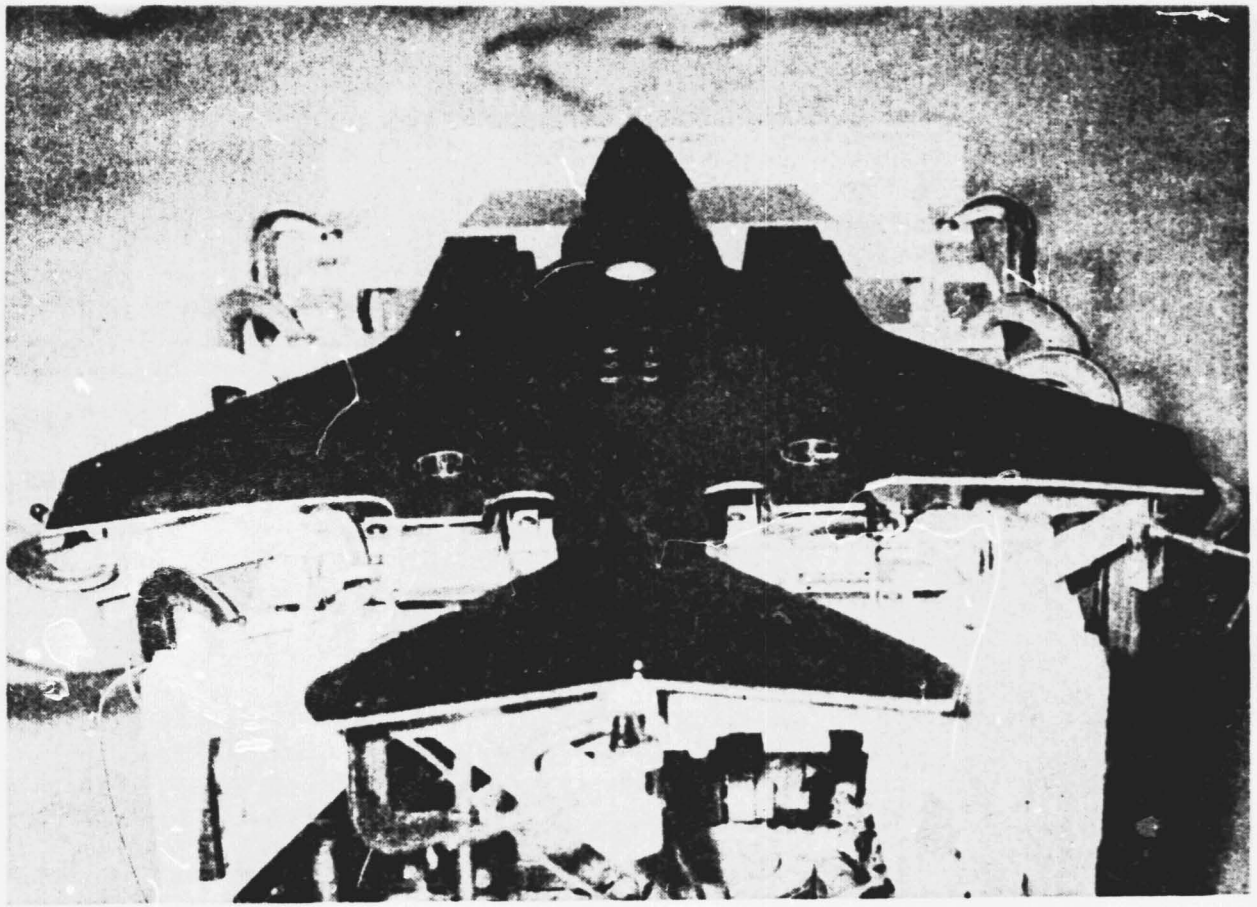

Figure 10. Plate model 3 mounted on the test rig.

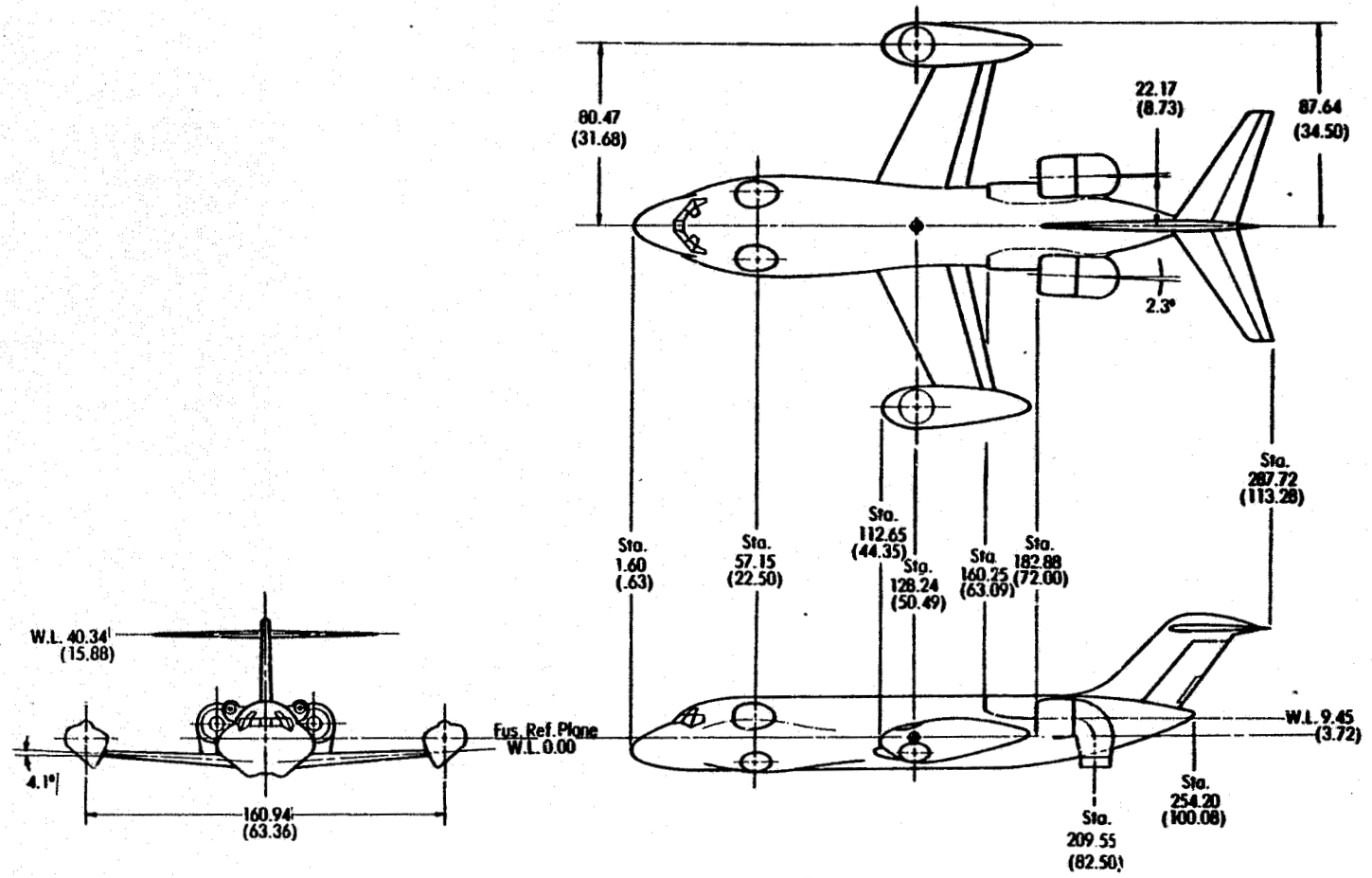

Figure 11. Tunnel model 1 shown in the static hover configuration. $\delta_L = 0°$, $\delta_{LC} = 0°$. All dimensions are in cm (in.).

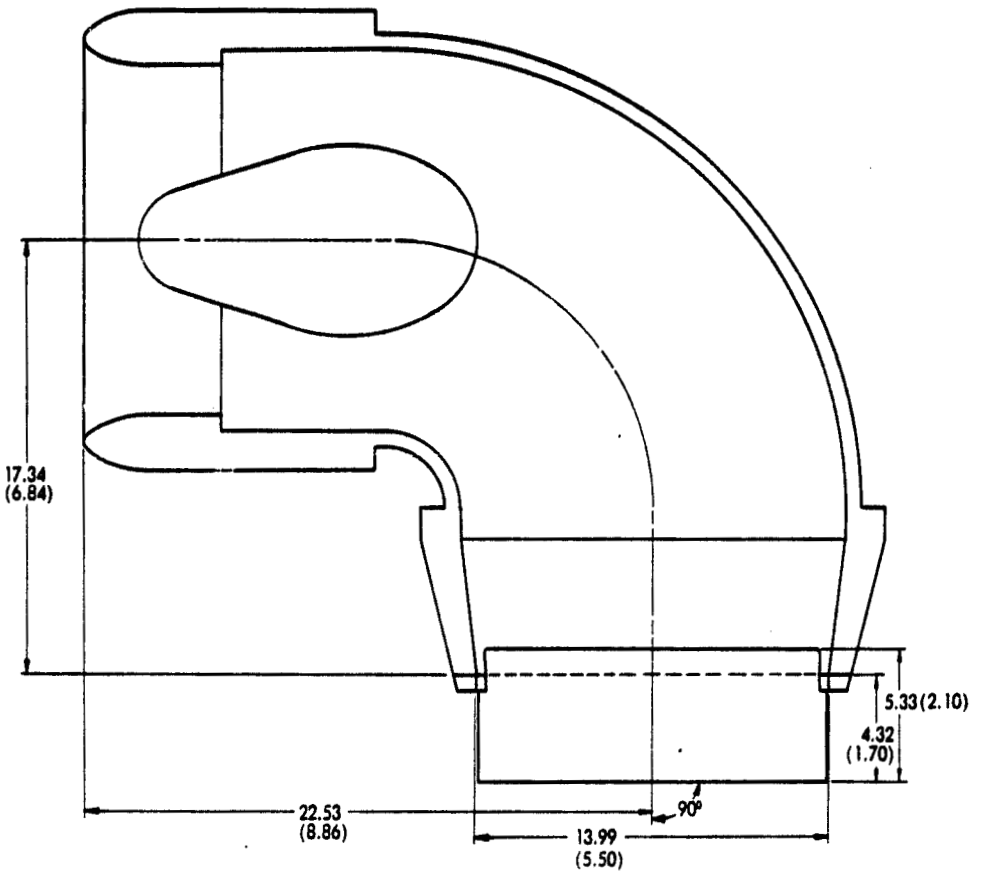

Figure 12. Tunnel model 1 forward fuselage lift fan in the static hover configuration, δ_L = 0°. All dimensions are in cm (in.).

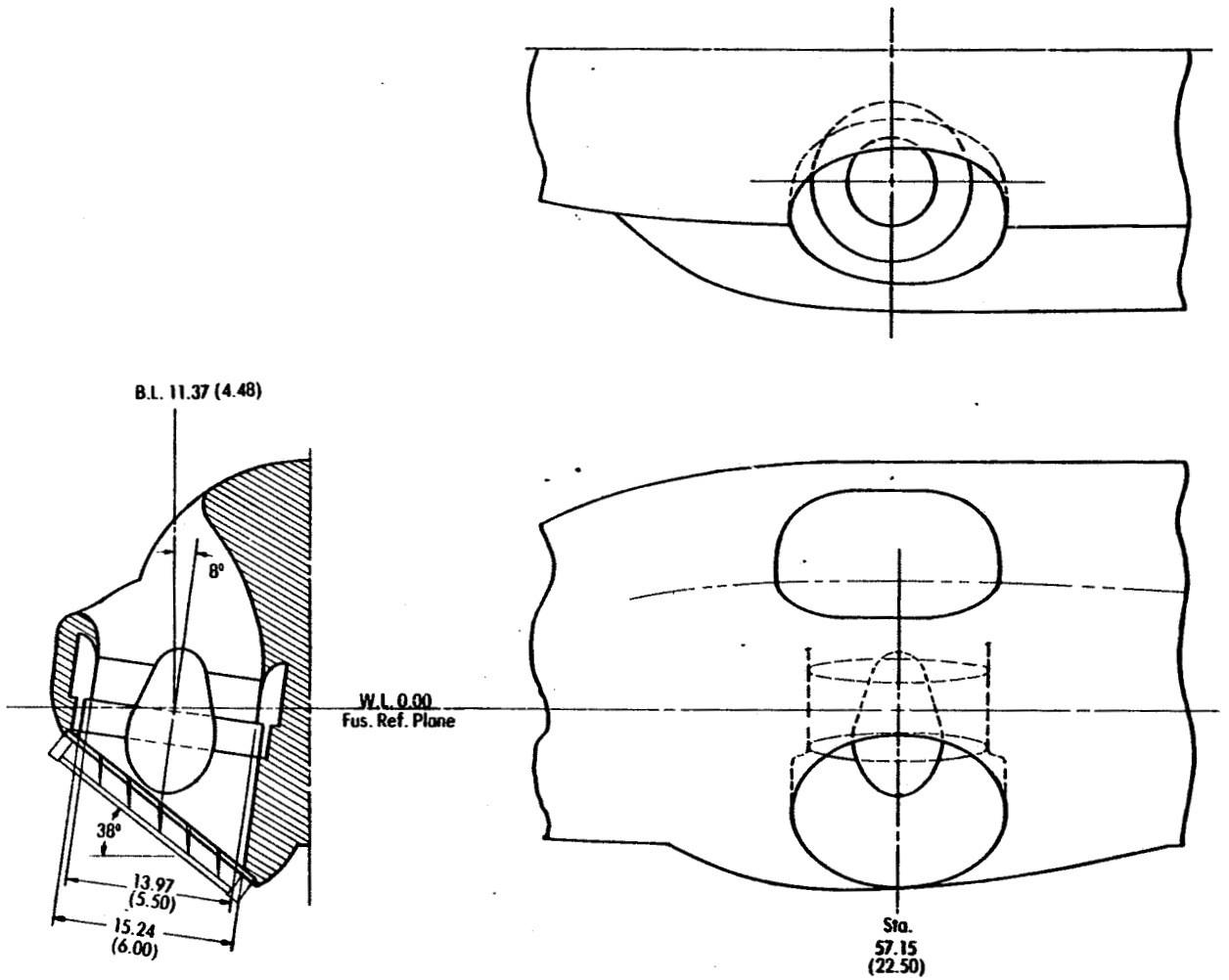

Figure 13. Tunnel model 1 deflected-cruise fan, hood and nozzle in static hover configuration, $\delta_{LC} = 0°$. All dimensions are in cm (in.).

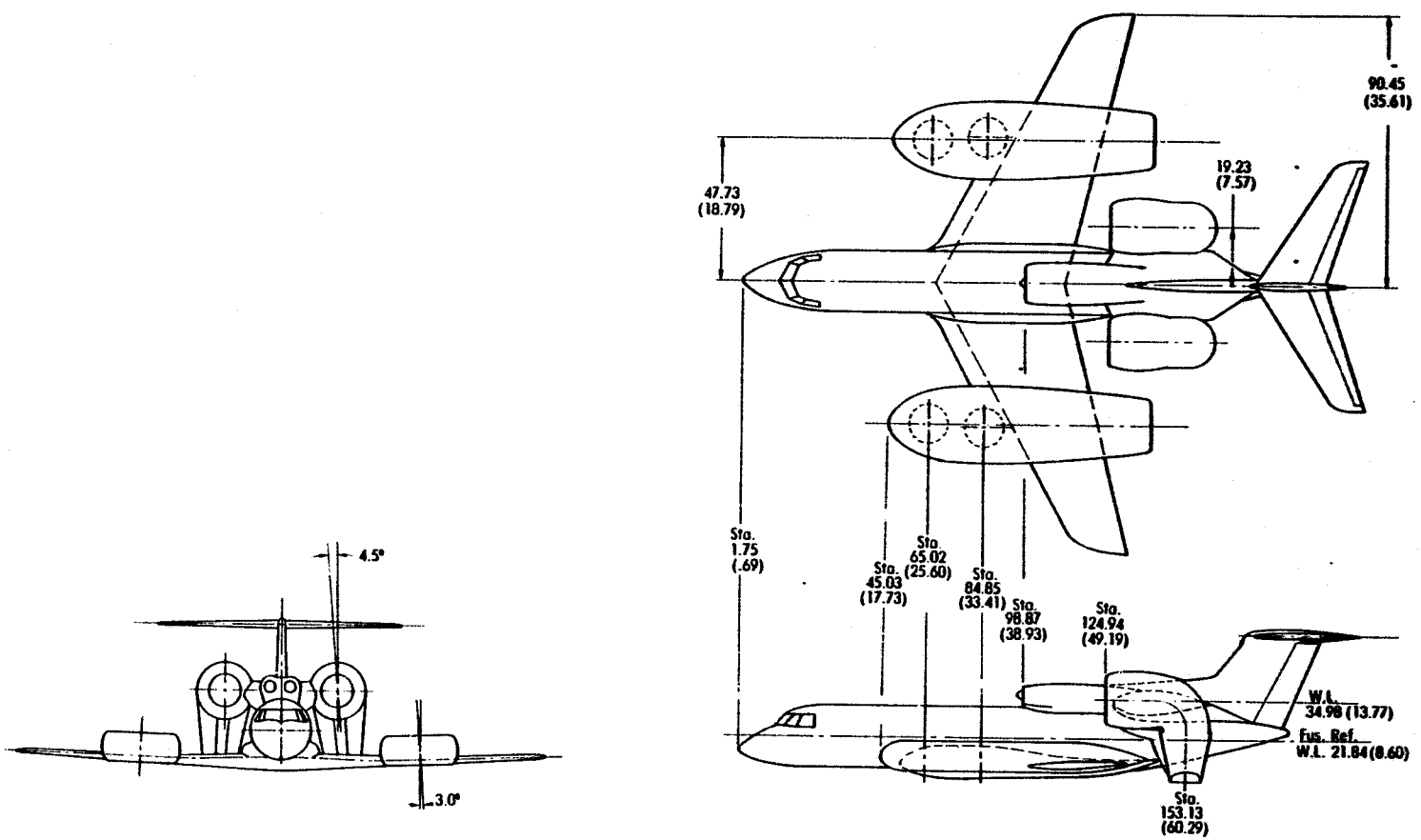

Figure 14. Tunnel model 2 shown in the static hover configuration, $\delta_L = 0°$, $\delta_{LC} = 0°$. All dimensions are in cm (in.).

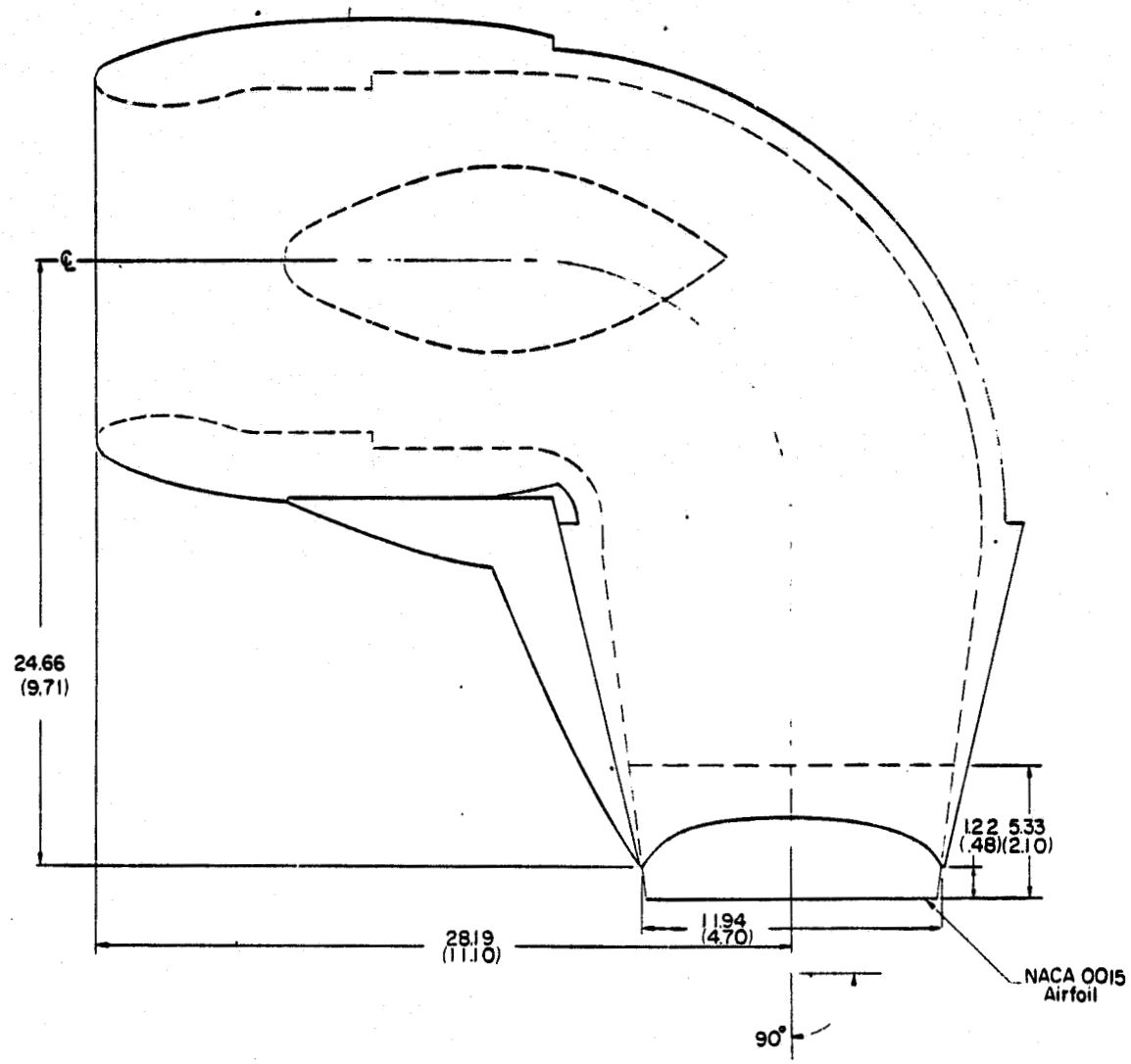

Figure 15. Tunnel model 2 pod lift fan in static hover configuration, $\delta_L = 0°$. All dimensions are in cm (in.).

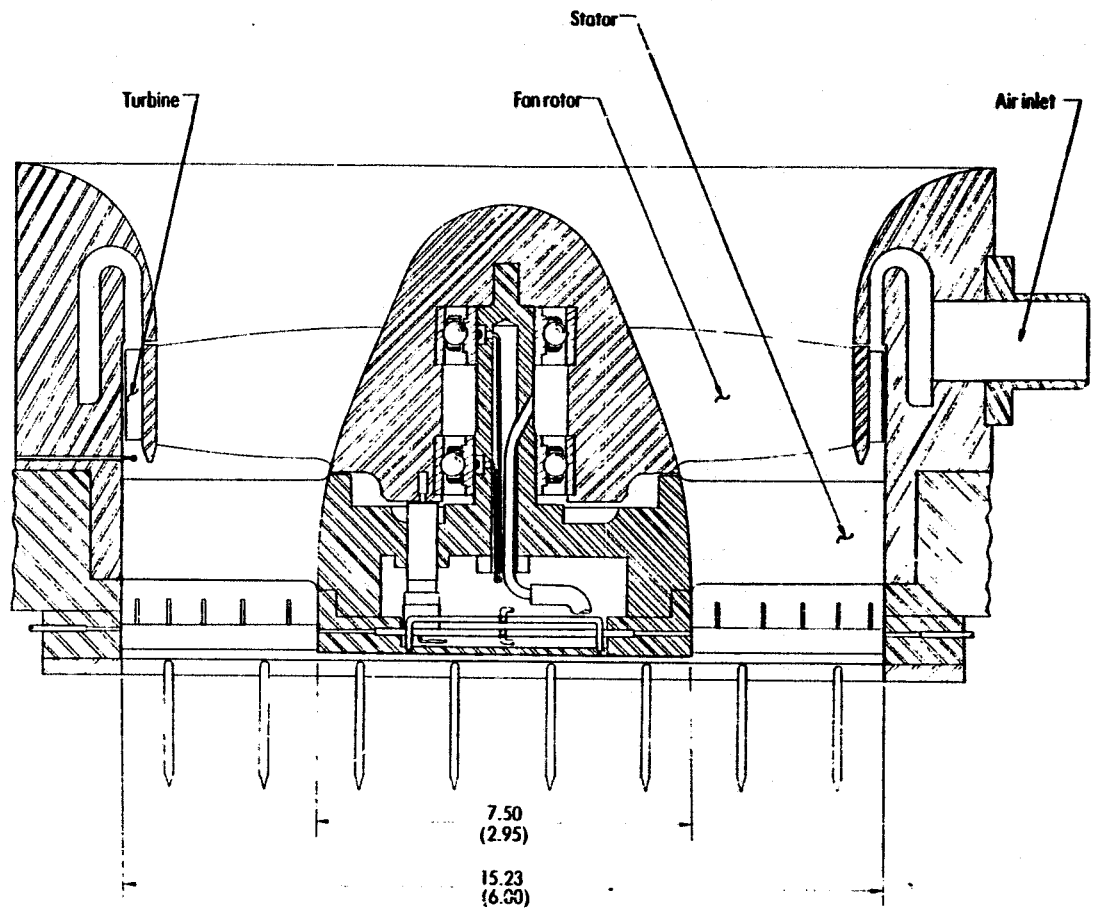

Figure 16. Tunnel model 2 deflected-cruise fan, hood and nozzle in static hover configuration, $\delta_{LC} = 0°$. All dimensions are in cm (in.).

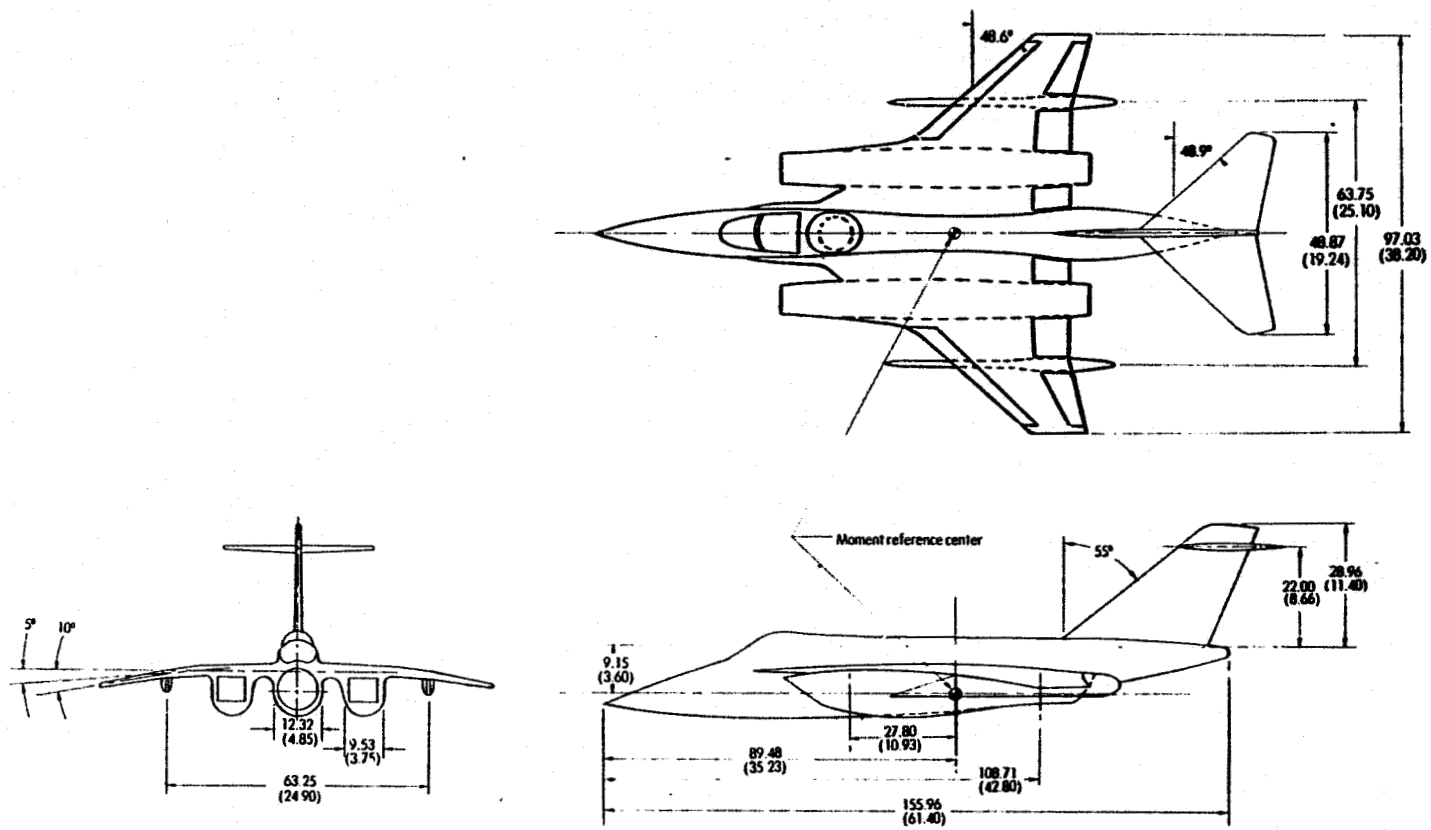

Figure 17. Tunnel model 3 shown in the static hover configuration.

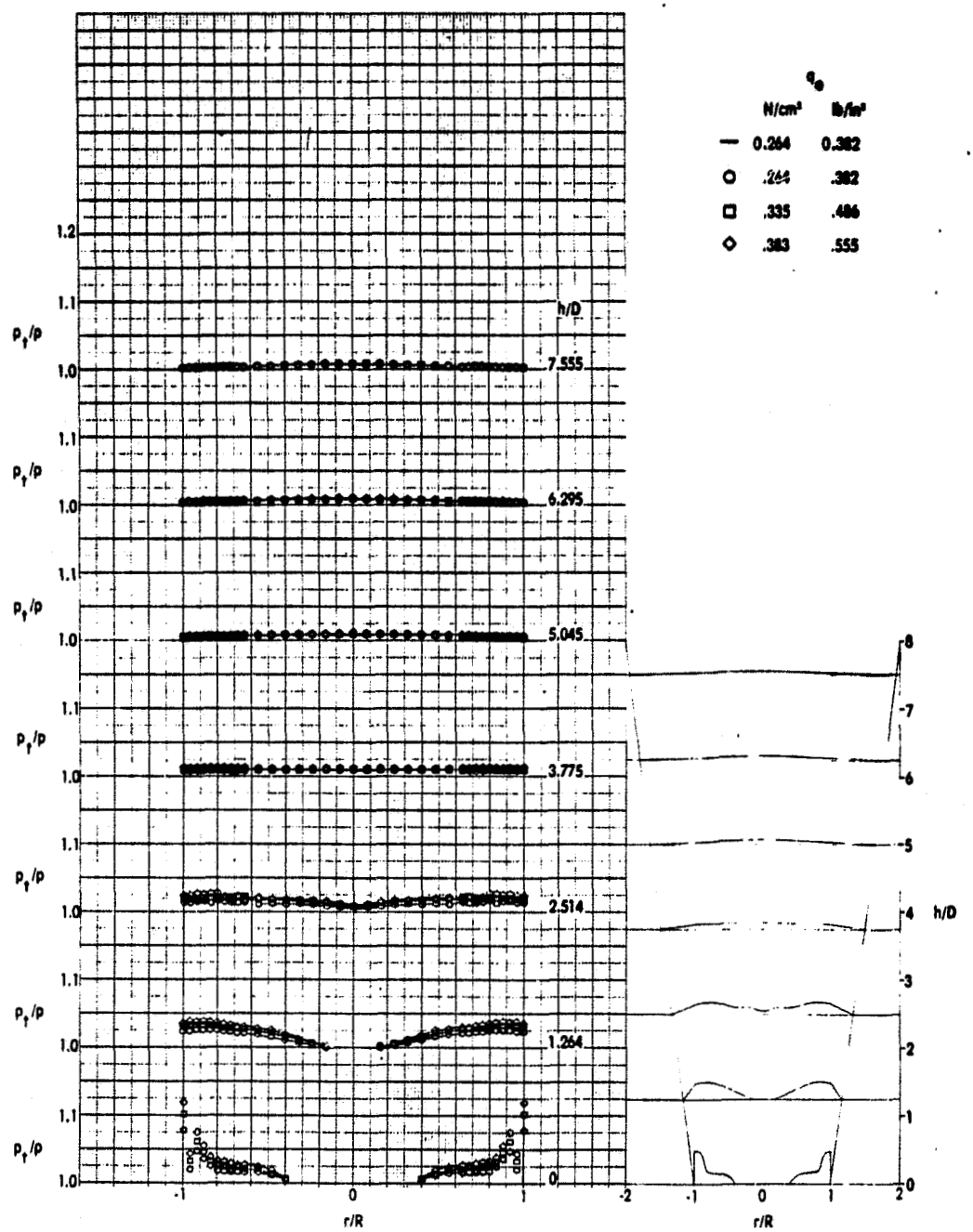

Figure 18. Efflux pressure profiles for plate and contour model 1, Configuration A.

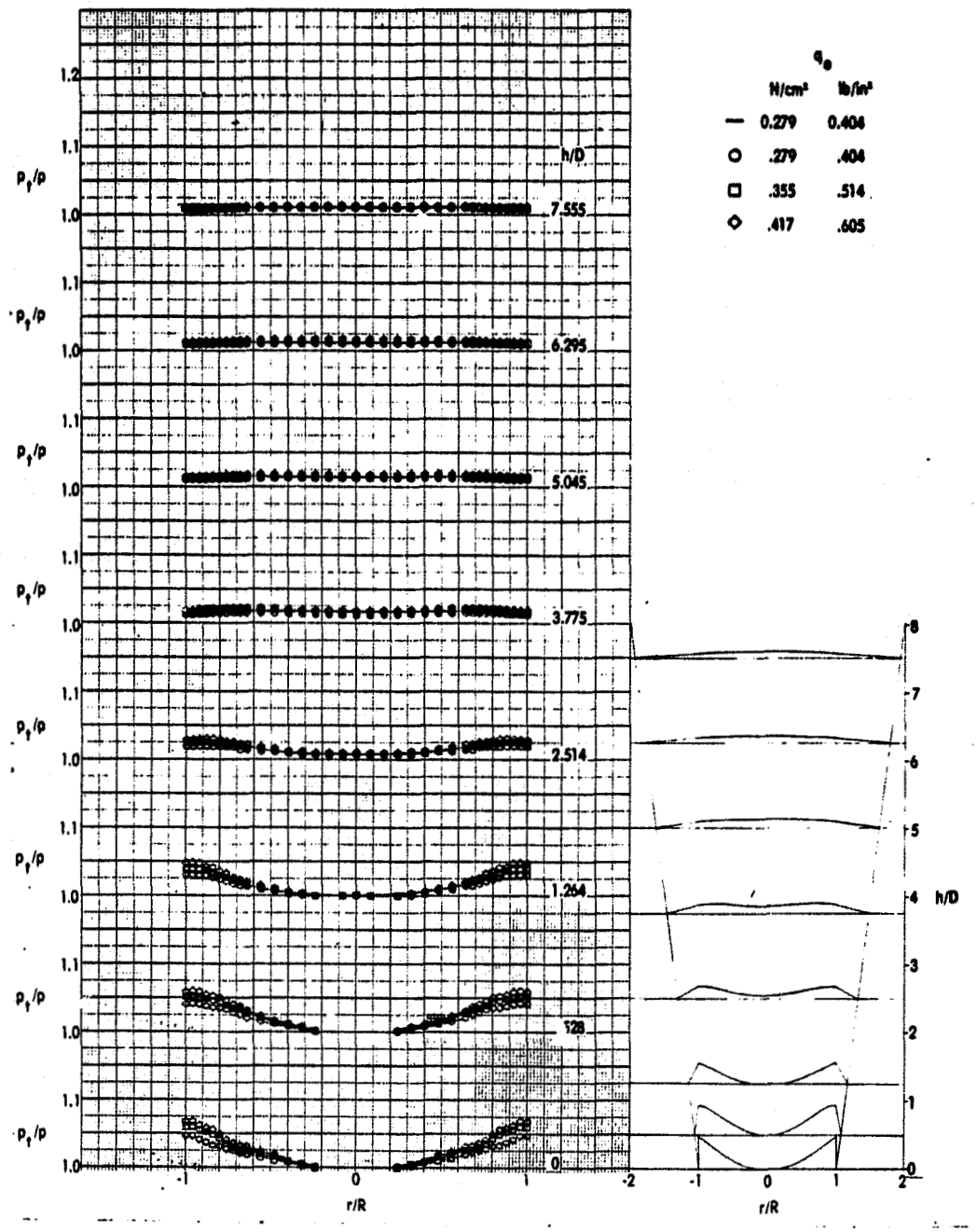

Figure 19. Efflux pressure profiles for contour model 1, Configuration A'.

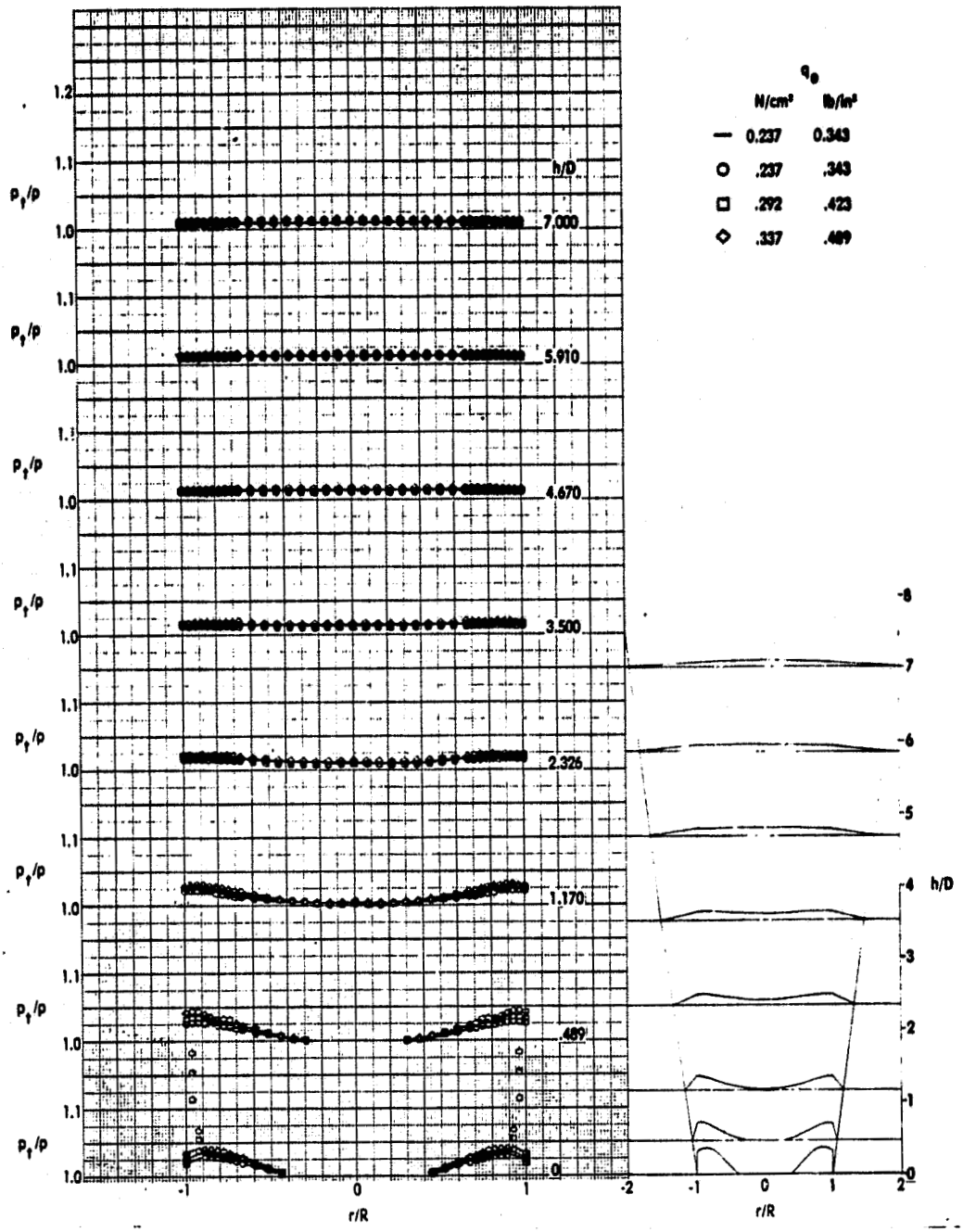

Figure 20. Efflux pressure profiles for plate model 1, Configuration B.

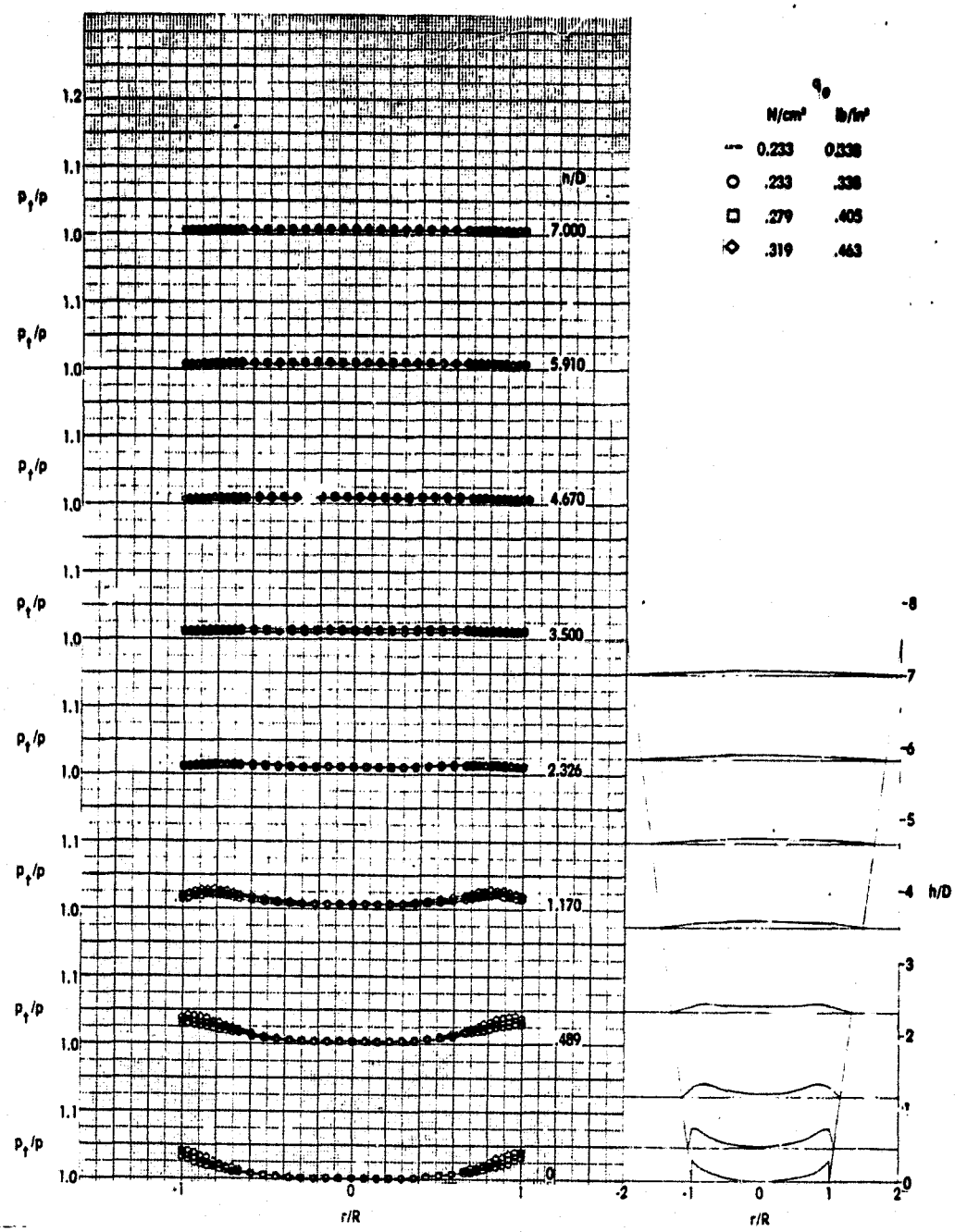

Figure 21. Efflux pressure profiles for plate model 1, Configuration B'.

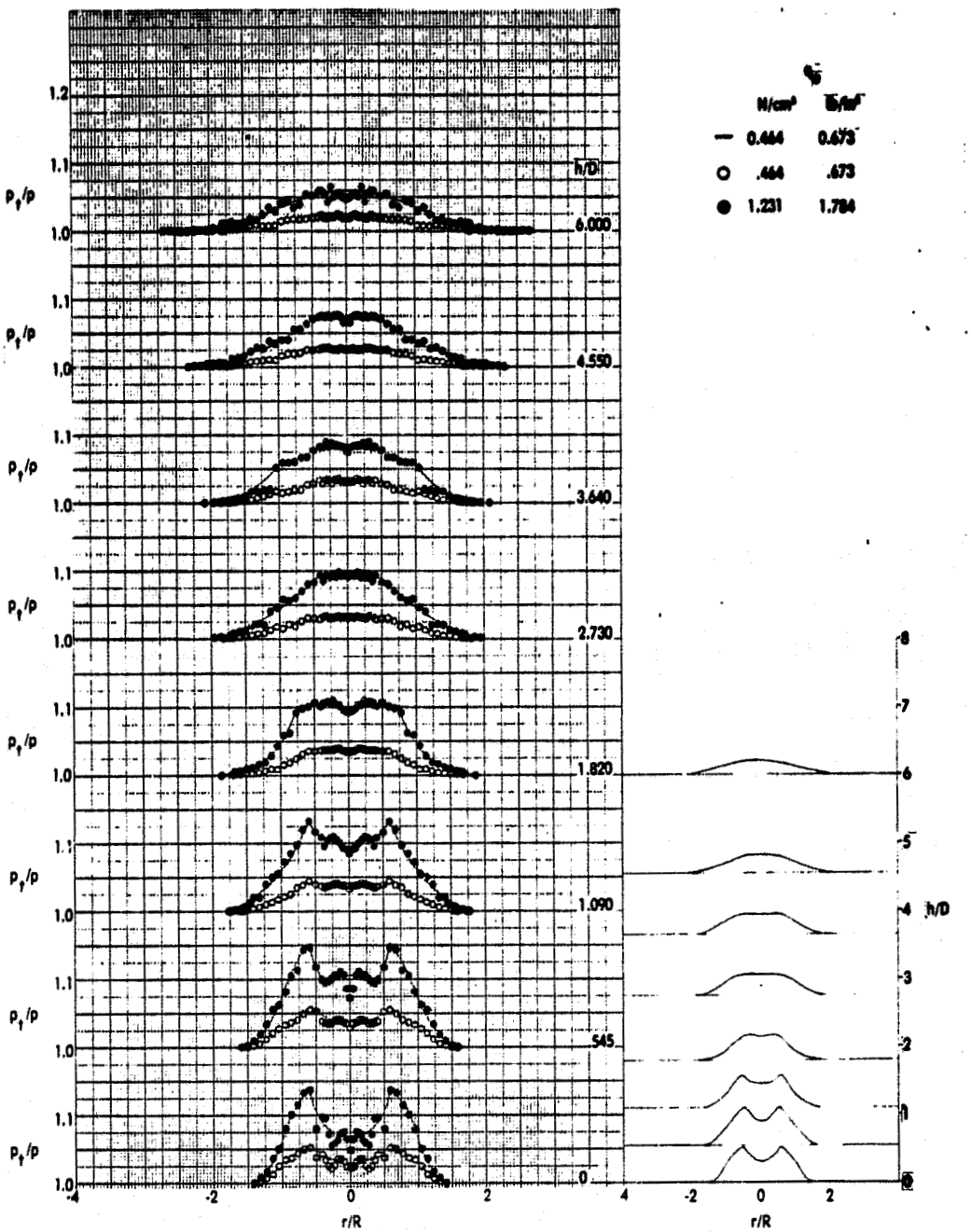

Figure 22. Efflux pressure profiles for tunnel model 1, δ_L = 0°, Configuration C.

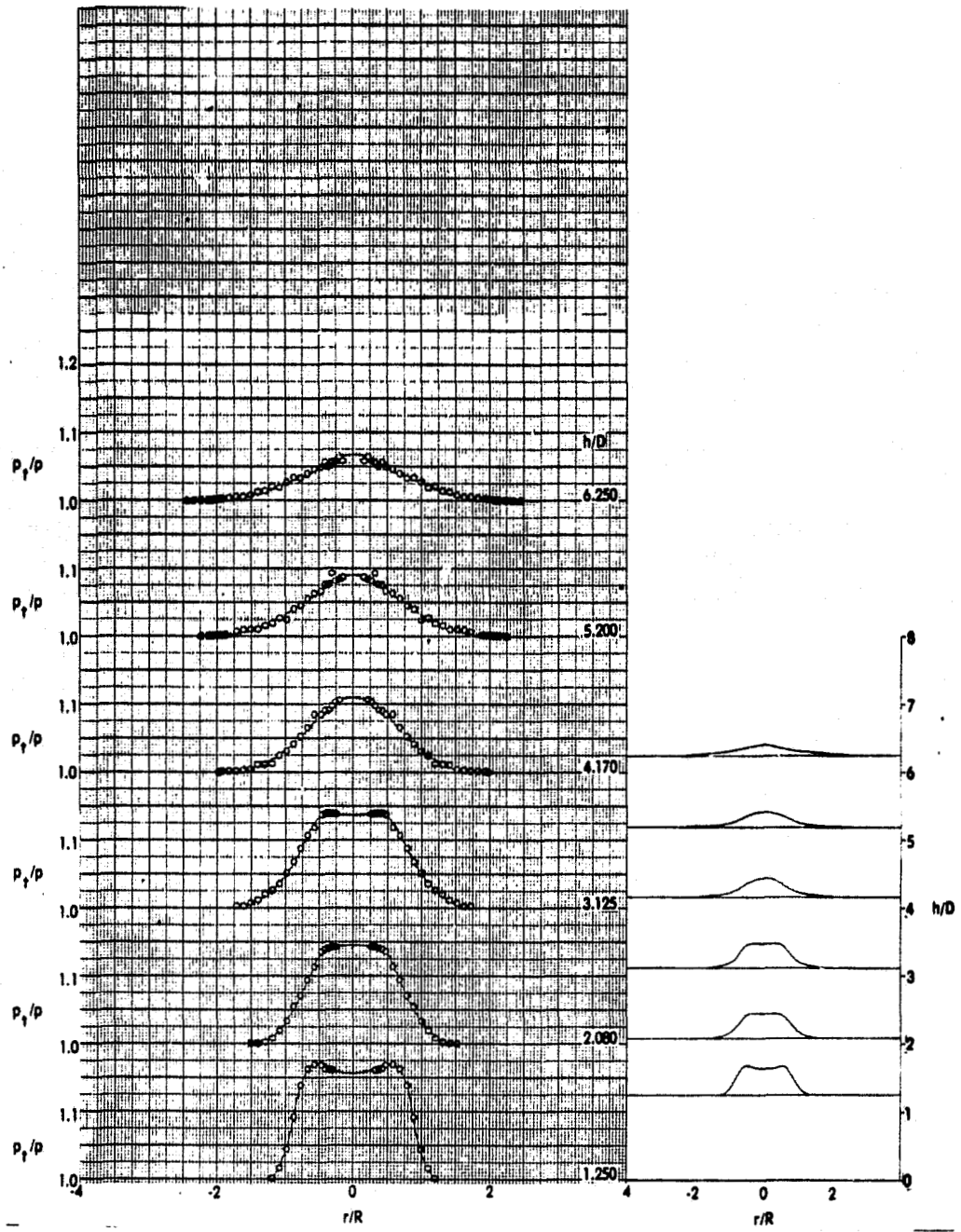

Figure 23. Efflux pressure profiles for tunnel model 2, q_e = 1.15 N/cm^2 (1.67 lb/in^2), Configuration D.

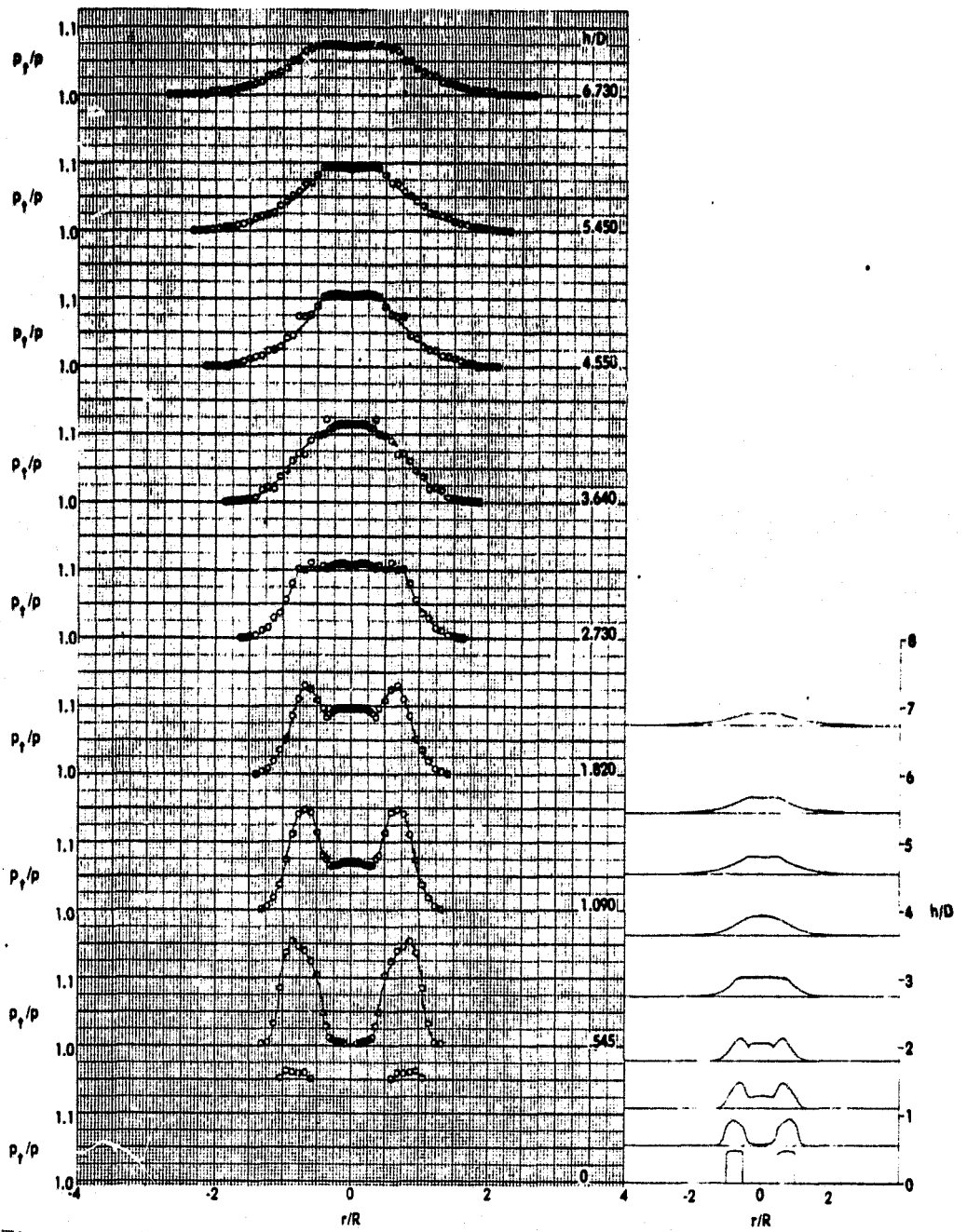

Figure 24. Efflux pressure profiles for tunnel model 2, $\delta_L = 0°$, $q_e = 1.64$ N/cm^2 (2.38 lb/in^2), Configuration E.

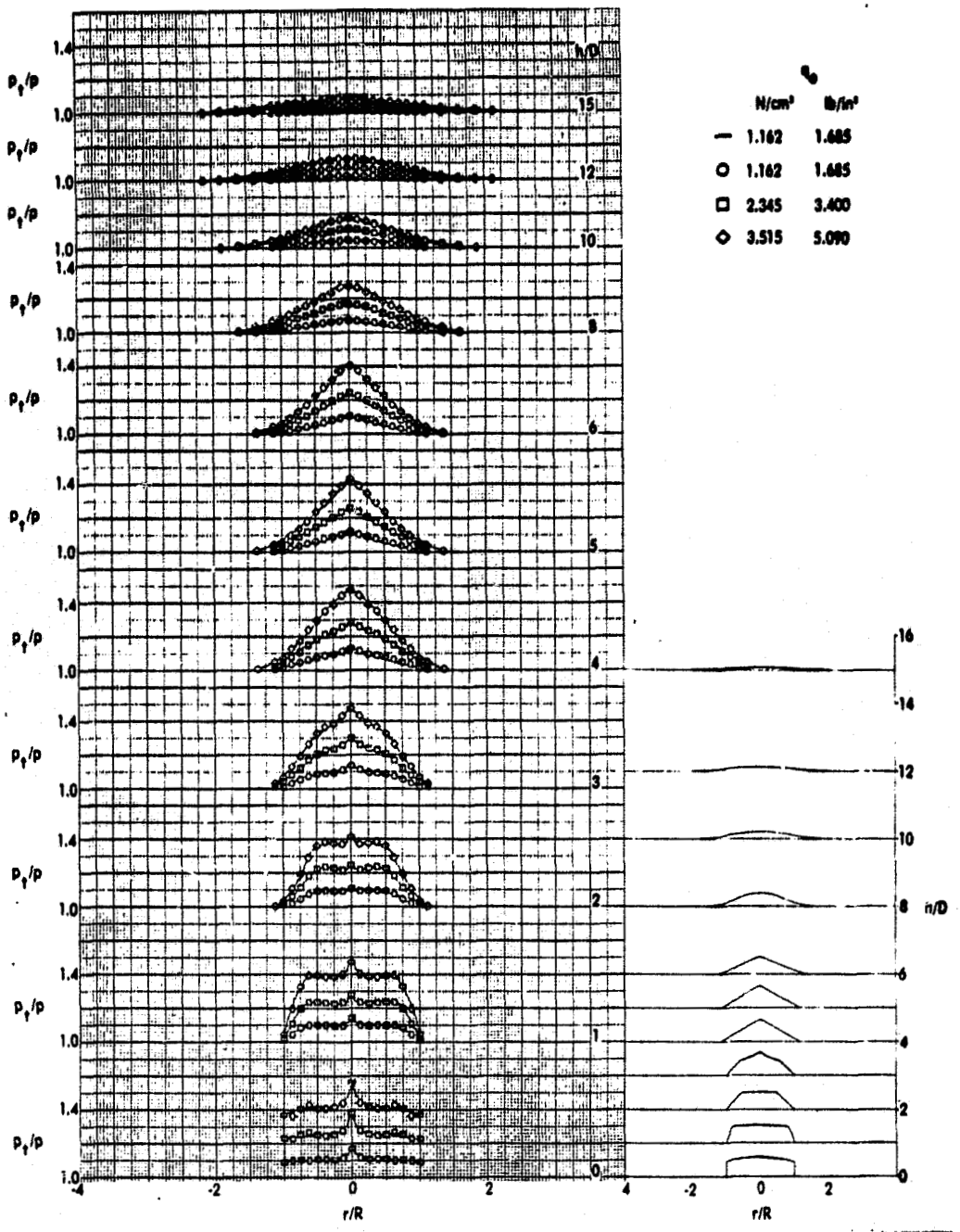

Figure 25. Efflux pressure profiles for plate models 2 and 3, Configuration F.

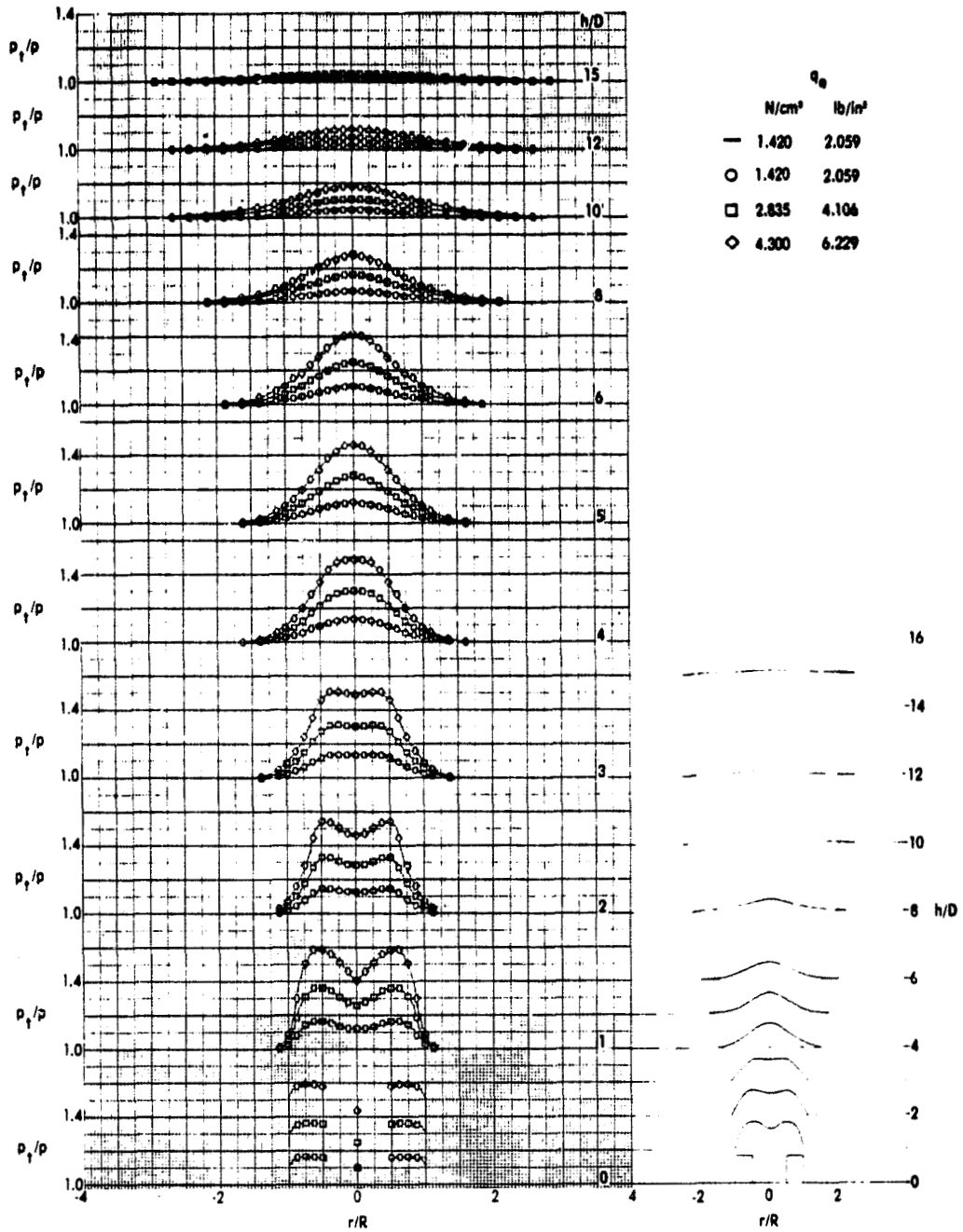

Figure 26. Efflux pressure profiles for plate model 2, Configuration G.

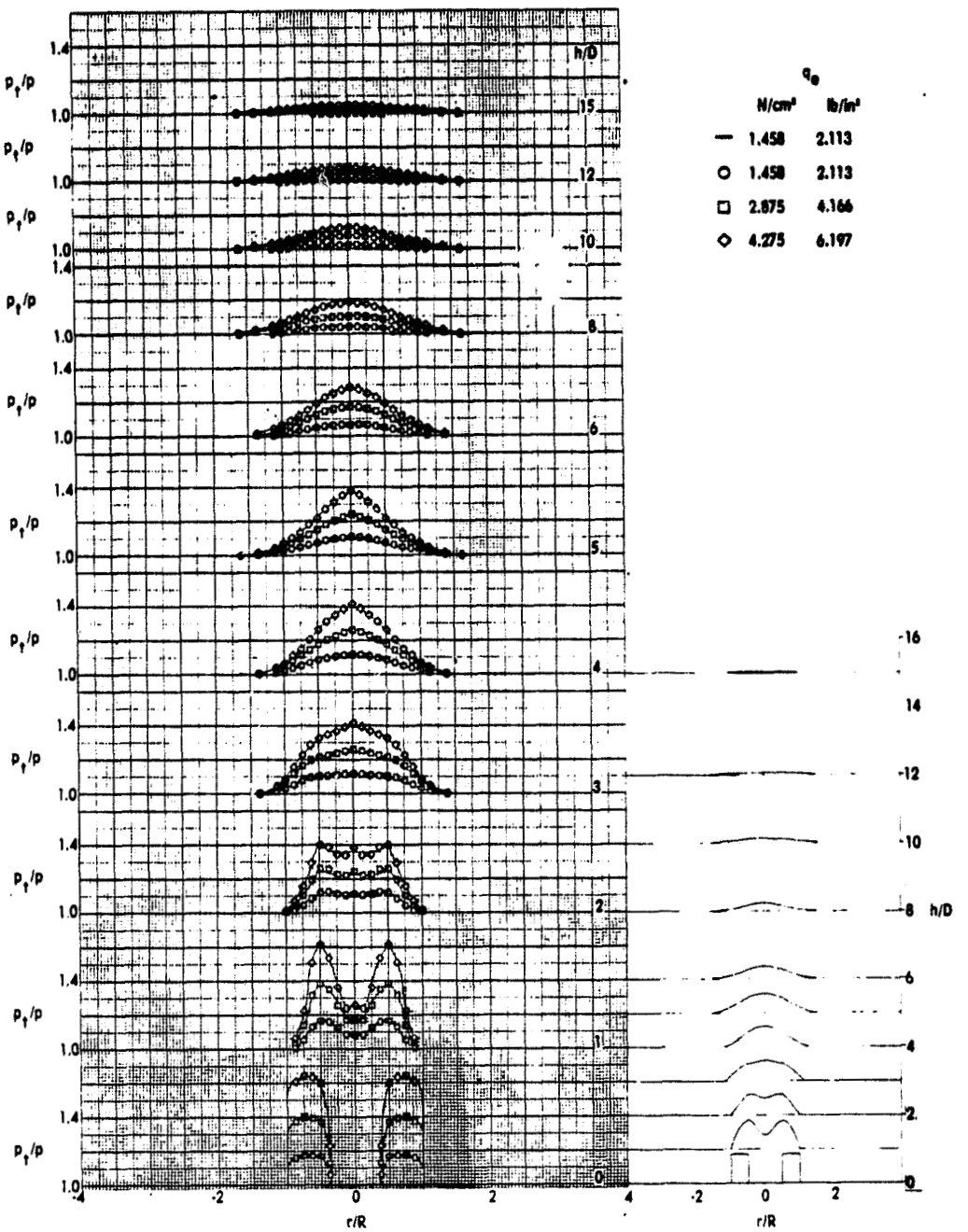

Figure 27. Efflux pressure profiles for plate model 2, Configuration G'.

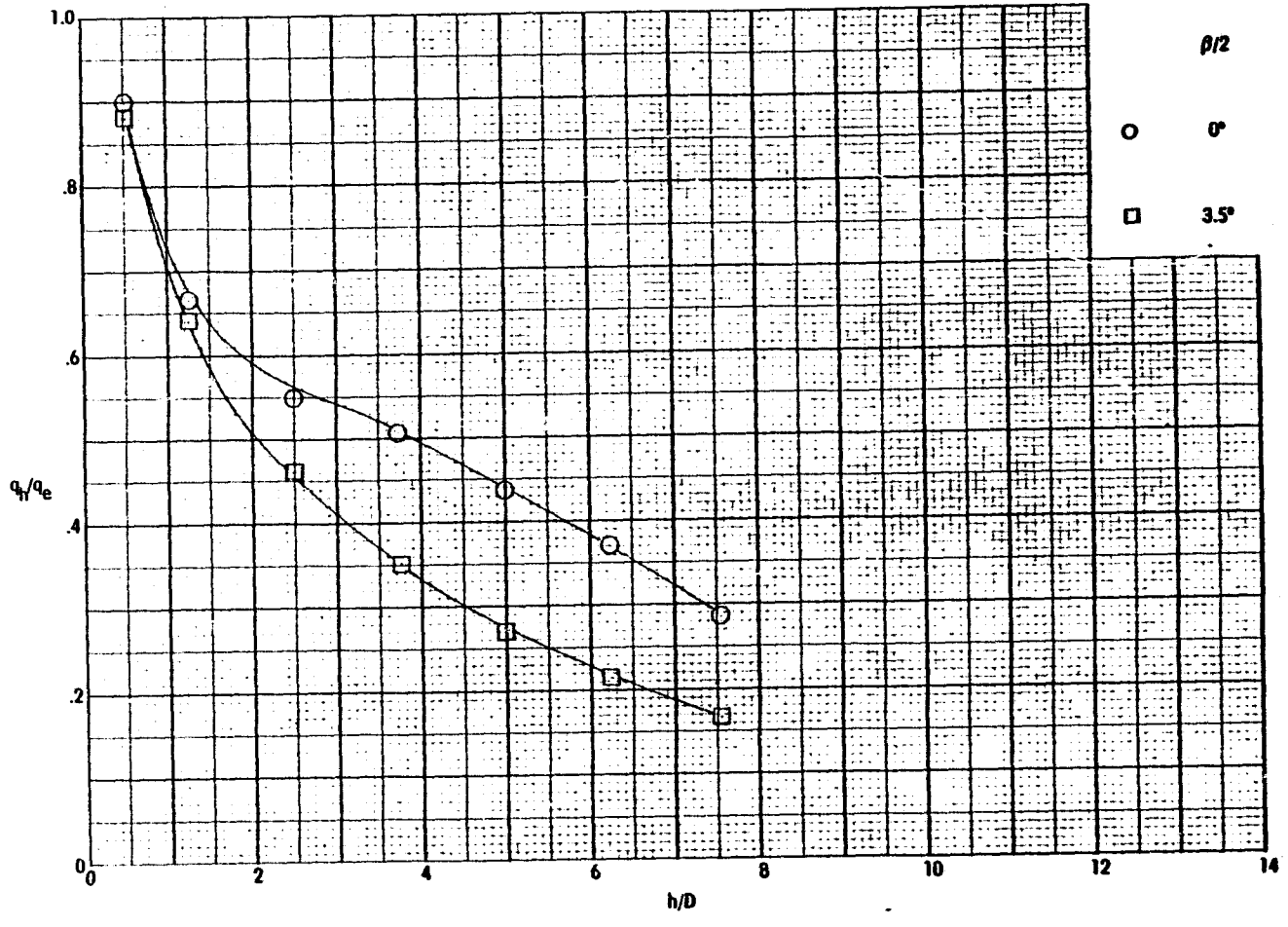

Figure 28. Effect of correcting the exhaust boundary by comparison of calculated thrust for q_e = 0.417 N/cm^2 (.605 lb/in^2), Configuration A.

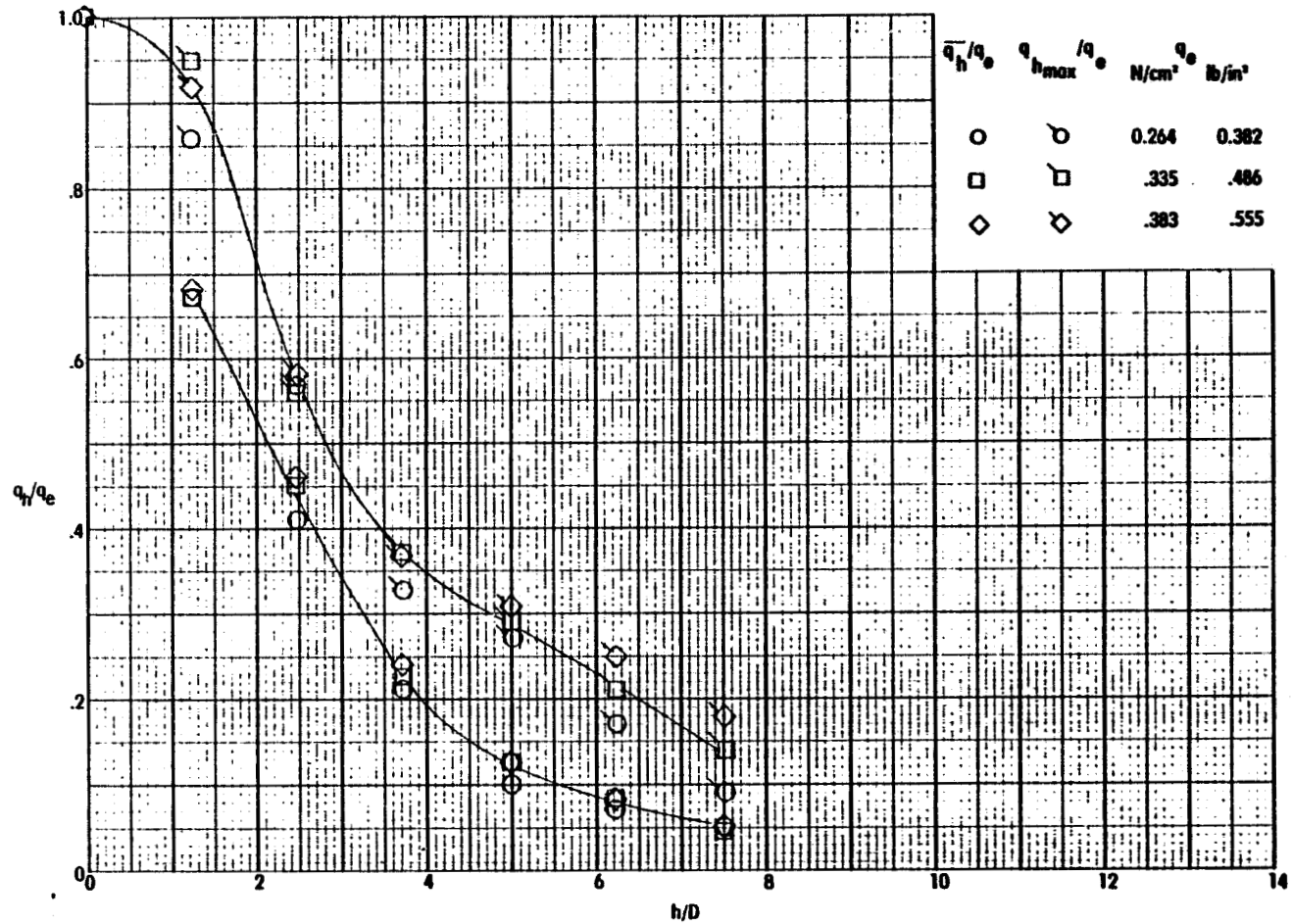

Figure 29. Thrust effects on q decay for a plate model 1 fan, Configuration A.

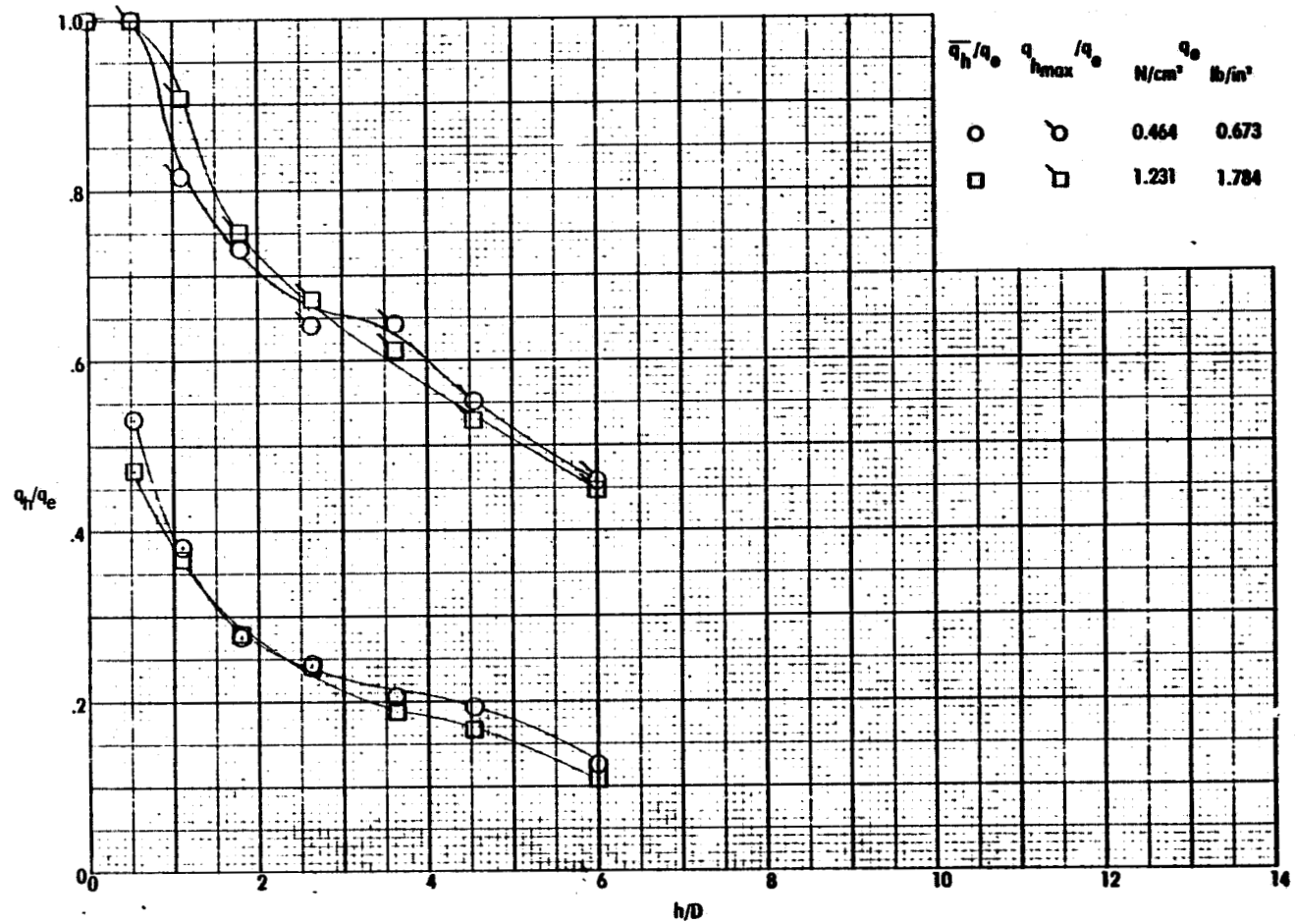

Figure 30. Thrust effects on q decay for a tunnel model 1 fan, Configuration C.

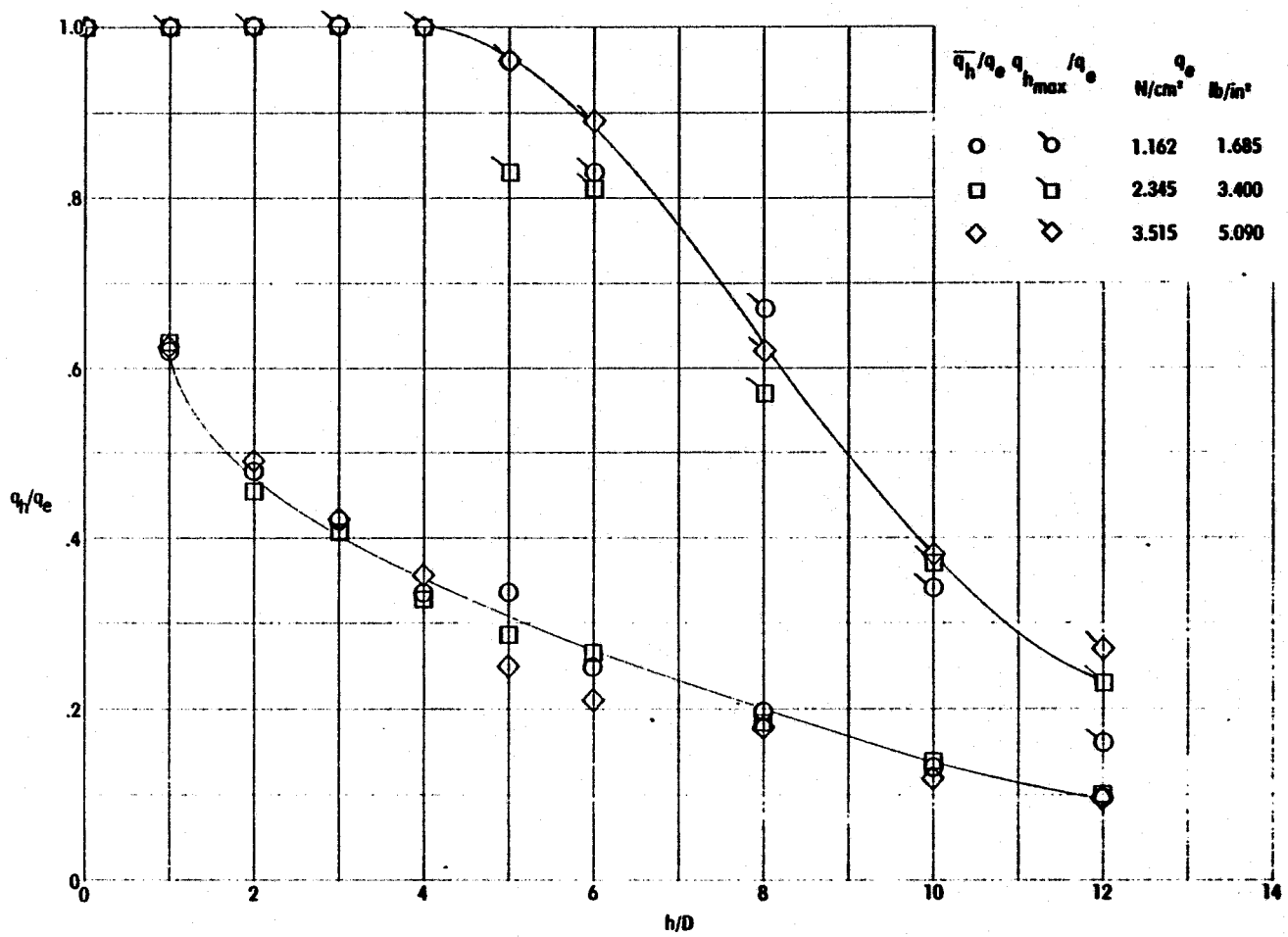

Figure 31. Thrust effects on q decay for a plate model 2 and 3 ejector, Configuration F.

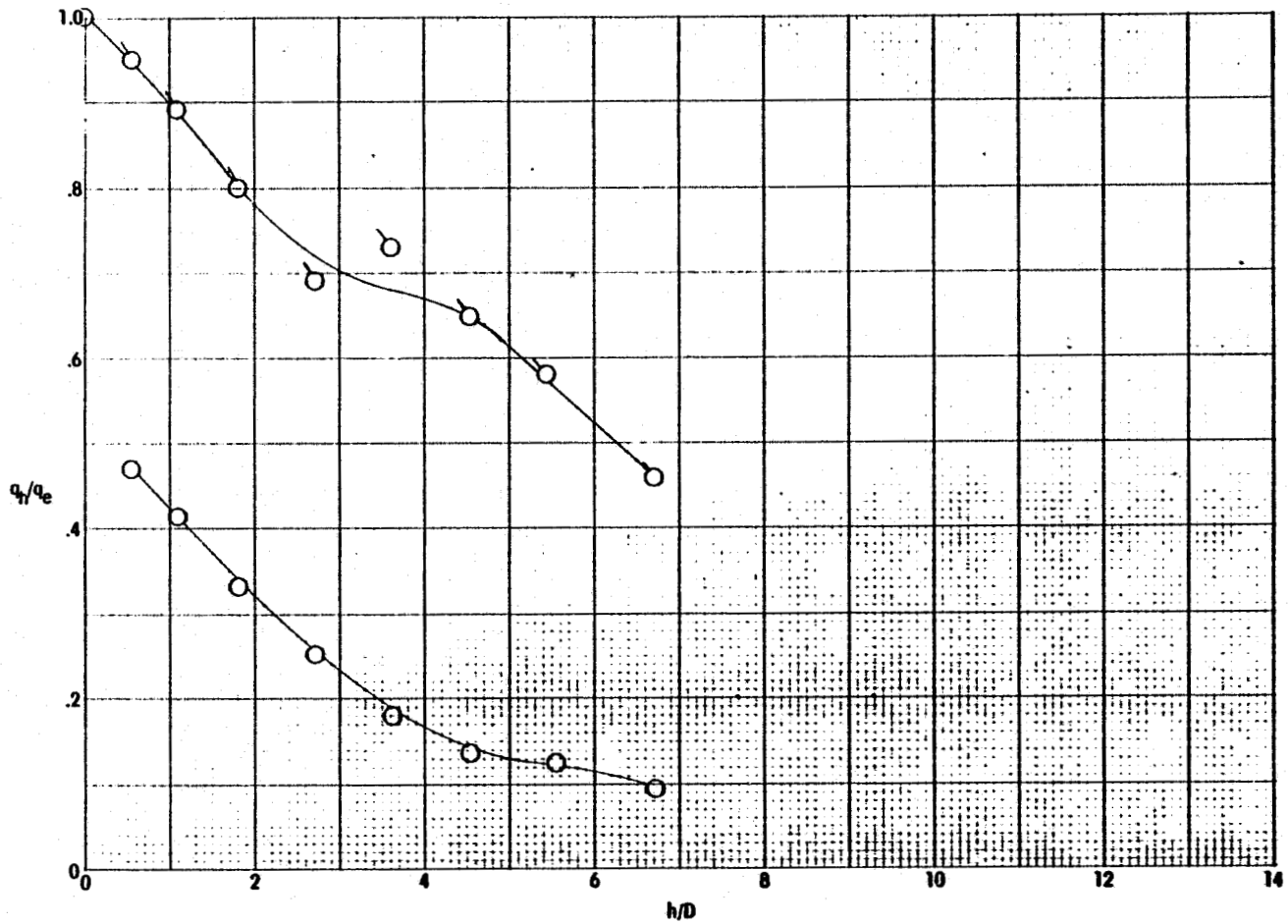

Figure 32. Thrust effects on q decay for a tunnel model 2 fan, q_e = 1.64 N/cm^2 (2.38 lb/in^2), Configuration E. Symbols are average q decay, flags indicate maximum q decay.

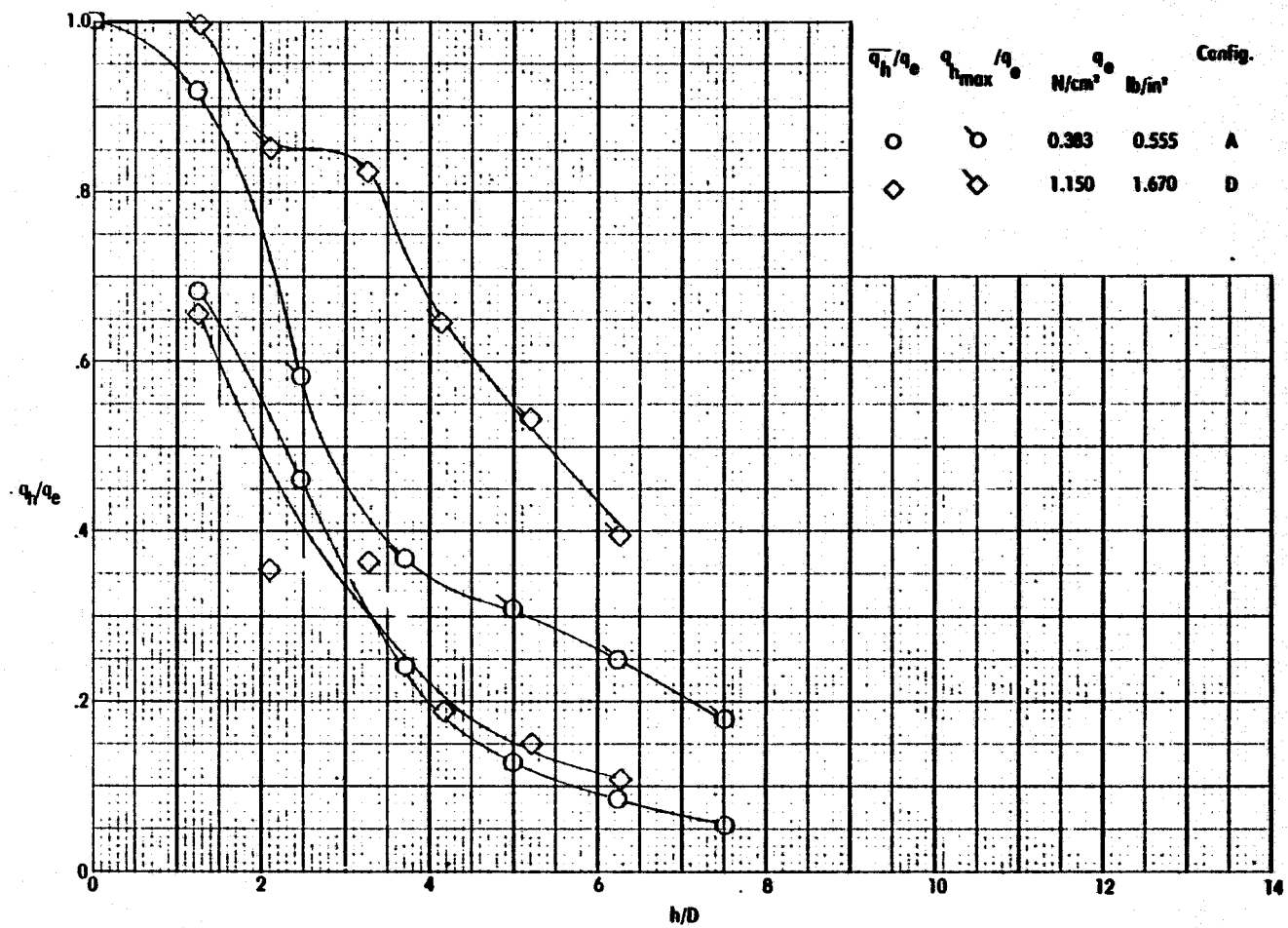

Figure 33. Comparisons of q decay for model 1 cruise engines for unscaled thrusts.

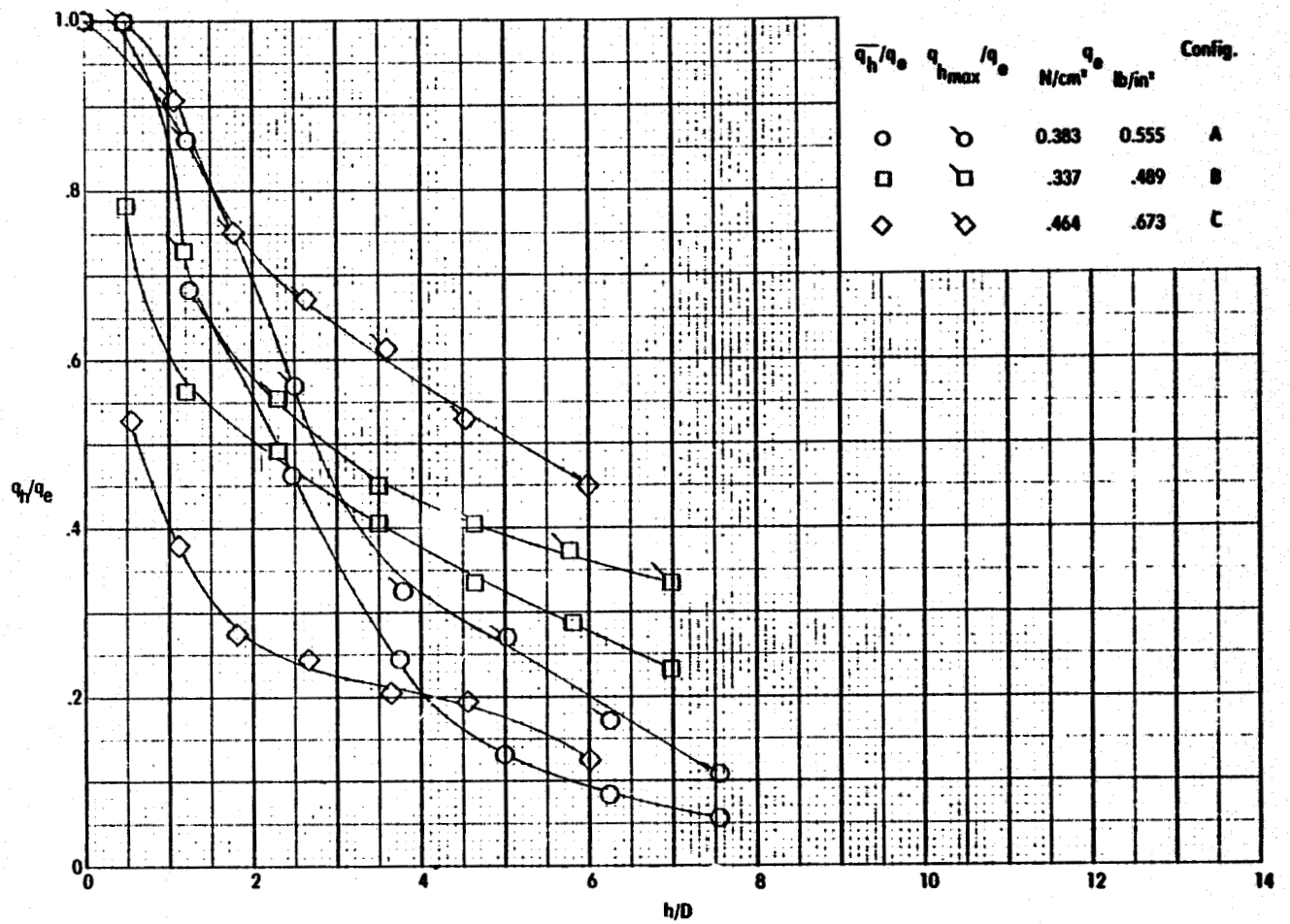

Figure 34. Comparisons of q decay for the model 1 lift engines for scaled thrusts.

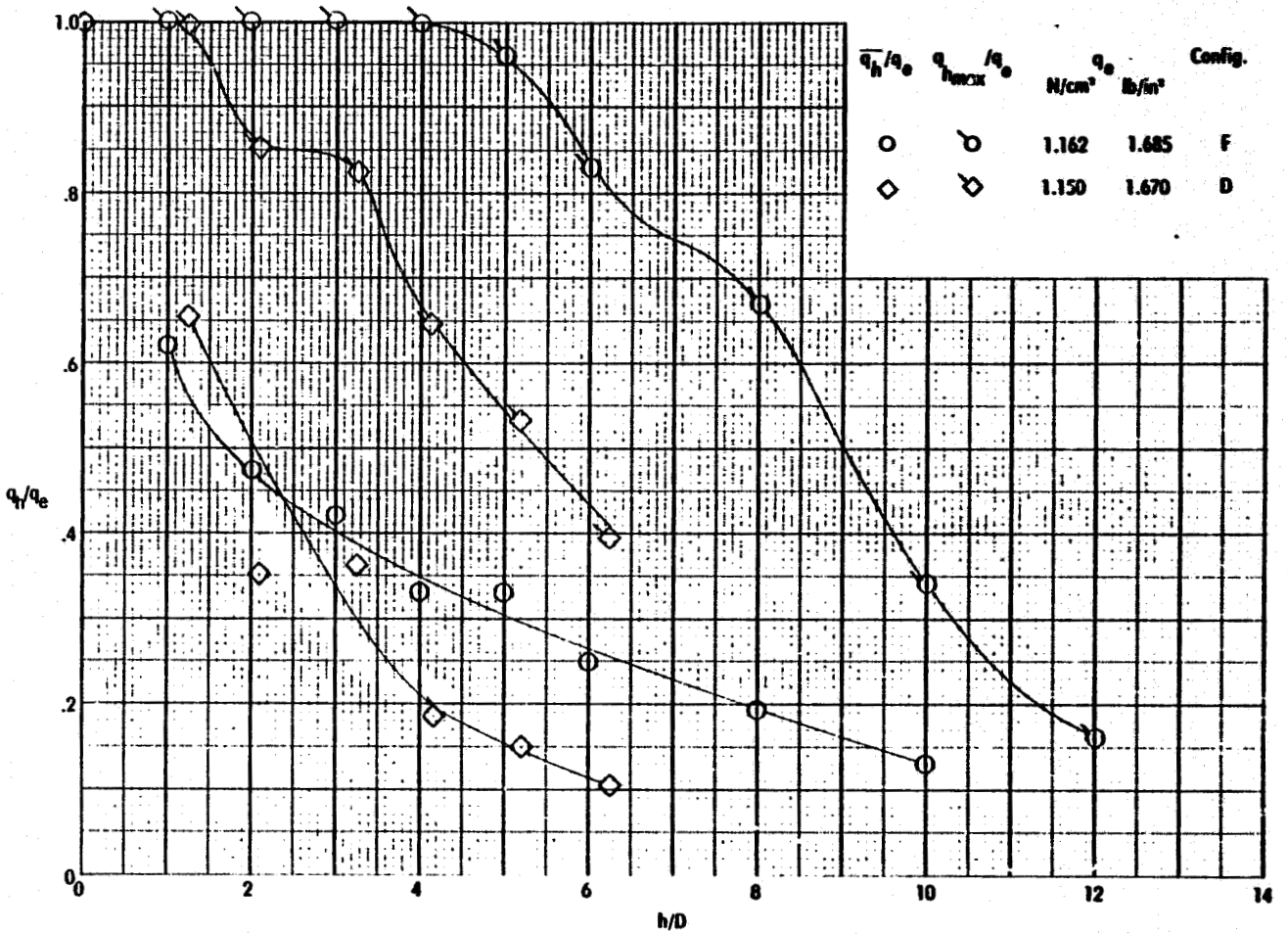

Figure 35. Comparisons of q decay for the model 2 cruise engines for scaled thrusts.

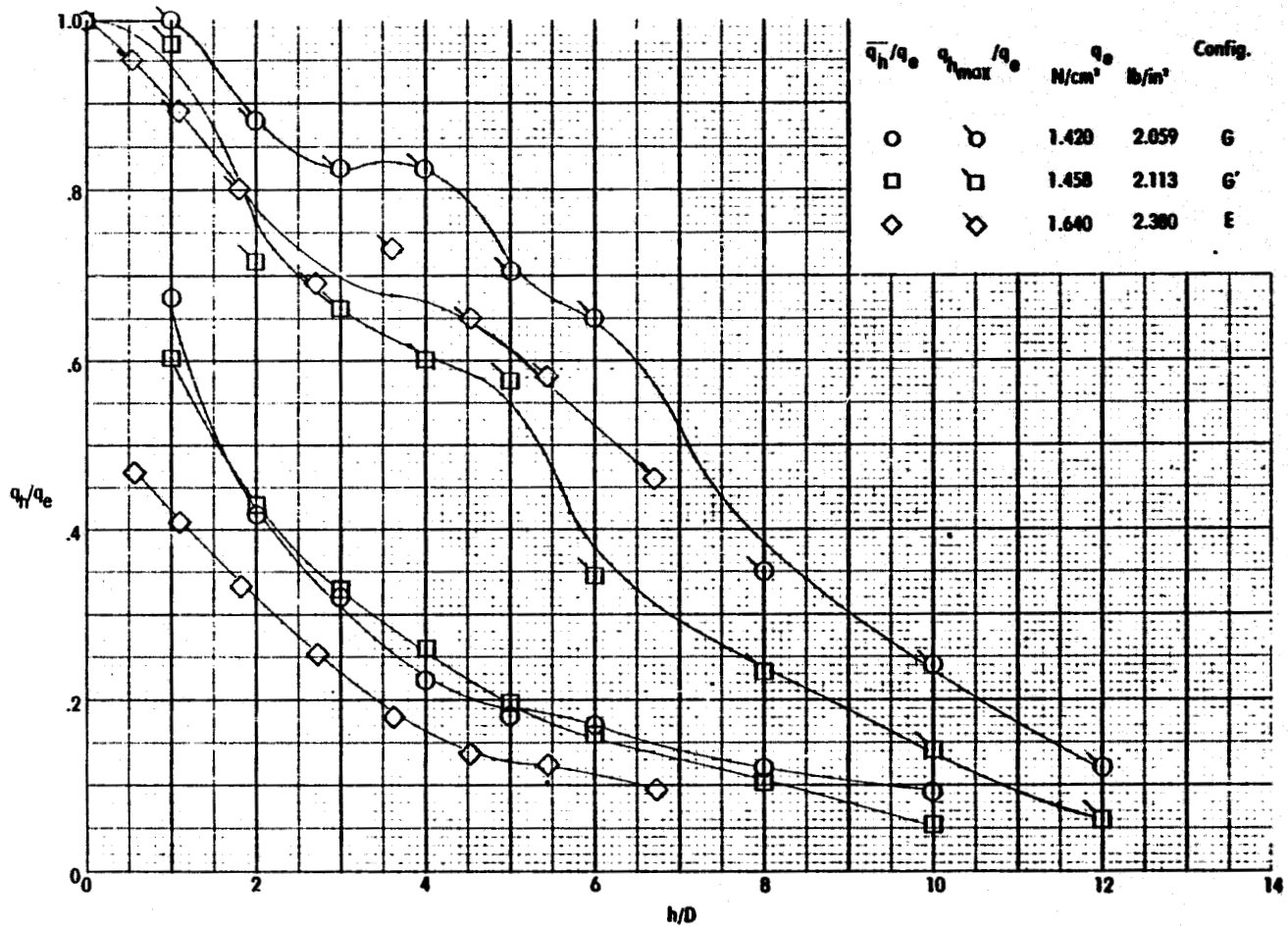

Figure 36. Comparisons of q decay for model 2 lift engines for scaled thrusts.

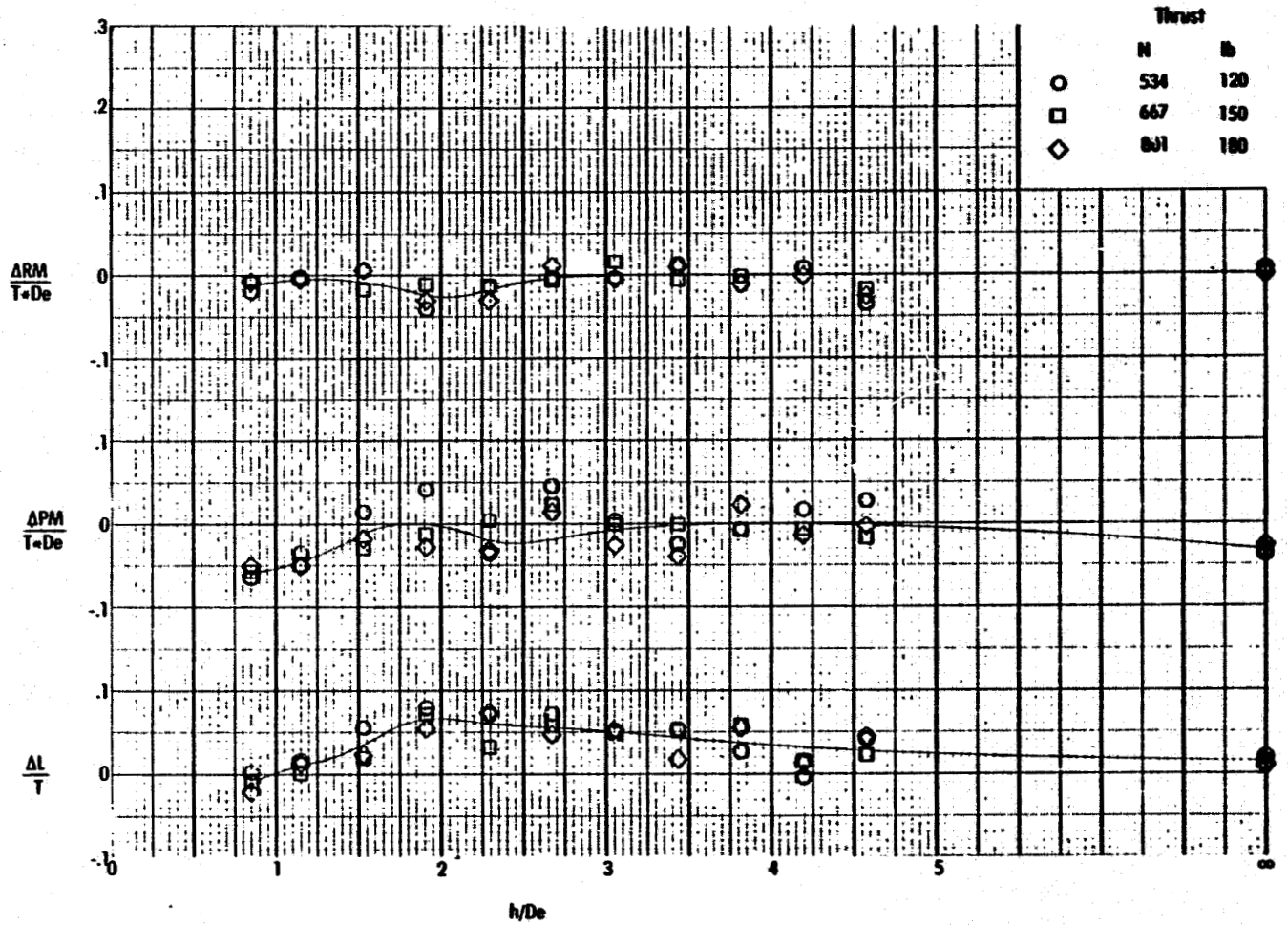

Figure 37. Effect of thrust level on induced loads for plate model 1.

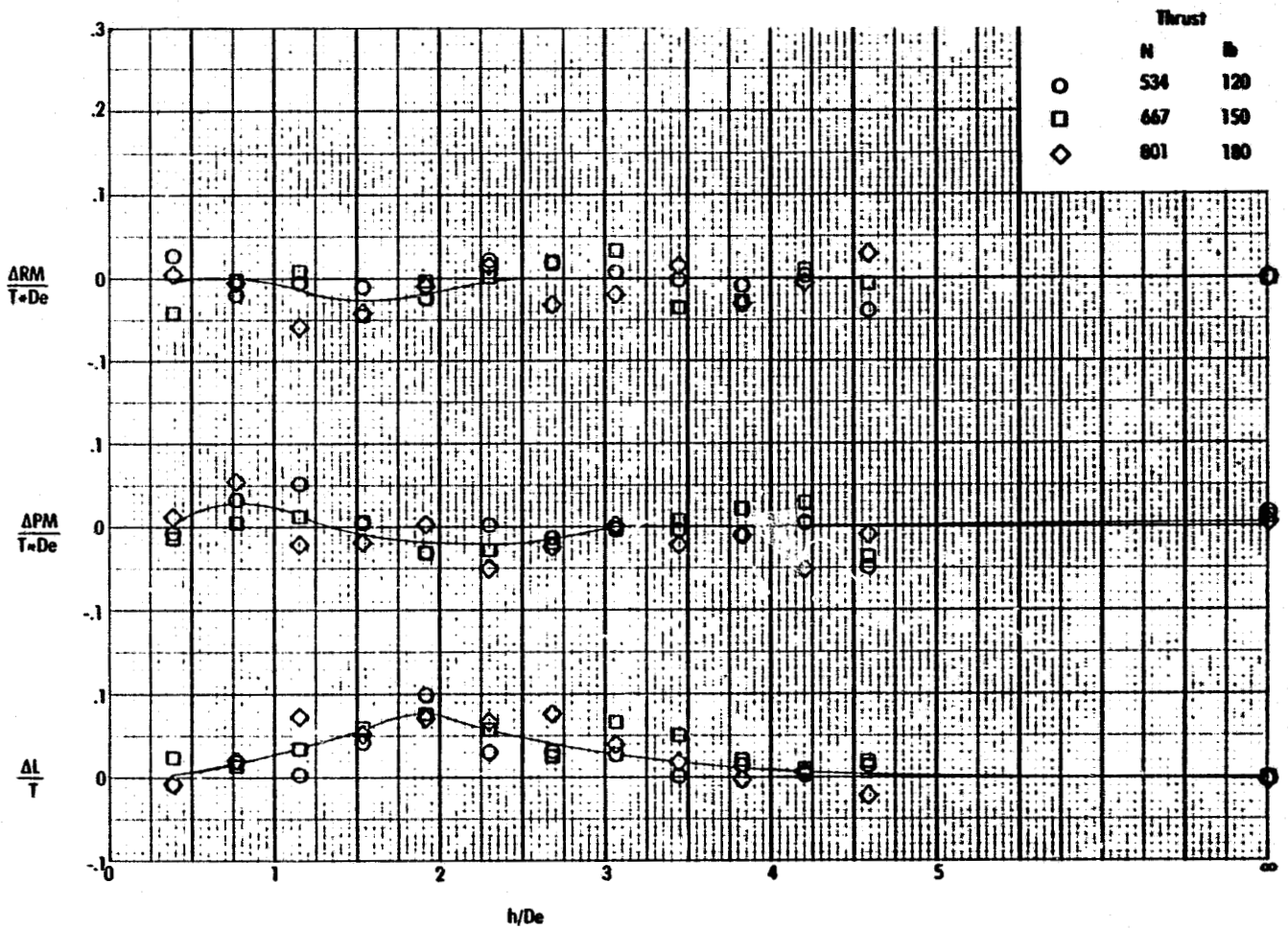

Figure 38. Effect of thrust level on induced loads for contour model 1.

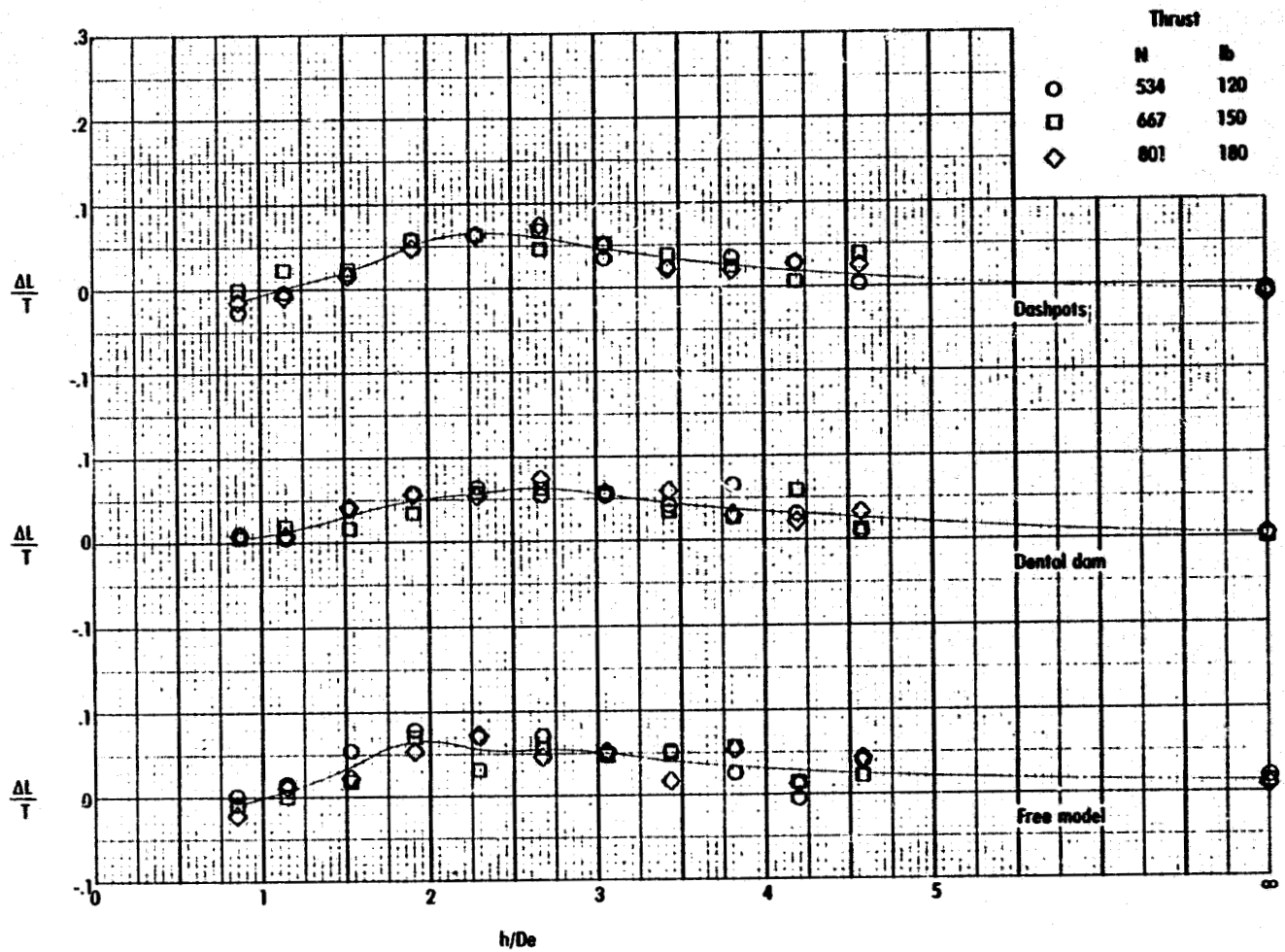

Figure 39. Influence of dental dam and dashpots on the induced lift for plate model 1.

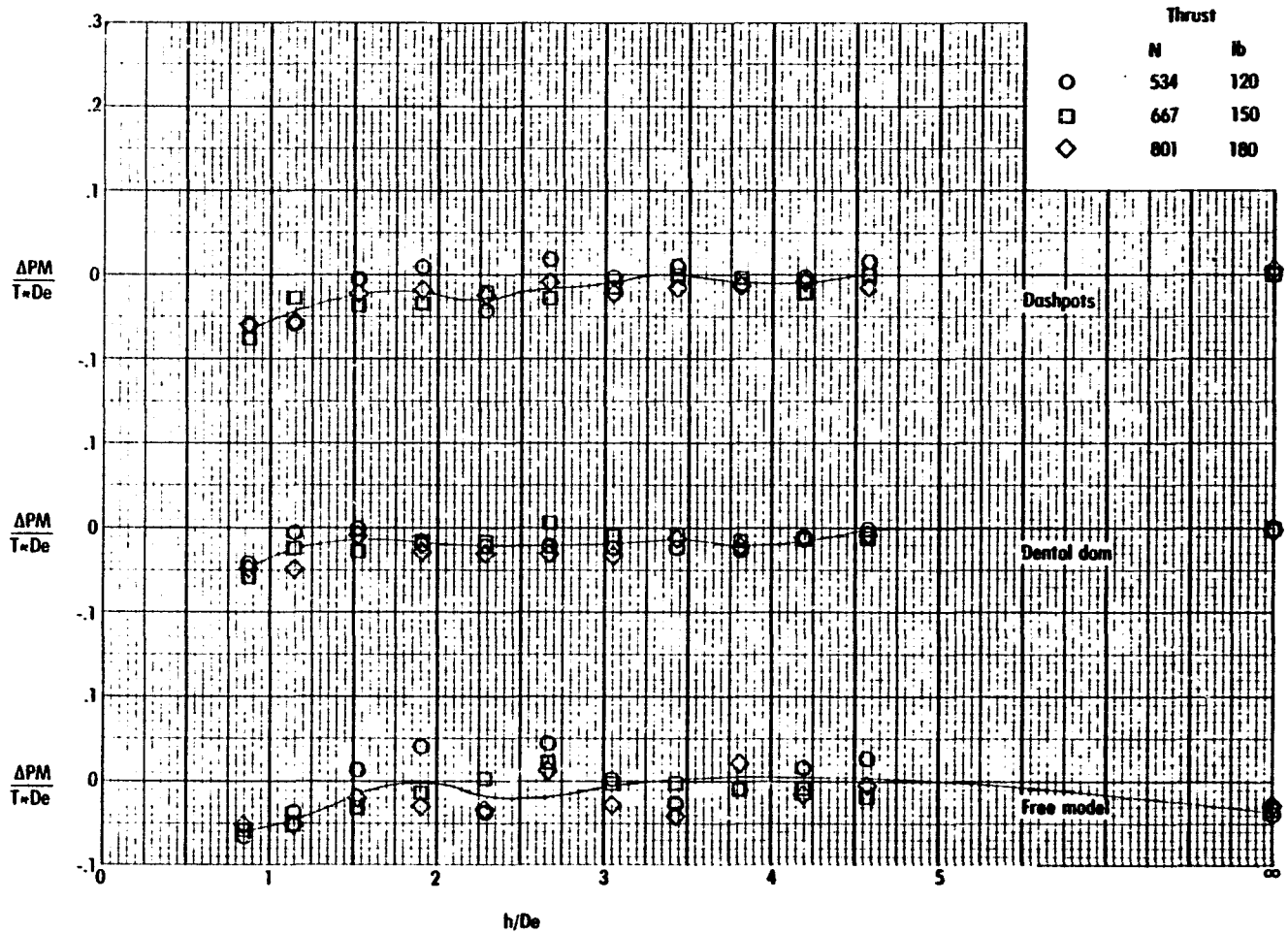

Figure 40. Influence of dental dam and dashpots on the induced pitching moment for plate model 1.

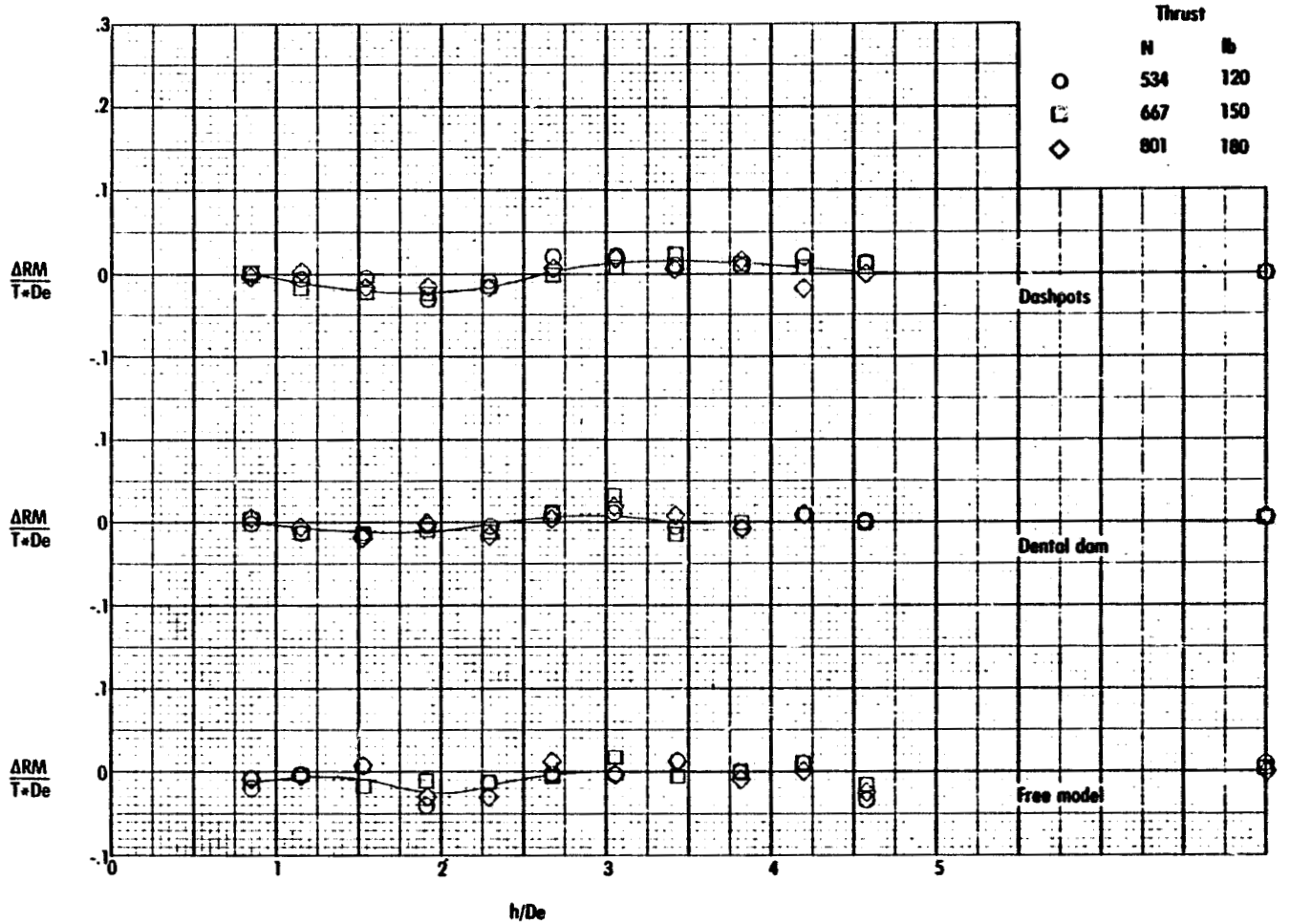

Figure 41. Influence of dental dam and dashpots on the induced rolling moment for plate model 1.

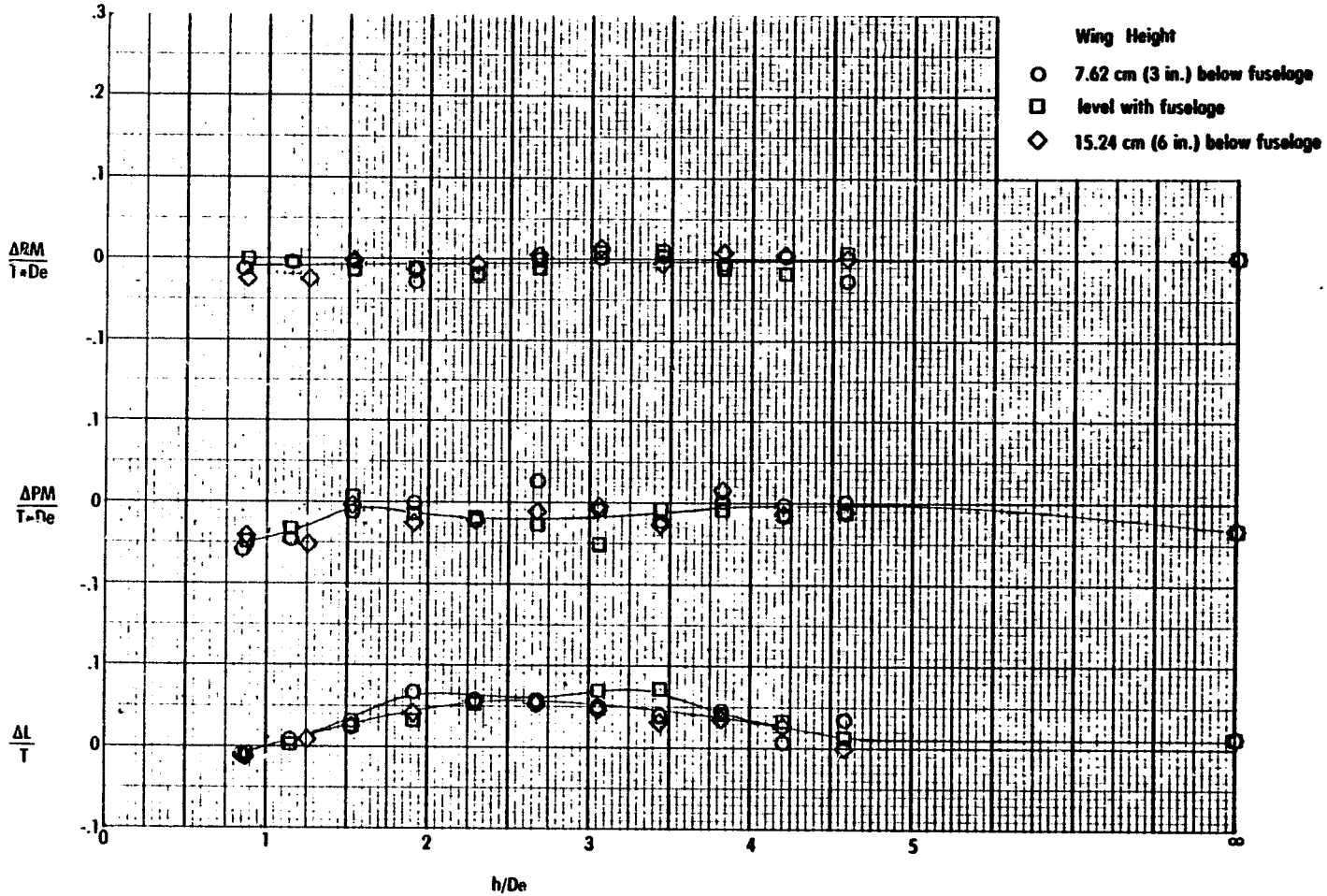

Figure 42. Influence of wing height variation on the induced loads of plate model 1.

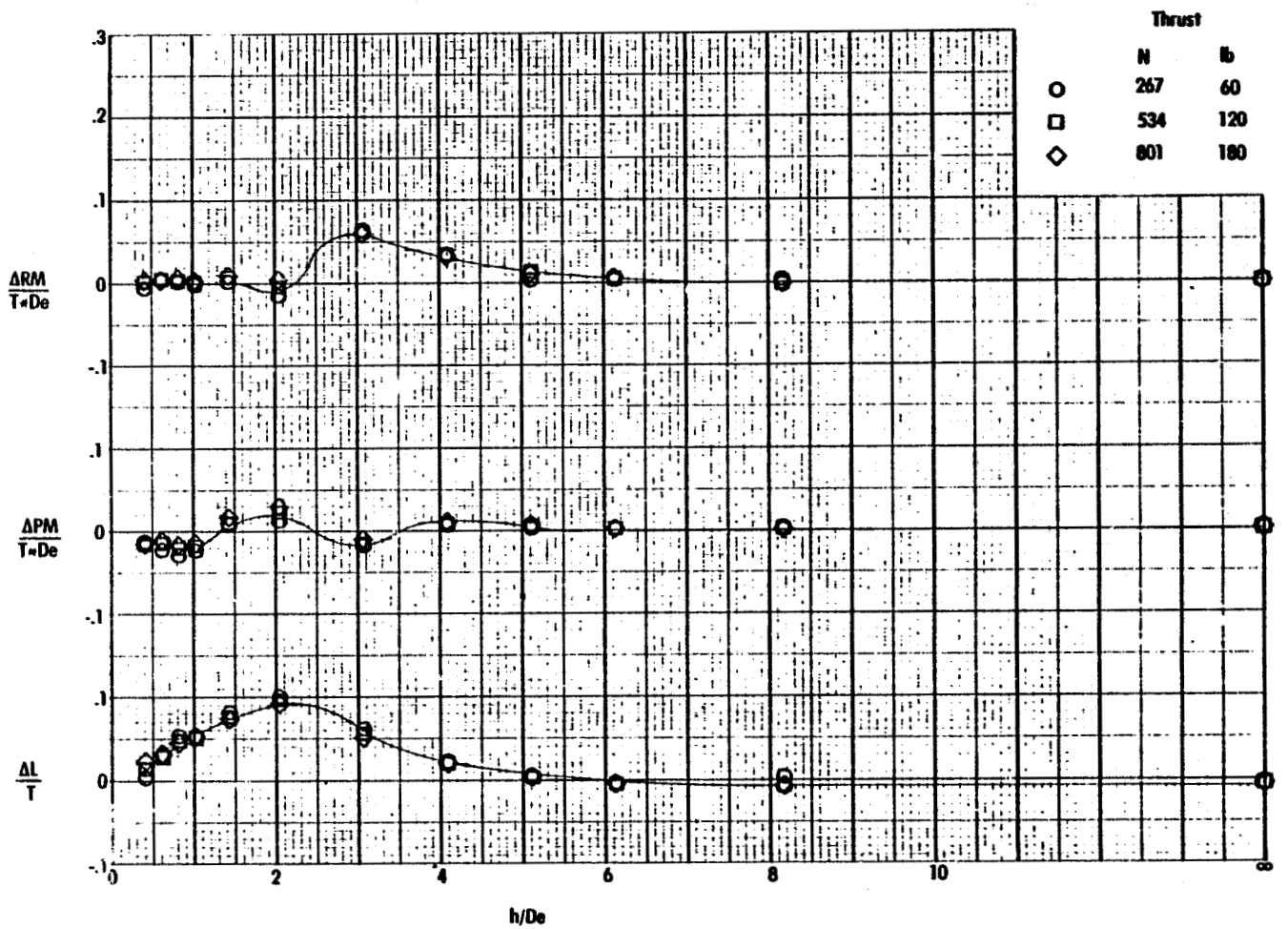

Figure 43. Effect of thrust level on the induced loads for plate model 2.

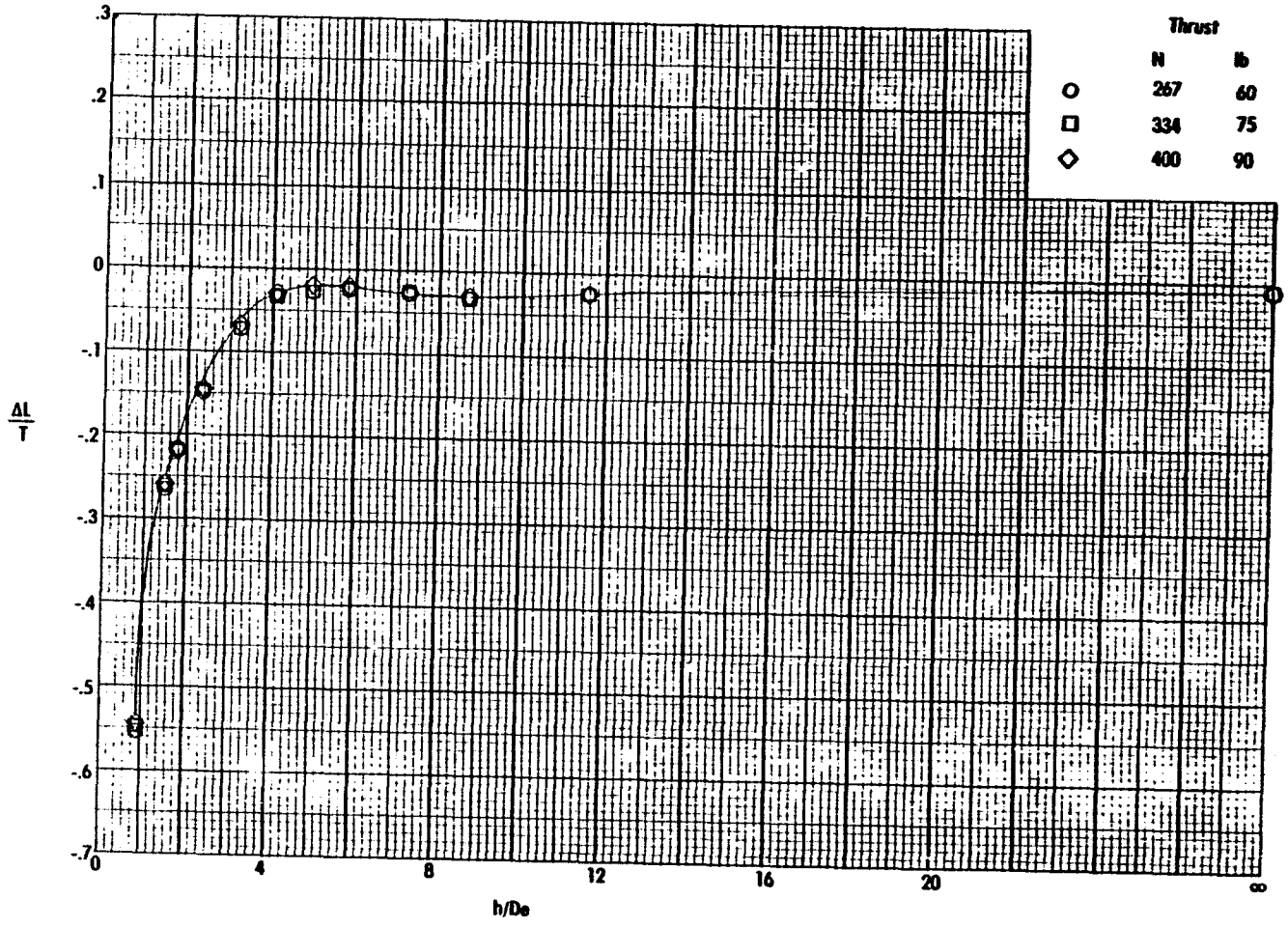

Figure 44. Effect of thrust level on the induced lift for plate model 3.

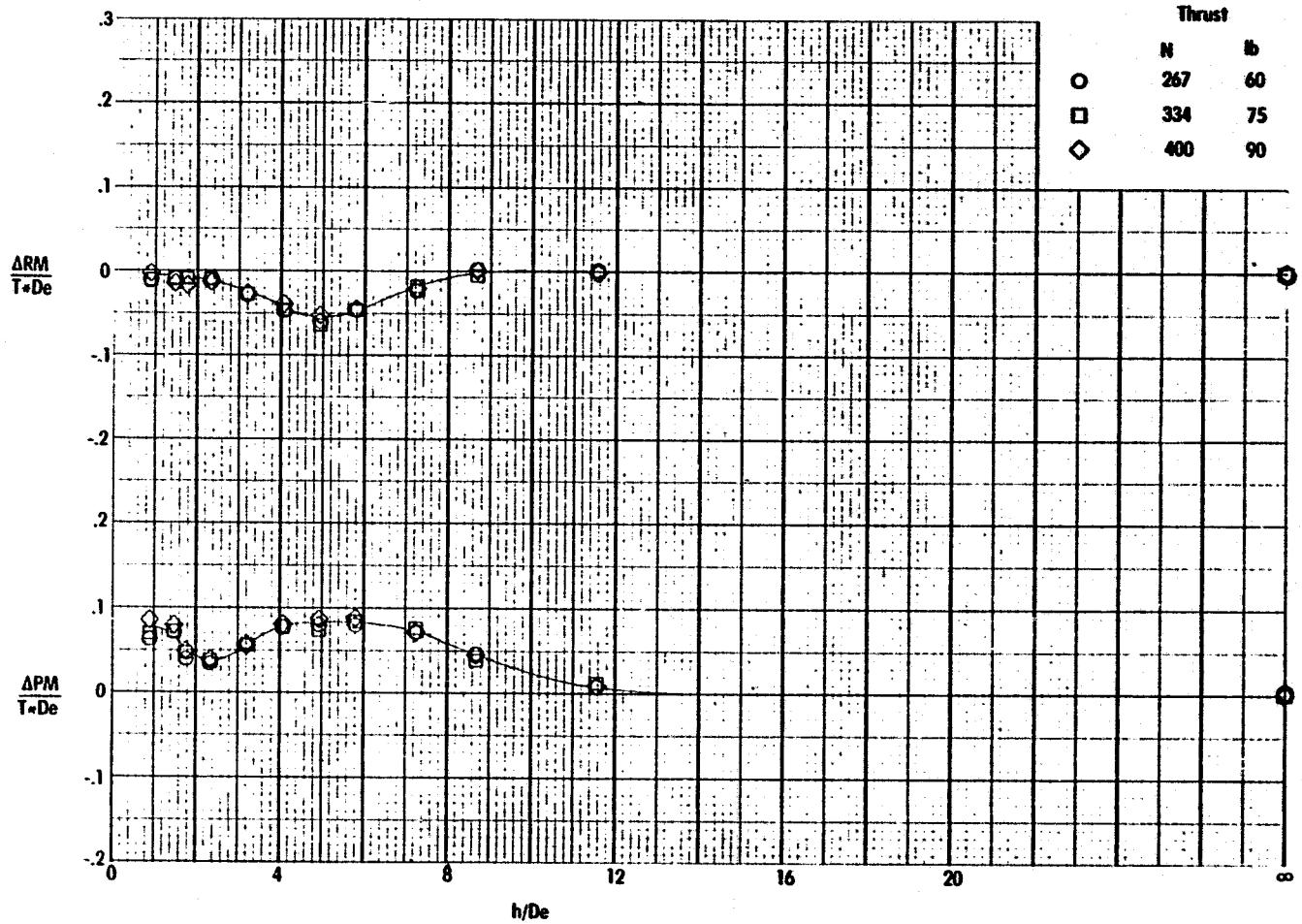

Figure 45. Effect of thrust level on the induced pitching and rolling moment for plate model 3.

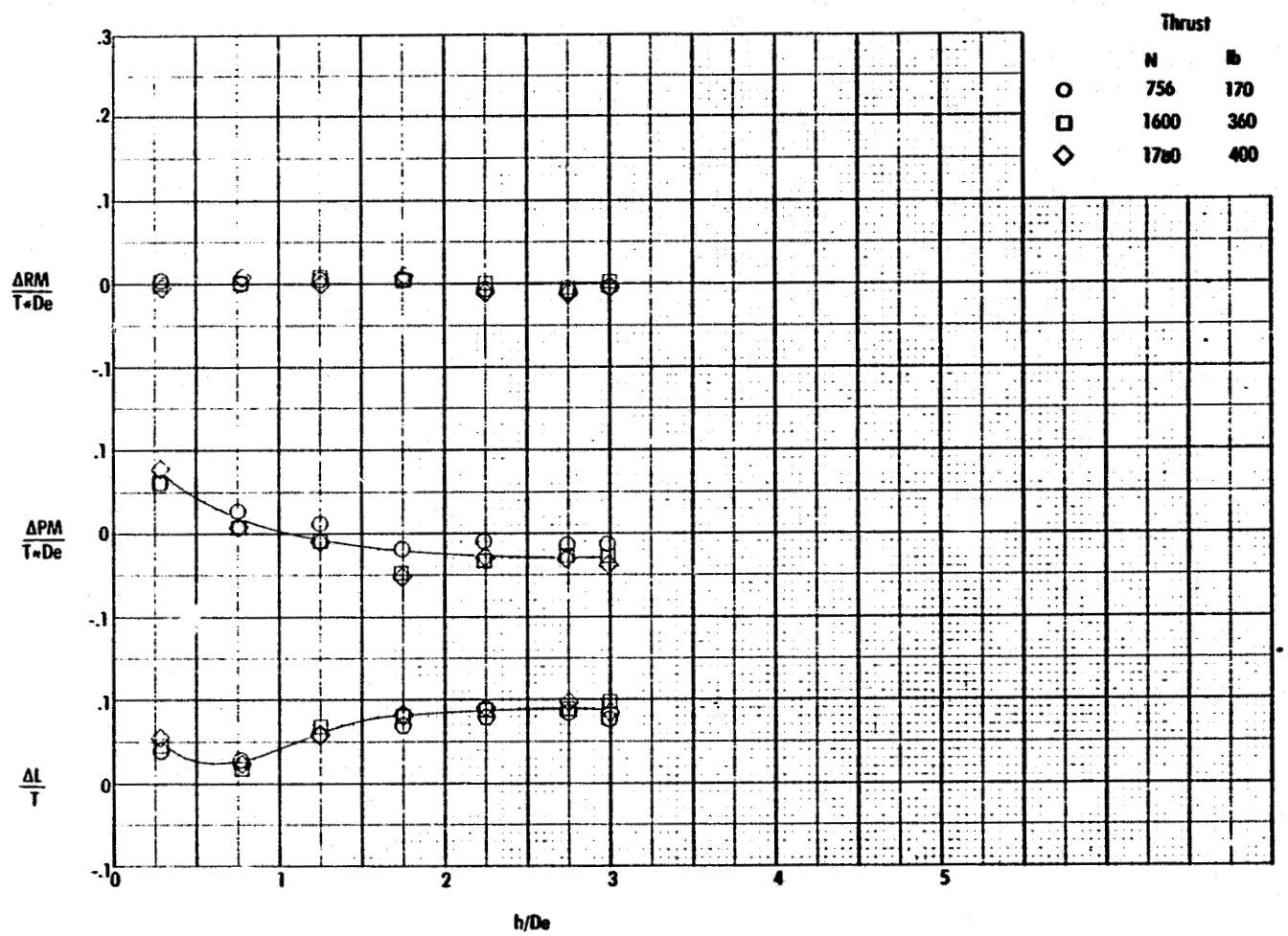

Figure 46. Effect of thrust level on the induced loads of tunnel model 1.

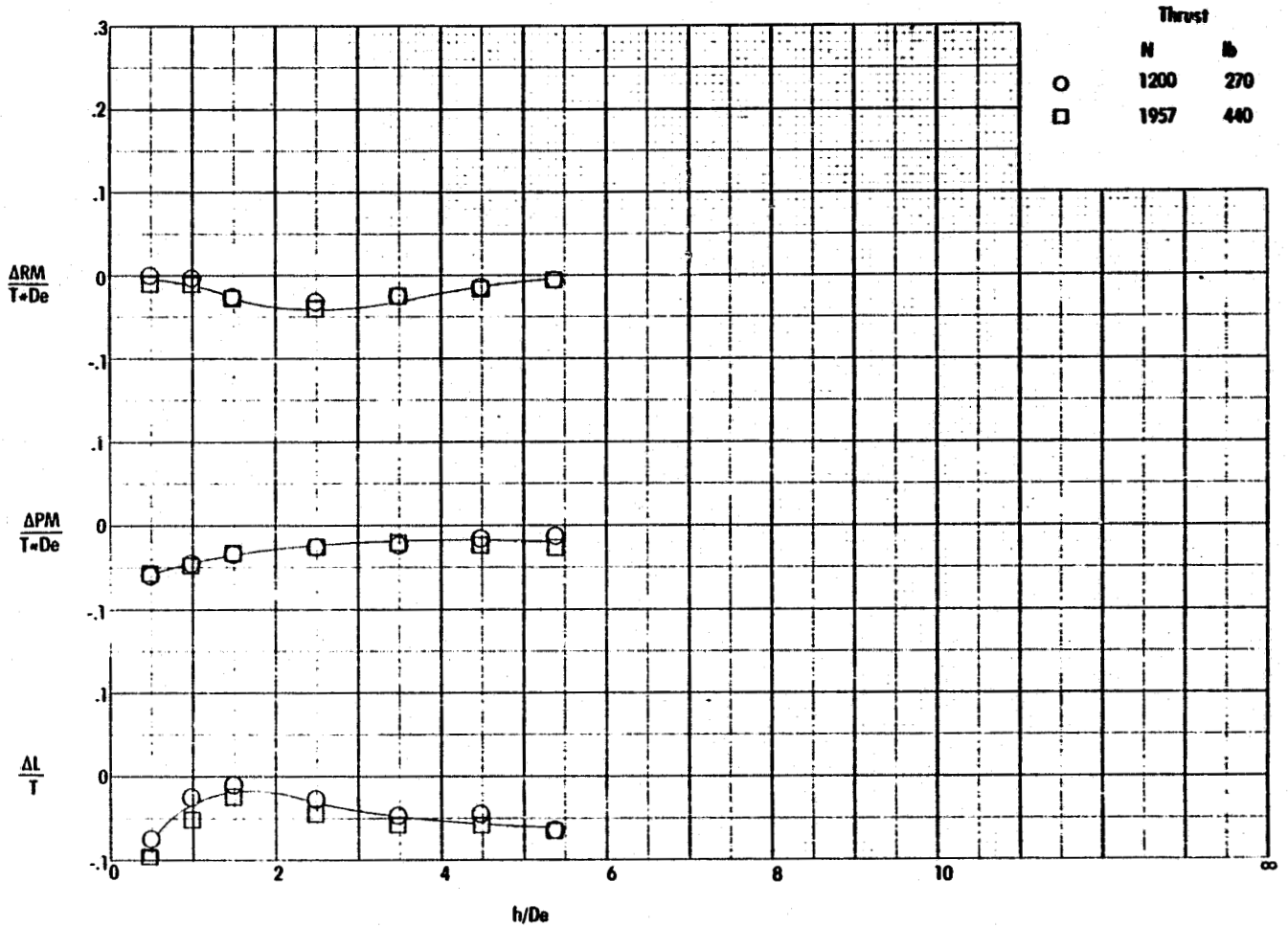

Figure 47. Effect of thrust level on the induced loads of tunnel model 2.

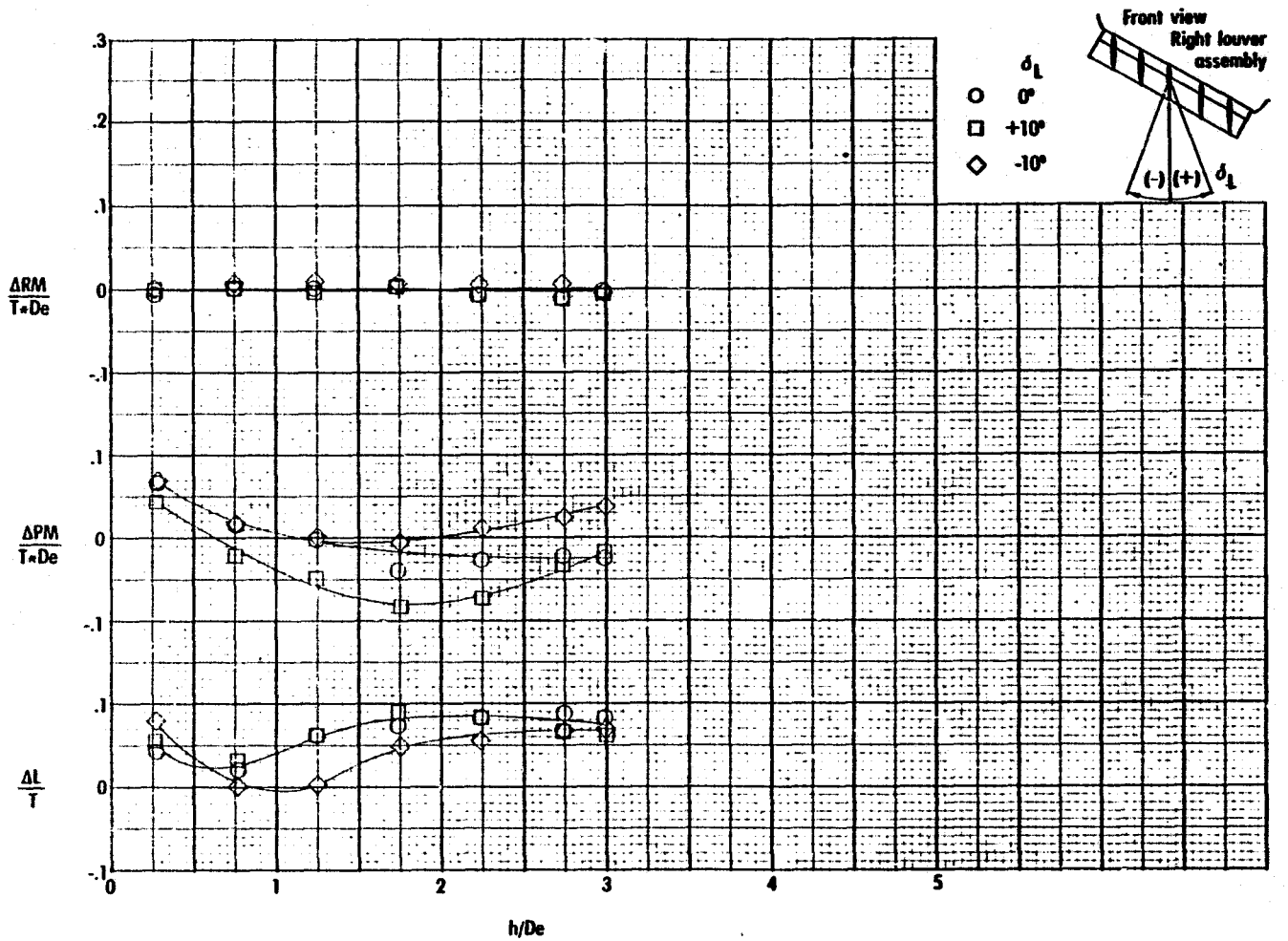

Figure 48. Influence of thrust deflection on the induced loads of tunnel model 1. (Thrust averaged data)

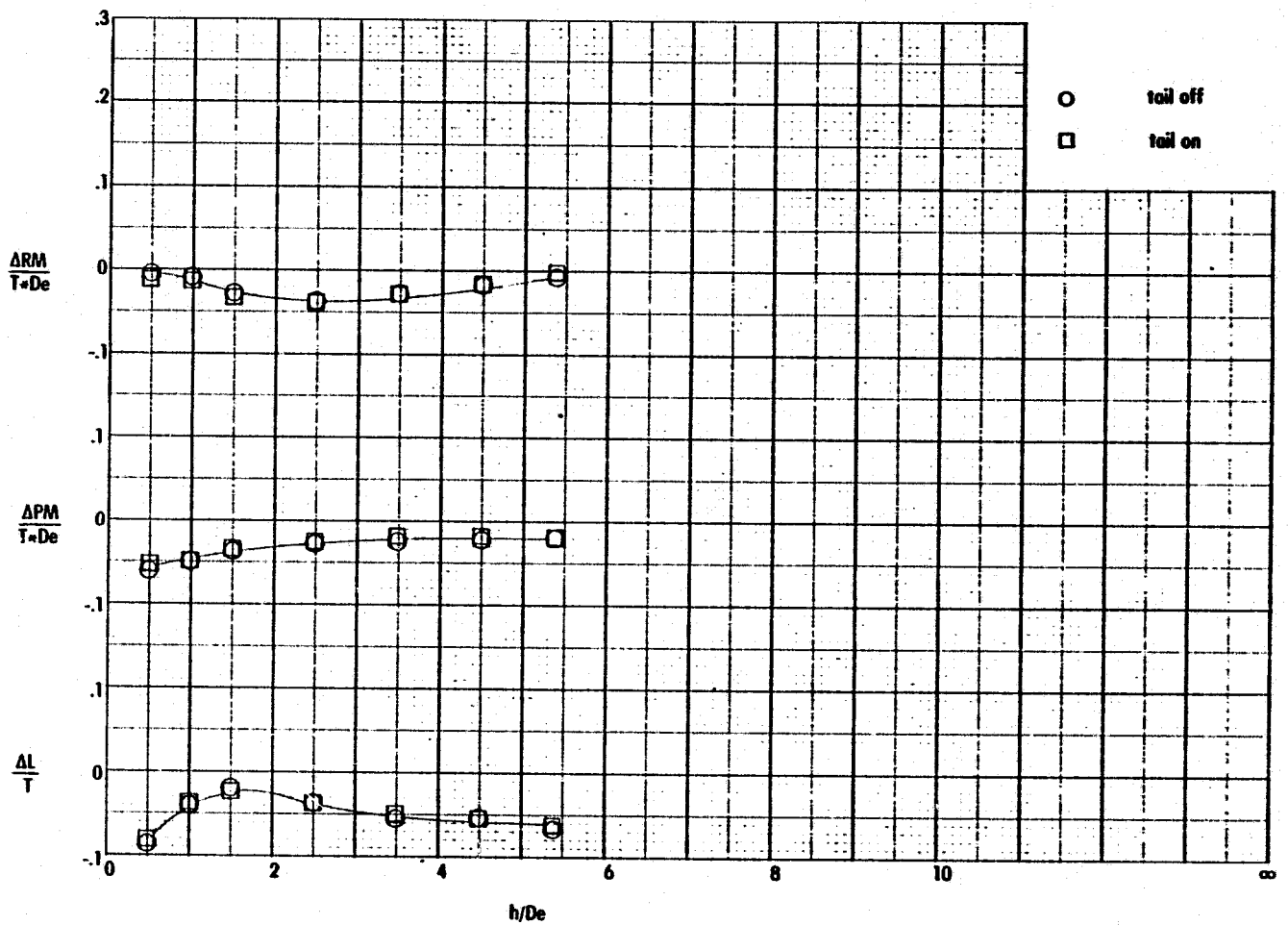

Figure 49. Influence of T-tail on the induced loads of tunnel model 2.

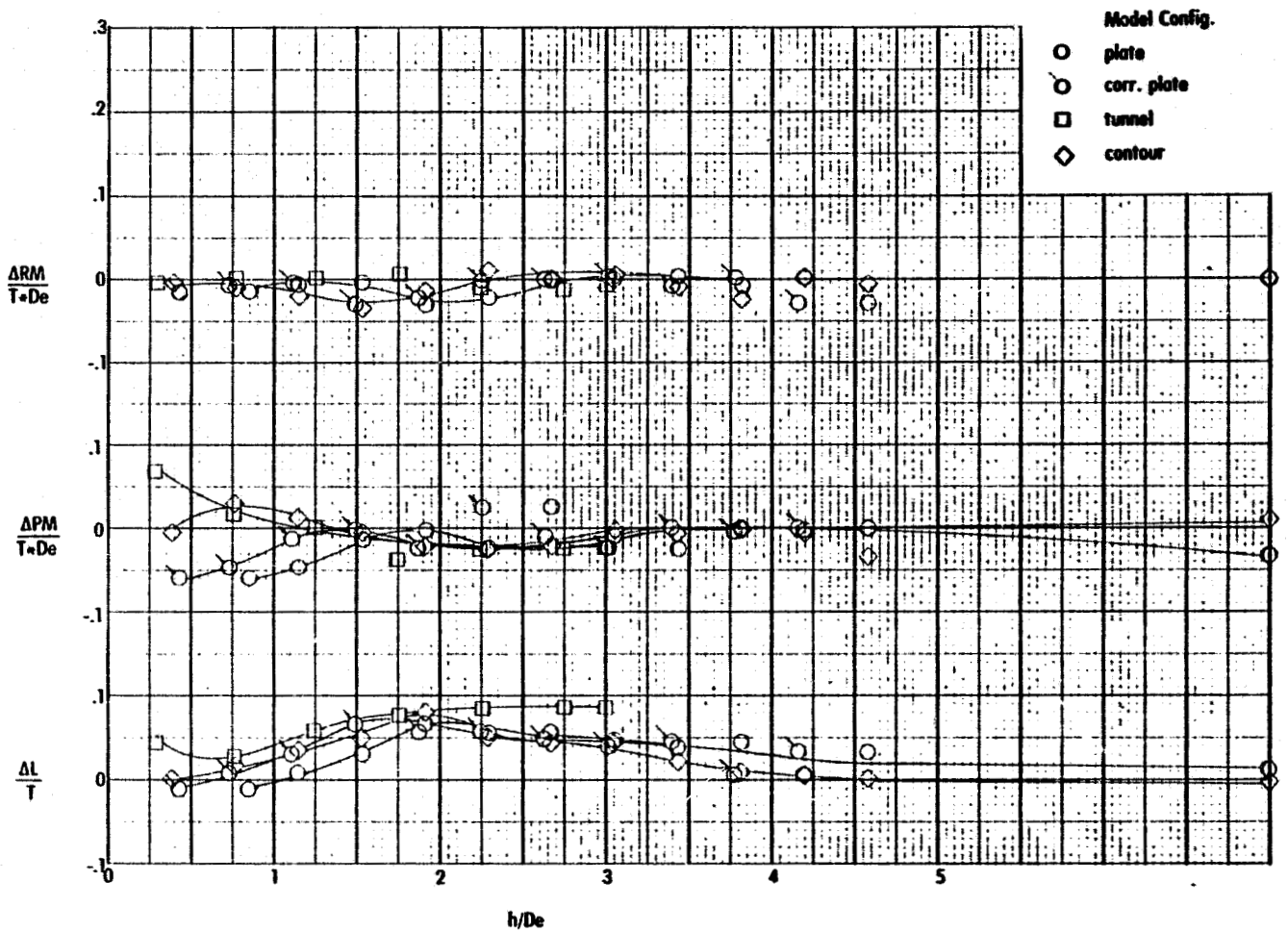

Figure 50. Comparison of induced loads for model 1, $\theta = 0$, $\phi = 0$. (Thrust averaged data)

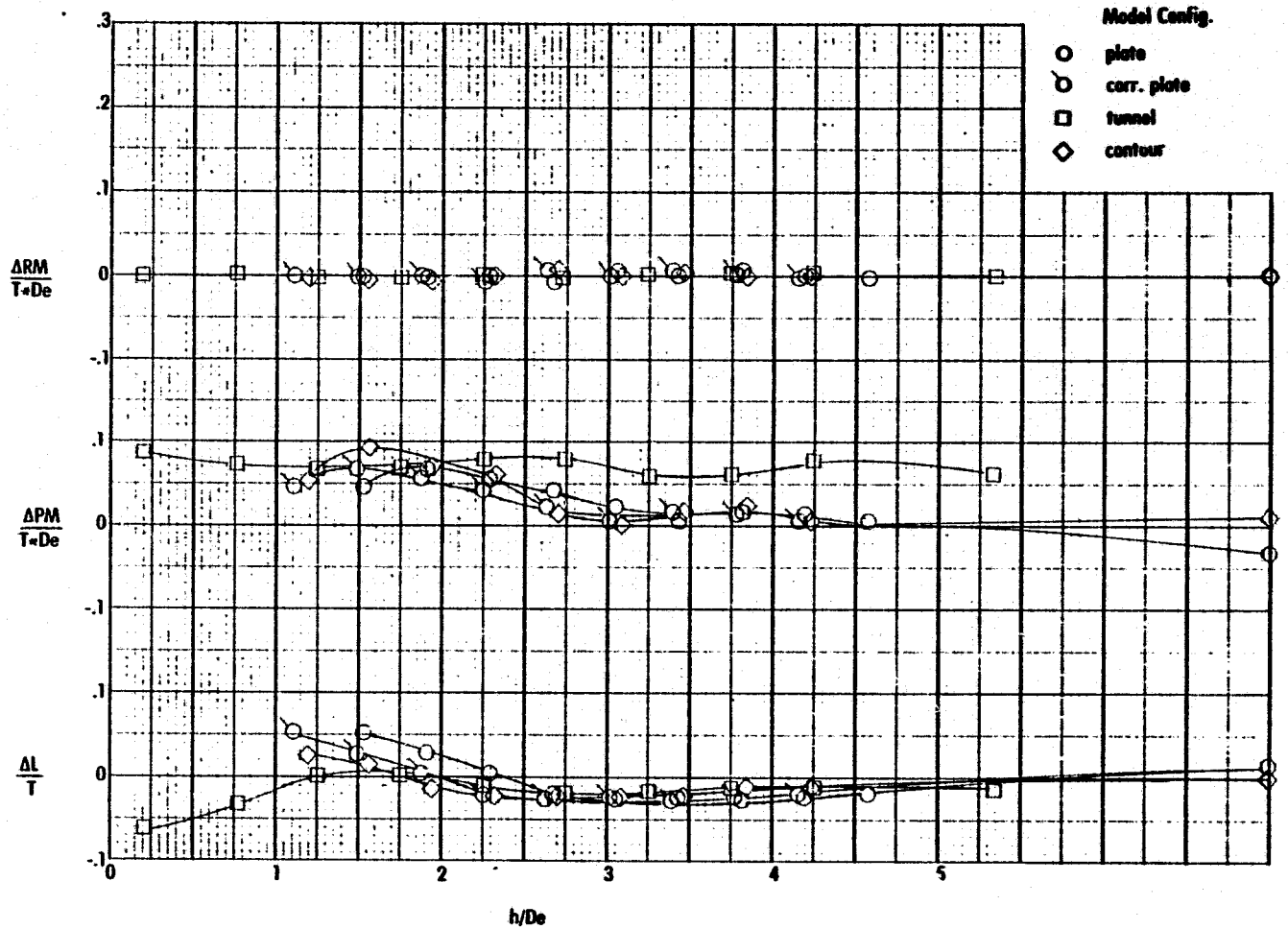

Figure 51. Comparison of induced loads for model 1, $\theta = +10$, $\phi = 0$. (Thrust averaged data)

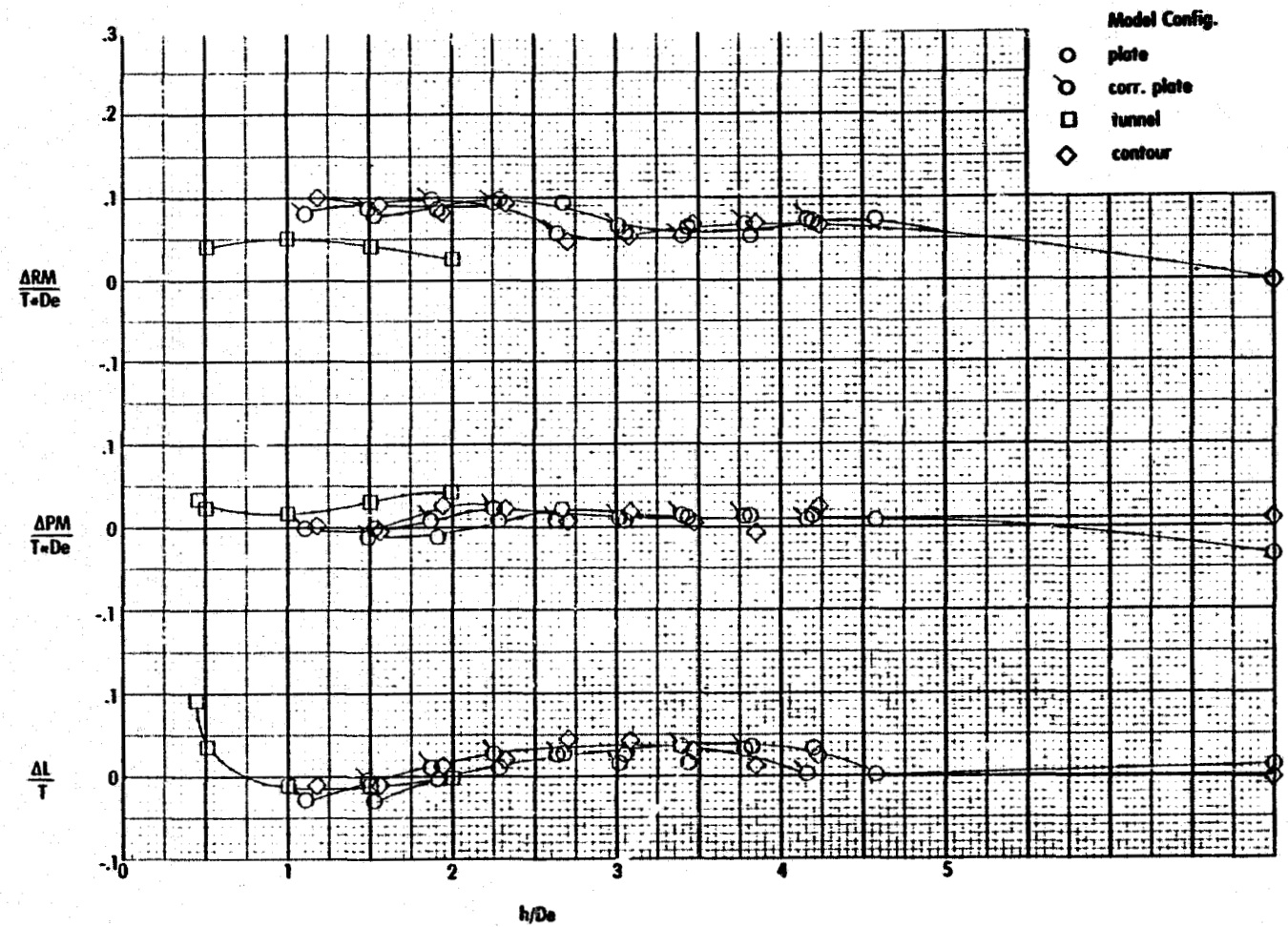

Figure 52. Comparison of induced loads for model 1, $\theta = 0$, $\phi = +10$. (Thrust averaged data)

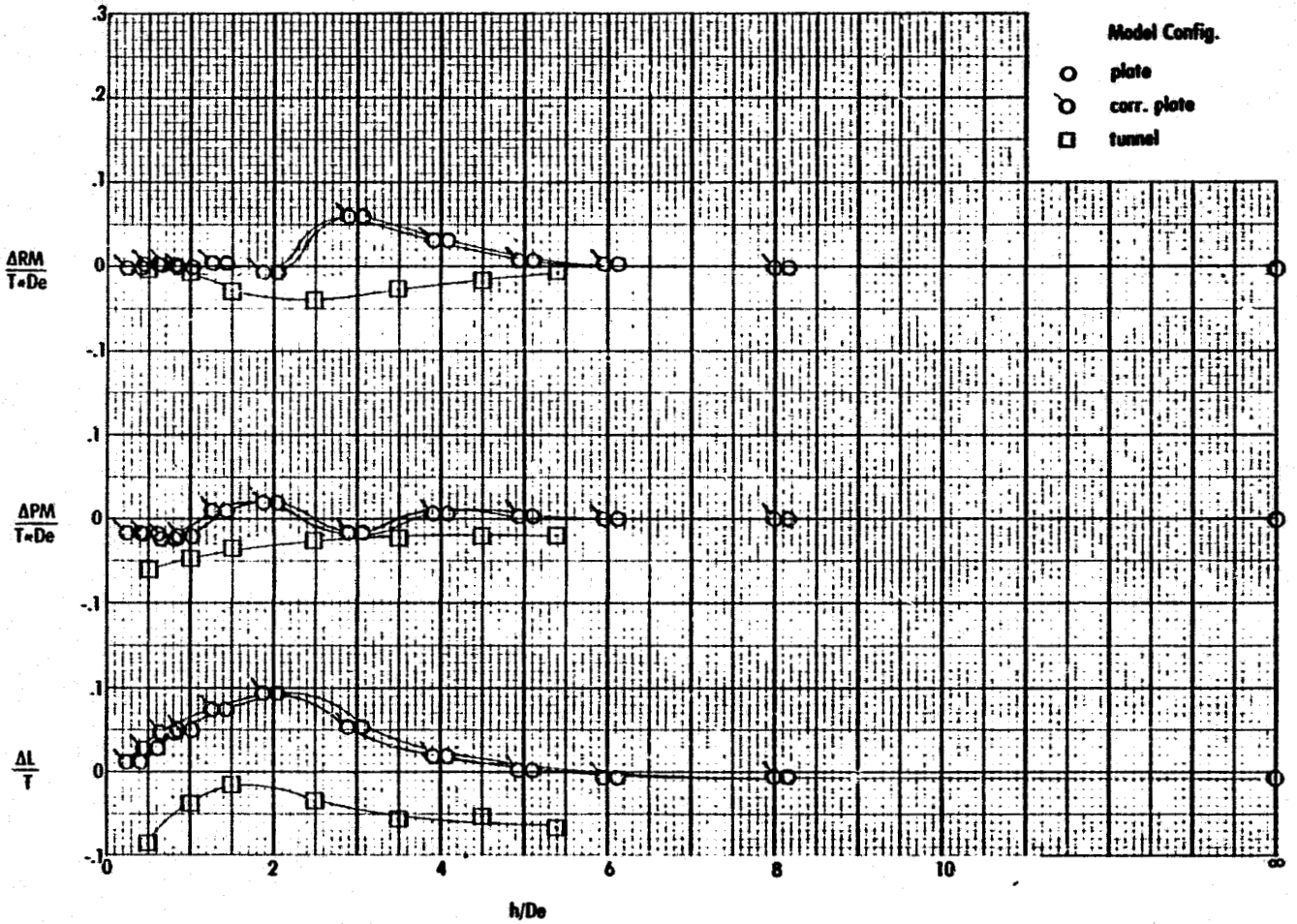

Figure 53. Comparison of induced loads for model 2, $\theta = 0$, $\phi = 0$. (Thrust averaged data)

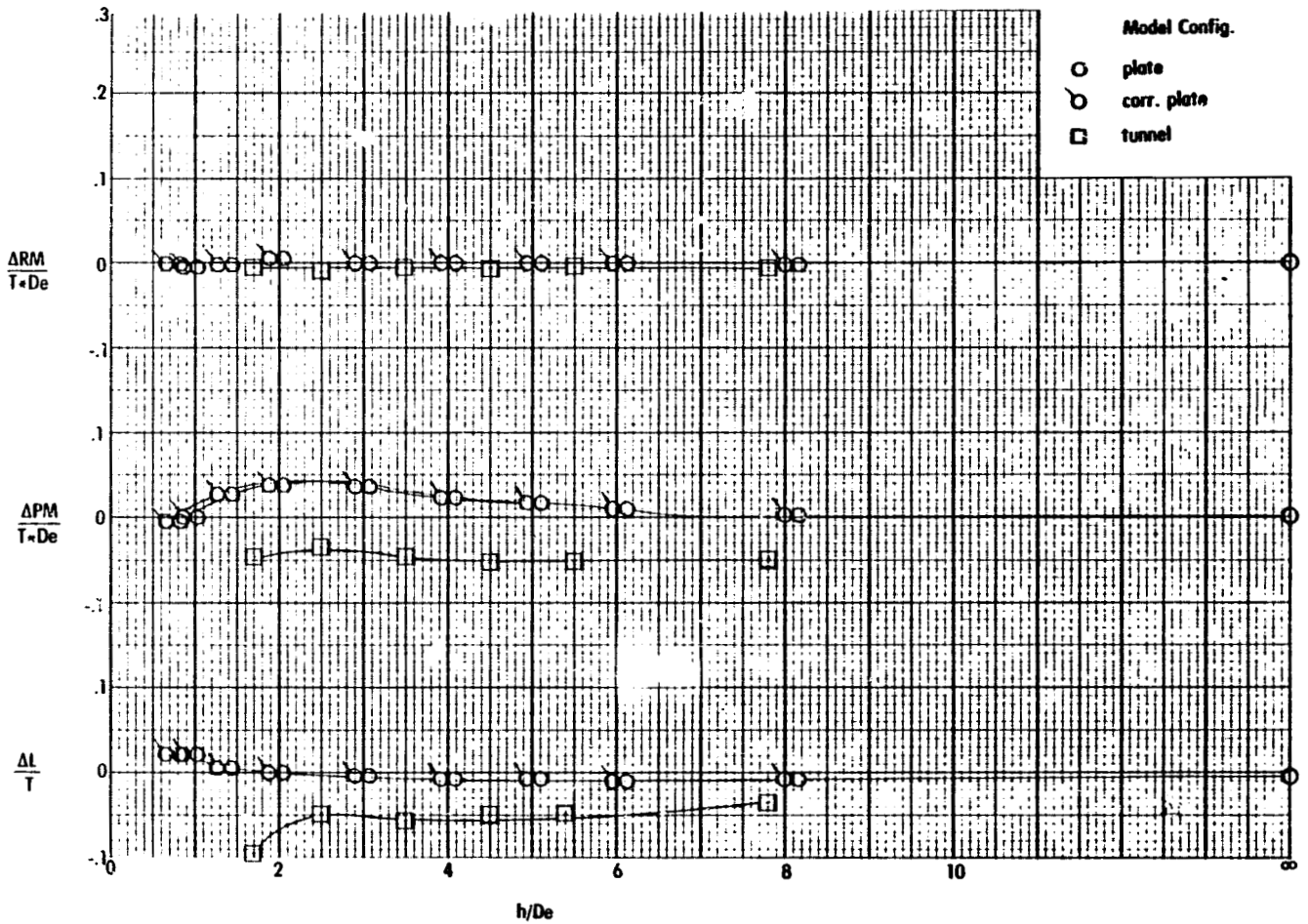

Figure 54. Comparison of induced loads for model 2, θ = +10, ϕ = 0. (Thrust averaged data)

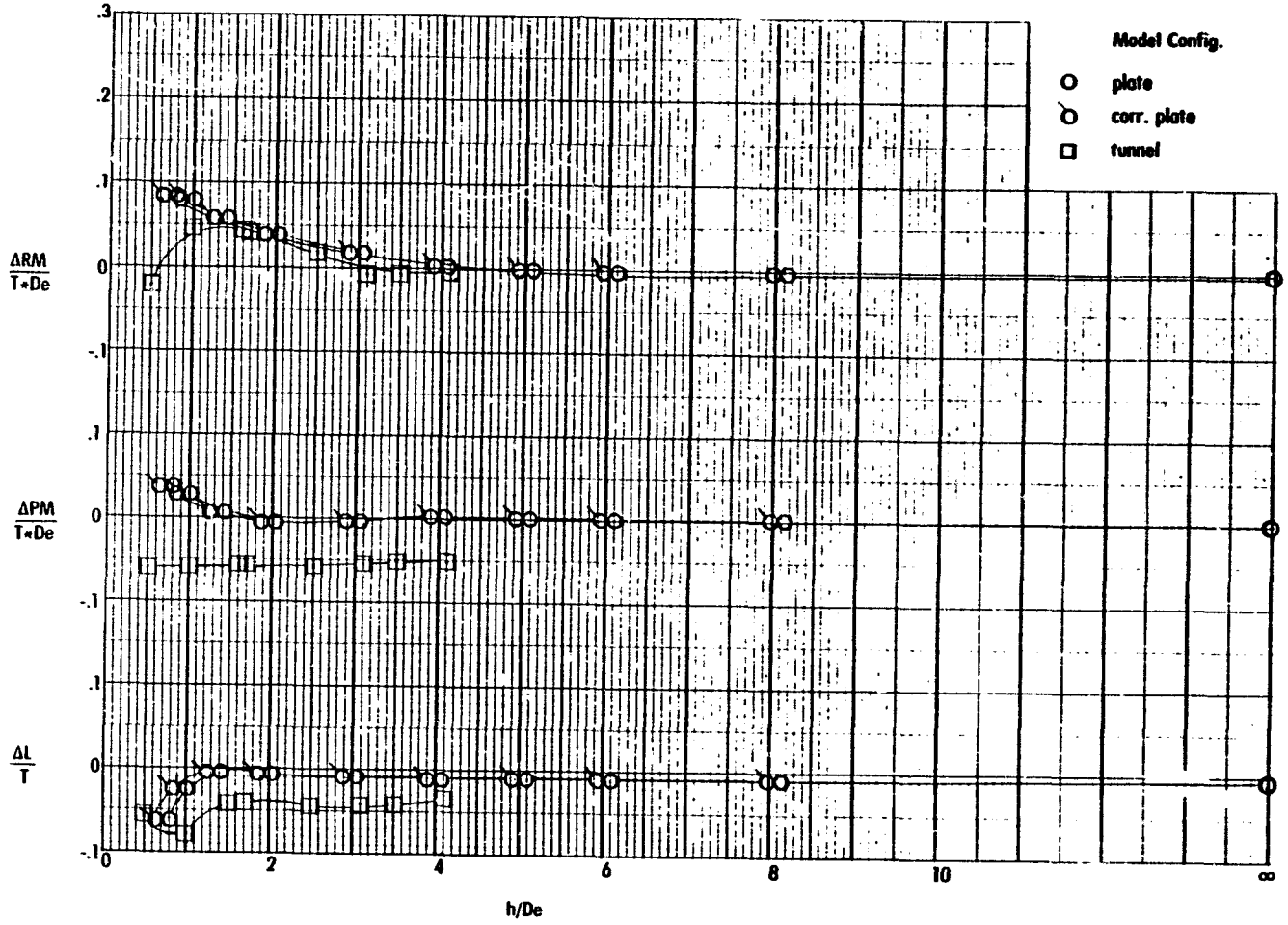

Figure 55. Comparison of induced loads for model 2, $\theta = 0$, $\phi = +10$. (Thrust averaged data)

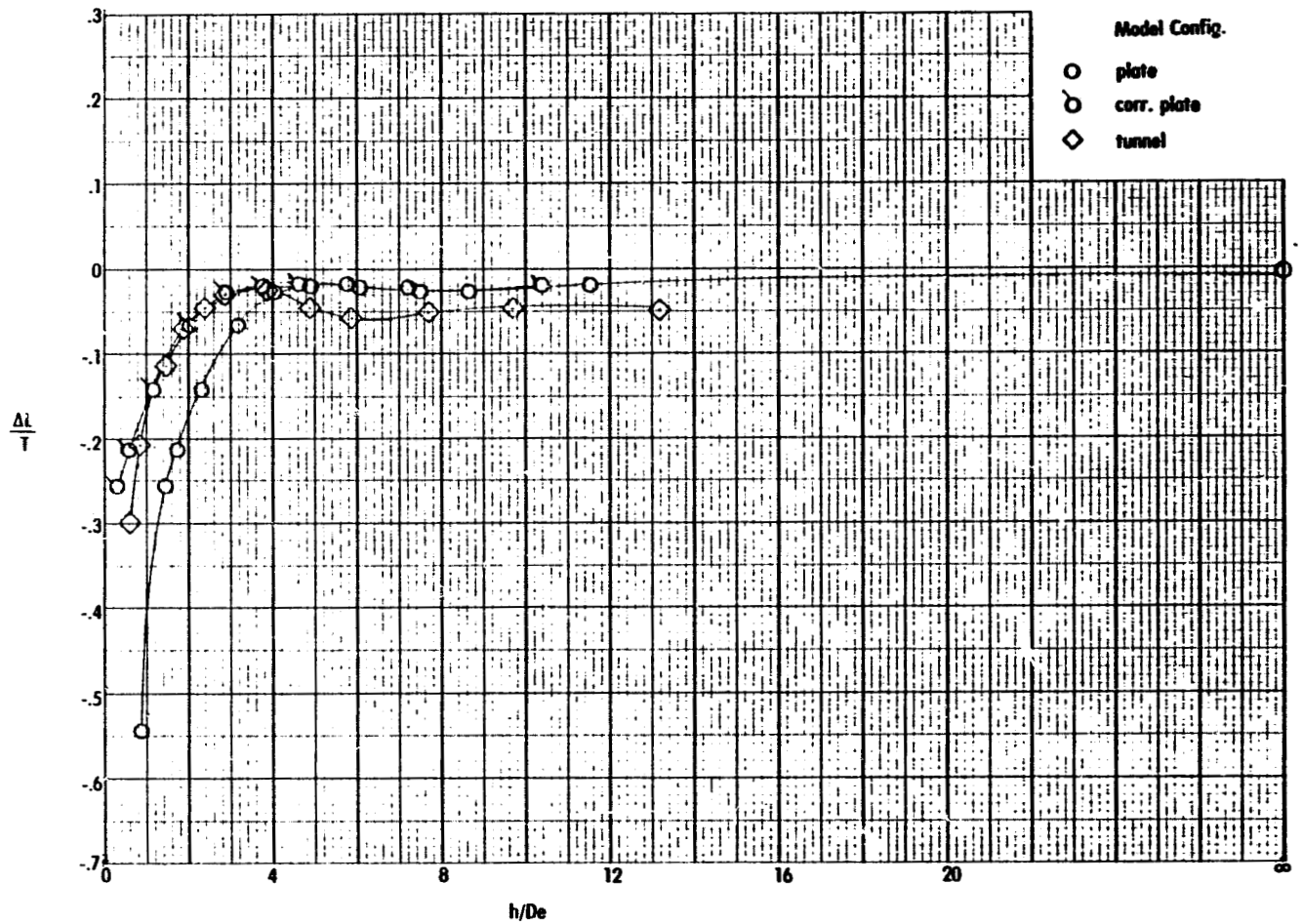

Figure 56. Comparison of induced lift force for model 3, $\theta = 0$, $\phi = 0$. (Thrust averaged data)

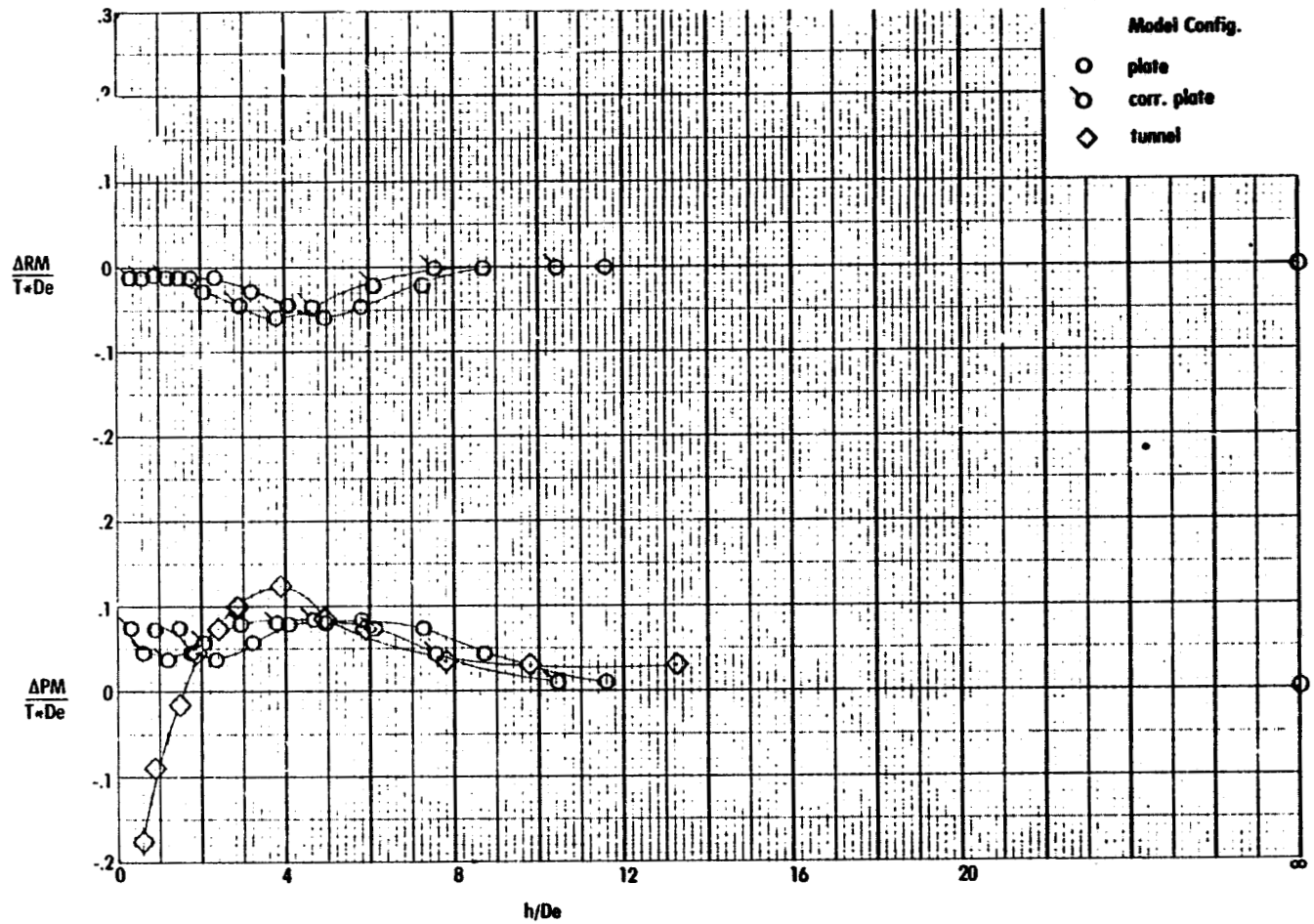

Figure 57. Comparison of induced pitching moment for model 3, $\theta = 0$, $\phi = 0$. (Thrust averaged data)

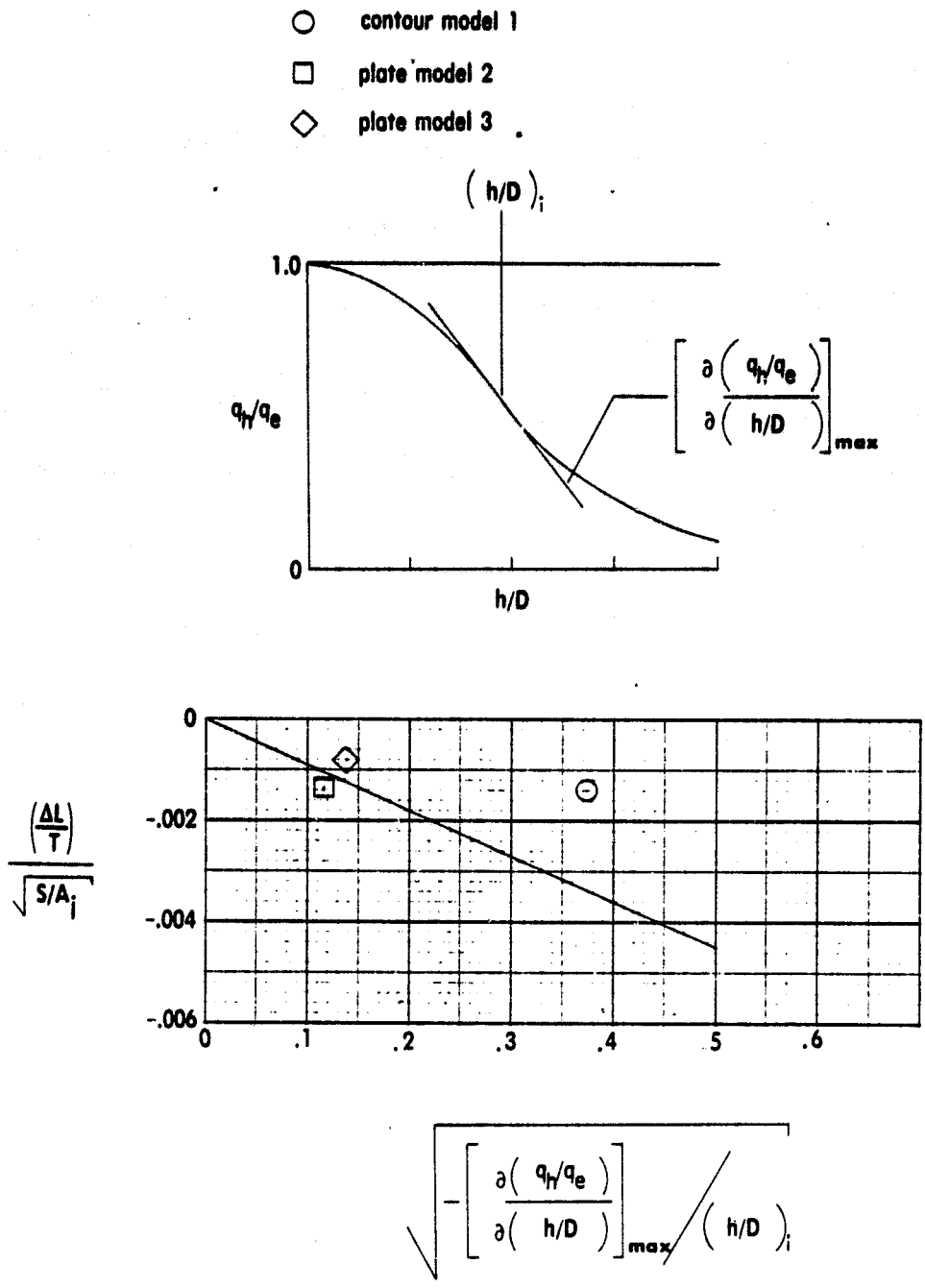

Figure 58. Correlation of induced loads with jet decay parameter. (Thrust averaged data)

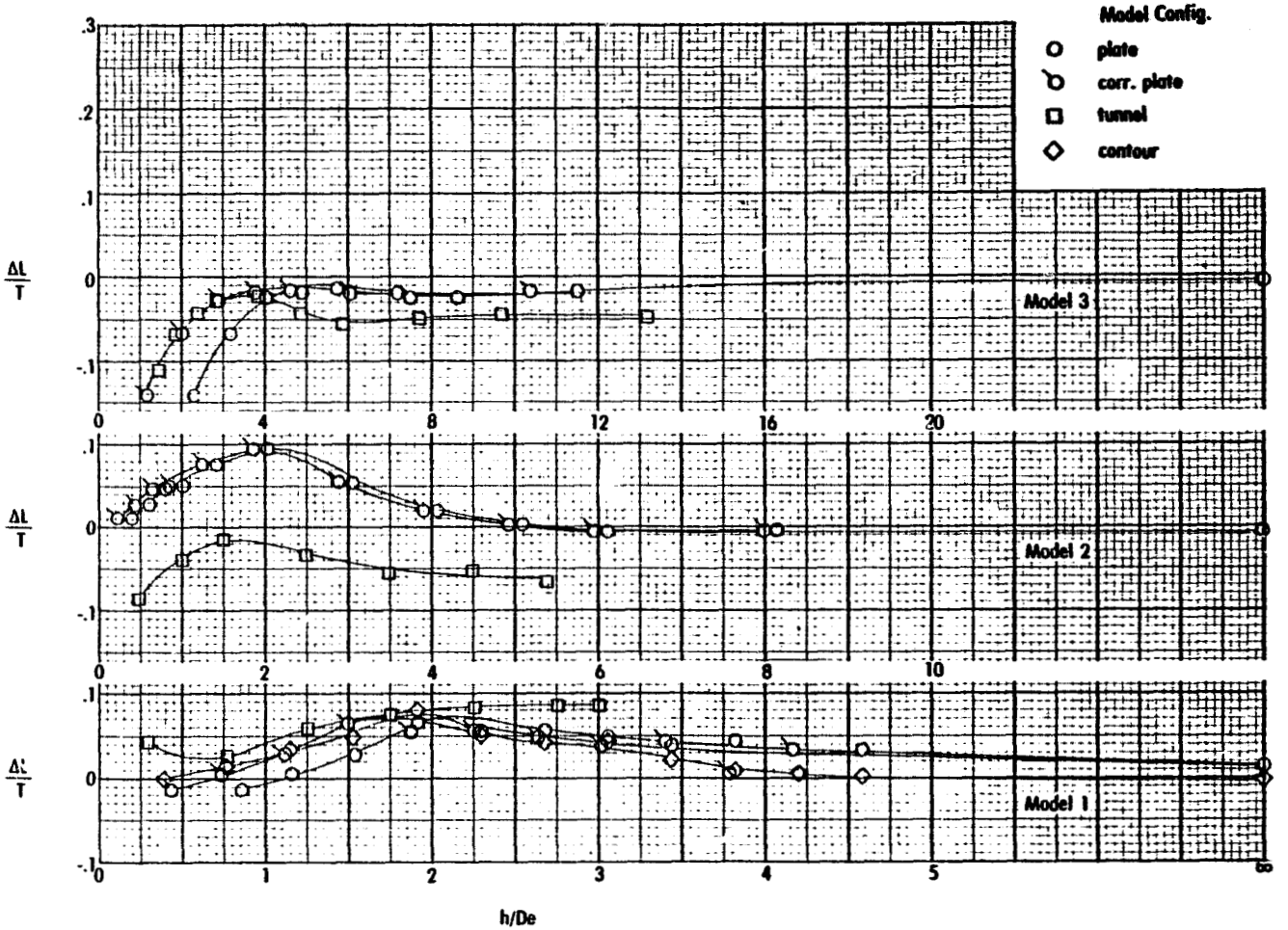

Figure 59. Summary of induced lift forces for all model configurations, $\theta = 0$, $\phi = 0$. (Thrust averaged data)